Torbjørn Gjervan

Studies of bimetallic particle formation in reforming catalysts

NTNU Trondheim
Norges teknisk-naturvitenskapelige universitet

Doktor ingeniøravhandling 2000:102
Institutt for kjemisk prosessteknologi

The Norwegian University of Science and Technology
Department of Chemical Engineering

Studies of bimetallic particle formation in reforming catalysts

by

Torbjørn Gjervan

A Thesis Submitted for the degree
Doctor Ingeniør
November 2000

ISBN 82-7984-131-8
ISSN 0809-103X

Acknowledgement

I first wish to thank my supervisor Professor Anders Holmen for his enthusiasm, support, and guidance throughout the work of this thesis. He was very much responsible for my decision to start as a doctoral student.

I am also very grateful to my co-supervisor Dr. Rune Prestvik for his supervision, helpful discussions, and sharing of frustrations in relation to some of the experimental work. His knowledge and experience in the field of catalytic reforming has been very valuable.

Associate Professor Bård Tøtdal and Dr. Magnus Rønning in collaboration with Professor David G. Nicholson are gratefully acknowledged for their contribution to this thesis by performing the STEM/EDX and EXAFS experiments, respectively. I would also like to thank Professor Charles E. Lyman for providing the opportunity to use the STEM/EDX instrumentation at Lehigh University, Bethlehem (U.S.).

My colleagues at the Department of Chemical Engineering and SINTEF are highly appreciated for their support and friendship.

This work was made possible through the financial support from the Norwegian Scientific Foundation VISTA, the Department of Chemical Engineering at the Norwegian University of Science and Technology (NTNU), and SINTEF Catalysis and Kinetics group.

Abstract

The formation of bimetallic particles in reforming catalysts has been studied employing various experimental techniques. Emphasis was put on investigations of the effect of the pre-treatment conditions, reduction conditions, and the chlorine content of the catalyst prior to reduction. Most of the studies involved a commercial Pt-Re/Al_2O_3 catalyst, but also a Pt-Sn/Al_2O_3 catalyst was synthesised and studied.

Dehydrogenation of methylcyclohexane (MCH) (270°C, 1.75 bar abs., pulse = 0.74 ml, carrier gas flow = 250 ml/min, H_2/MCH = 35) was used as a model reaction to investigate changes in the dispersion of the Pt-Re/Al_2O_3 catalyst. By using a specially designed pulse apparatus it was found that the dispersion was not affected by increasing the drying temperature from 240°C to 550°C. However, reducing the catalyst without any pre-treatment resulted in low dispersion. The latter result may be rationalised in terms of the effect of too much water present during reduction. Water may have a sintering effect on Pt particles. In addition, water may suppress the reduction of rhenium and thus prevent the formation of bimetallic particles.

Hydrogenolysis of cyclopentane and n-butane (250°C, 1.75 bar abs., pulse = 1.20 ml, carrier gas flow = 250ml/min) were used as model reactions in order to study changes the in alloy formation of the Pt-Re/Al_2O_3 catalyst. The same apparatus as for dehydrogenation of methylcyclohexane was used. Using the selectivity to methane as a measure of the degree of alloy formation it was found that drying at 240°C in air prior to reduction resulted in the most alloyed catalyst. Drying at 550°C resulted in less bimetallic particles, whereas no drying prior to reduction yielded even lower methane selectivity. Drying at 240°C in air leaves the catalyst surface relatively hydrated yielding good conditions for Re oxide surface mobility. The surface is less hydrated after drying at 550°C and therefore less bimetallic particles are formed during

reduction. If the catalyst is reduced without any drying too much water seems to suppress the reduction of Re and the formation of bimetallic particles.

The changes in alloy formation have also been studied with volumetric chemisorption of hydrogen. Compared to the Pt/Al_2O_3 catalyst hydrogen chemisorption is suppressed in the $Pt\text{-}Re/Al_2O_3$ catalyst due to Pt-Re alloy formation. Rhenium does not chemisorb hydrogen, which imply that in an alloy particle the number of Pt neighbours required for dissociative chemisorption is reduced. The H/Pt ratio has therefore been interpreted as a measure of the degree of alloy formation. It was found that drying at low temperatures prior to reduction resulted in the lowest H/Pt ratios. However, the low H/Pt ratio of the catalyst that was not dried prior to reduction can not solely be due to a high degree of alloy formation regarding the results from the model reactions. Thus, it also reflects a low dispersion of Pt in this catalyst. Drying the catalyst in N_2 atmosphere at 680°C gave a catalyst with a similar low dispersion.

X-ray absorption spectroscopy (XAS) experiments were performed in order to obtain direct physical information of the metal particles. Extended X-ray absorption fine structure (EXAFS) analysis of the catalyst samples pre-treated at different temperatures in air and N_2 confirmed the findings from the chemical characterisation techniques. Investigation of the Re L_{III} edge and the Pt L_{III} showed that the samples dried at 240°C and 500°C have the highest amount of bimetallic particles. The sample not dried prior to reduction shows a significantly lower bimetallic coordination than the other samples. Treating the catalyst in N_2 atmosphere at 680°C resulted in less alloy formation, indicating both that the mobility of the Re oxide species is inhibited and that the Pt particles are sintered at these conditions. The Re L_{III} EXAFS and XANES data indicate that a large fraction Re is present in a low oxidation state and in intimate contact with the support. This tendency increases with increasing drying temperature.

No significant effect of the reduction procedure was found when varying the heating rate in the range 0.2°C/min to 3.3°C/min. When the reduction temperature was increased from 480°C to 530°C a higher degree of alloy

formation was found. The catalyst samples were analysed with pulse hydrogen chemisorption and the obtained H/Pt ratios were used as an indication of the degree of alloy formation. Addition of moisture during reduction has a significant effect on the H/Pt ratio reflecting the beneficial role of small amounts of water on the formation of bimetallic particles. Combined STEM/EDX measurements did not reveal any significant differences in composition of the individual metal particles when even more severe reduction conditions were employed.

The effect of the chlorine content was investigated with n-butane and cyclopentane hydrogenolysis used as model reactions, combined STEM/EDX, temperature programmed reduction (TPR) and volumetric chemisorption. By oxychlorination the chlorine content was varied in the range 0.65 wt% Cl to 1.50 wt% Cl and the results obtained from the model reactions and volumetric chemisorption experiments indicated that small amounts of chlorine is beneficial when alloy formation is regarded. No significant differences could be found from the STEM/EDX analysis. Reducing the oxychlorinated samples in moist atmosphere yielded larger metal particles with a slightly higher Re content.

There were only conducted a limited number of investigations involving Pt-Sn/Al_2O_3 catalysts and it was evident from TPR studies that the drying temperature prior to reduction has a significant effect on the final state of the metal particles. The results obtained can be rationalised in terms of higher degree of Sn reduction and bimetallic formation when the catalyst sample was dried in high temperatures in air.

Table of contents

List of publications and presentations

List of publications

The following publications related to this thesis have been prepared:

I. T. Gjervan, M. Rønning, R. Prestvik, B. Tøtdal, C. E. Lyman, and A. Holmen: "Bimetallic nano-particle formation in the Pt-Re reforming catalysts revealed by STEM/EDX, XANES/EXAFS and chemical characterization techniques. Effect of water and chlorine", in *Stud. Surf. Sci. Catal.*, A. Corma, F.V. Melo. S. Mendioroz, J.L.G. Fierro (Eds.), Proceedings of the 12th ICC, Granada, Spain, July 9 – 14 2000, Vol. 130 D (Elsevier, Amsterdam 2000) pp. 3189-3194

II. M. Rønning, T. Gjervan, R. Prestvik, D. Nicholson, and A. Holmen: "Influence of pre-treatment temperature on the bimetallic interactions in Pt-Re/Al_2O_3 reforming catalysts studied by X-ray absorption spectroscopy", *Submitted*

III. T. Gjervan, B. Tøtdal, C. E. Lyman, R. Prestvik, and A. Holmen: "The influence of chlorine content on the bimetallic particle formation in PtRe/Al_2O_3 studied by STEM/EDX, TPR, H_2 chemisorption and model reaction studies", *Submitted*

IV. T. Gjervan, R. Prestvik, and A. Holmen: "Catalytic Reforming" *in the monograph "Applied Catalysis"*, M. Baerns (Ed.) (Springer Verlag), *Submitted*

Copies of paper I-IV are given as appendices to the thesis.

International presentations

The author has given the following presentations of parts of the thesis:

I. T. Gjervan, B. Tøtdal, C. E. Lyman, R. Prestvik and A. Holmen: "Effect of the pre-treatment conditions and chlorine content on the formation of PtRe alloys in $PtRe/Al_2O_3$ catalysts". *Oral presentation at ICAT*, Technical University of Denmark, Denmark April 30 1999.

II. T. Gjervan, B. Tøtdal, C. E. Lyman, R. Prestvik and A. Holmen: "Effect of the pre-treatment conditions and chlorine content on the formation of PtRe alloys in $PtRe/Al_2O_3$ catalysts". *Oral presentation at Europacat-IV*, Rimini, Italy September 10 1999.

III. T. Gjervan, M. Rønning, R. Prestvik, B. Tøtdal, C. E. Lyman and A. Holmen: "Bimetallic nano-particle formation in the Pt-Re reforming catalysts revealed by STEM/EDX, XANES/EXAFS and chemical characterization techniques. Effect of water and chlorine". *Poster at the 12^{th} ICC*, Granada, Spain July 9^{th} – 14^{th} 2000.

The author's contribution

The author has had an active role in all stages of the work reported in this thesis. The author has been involved in the planning and the performance of all the experimental work. However, Dr. Magnus Rønning in collaboration with Professor David Nicholson has performed the XAS experiments at synchrotron facilities in Grenoble, France, and Brookhaven, U.S. and completed the corresponding data analysis. Associate Professor Bård Tøtdal has performed the STEM/EDX experiments with the support from Professor Charles E. Lyman at Lehigh University, U.S. The author has written paper I, III, and IV. He has also been involved in writing paper II.

List of symbols and abbreviations

AEM	Atomic Electron Microscopy
a.u.	Arbitrary units
BET	Surface area measured by Brunauer, Emmet, Teller method [m^2/g]
C_{Pt}	Atomic fraction (EXAFS) or weight fraction (EDX) of platinum in a metal particle
C_{Re}	Atomic fraction of rhenium in a metal particle
CCR	Continuous Catalytic Reforming
CP	Cyclopentane
$D_{Particle}$	Diameter of a metal particle [nm]
DR	Direct Reduction
EDX	Energy Dispersive X-ray Spectroscopy
ESRF	European Synchrotron Radiation Facility
EXAFS	Extended X-ray Absorption Fine Structure
FEG	Field Emission Gun
FID	Flame Ionisation Detector
GC	Gas Chromatograph
IR	Infrared absorption spectrocsopy
k	Wave number [$Å^{-1}$]
LFC	Liquid Flow Controller
MCH	Methylcyclohexane
MFC	Mass Flow Controller
MTBE	Methyl-Tert-Butyl Ether
Mx	Million times magnification
N	Number of atom neighbours
NSLS	National Synchrotron Light Source
R	Interatomic distance [Å]
RFG	Reformulated Gasoline
RVP	Reid Vapor Pressure [kPa]

S_a	Specific surface area [m^2/g]
Sel. C1	Selectivity to methane [%]
SNBL	Swiss-Norwegian Beamline
STEM	Scanning Transmission Electron Microscopy
TCD	Thermal Conductivity Detector
TEM	Transmission Electron Microscopy
TOF	Turnover Frequency
TPR	Temperature Programmed Reduction
Wt%	Weight percent
XANES	X-ray Absorption Near Edge Structure
XAS	X-ray Absorption Spectroscopy
XPS	X-ray Photoelectron Spectroscopy

1. Introduction

1.1. History of catalytic reforming

Catalytic reforming is a process where the octane number of naphthas is raised by changing the molecular structure of the hydrocarbons. This process is one of the most important industrial applications of catalyst, and according to *the International Petroleum Encyclopedia (1999)* [1] there are 755 catalytic reforming plants world-wide and with a total capacity of more than 11 million barrels per calendar day. The demand for high-octane fuels has been increasing as a consequence of the development of more efficient combustion engines with higher and higher compression ratios. The octane number is a measure of the tendency of the gasoline to knock during combustion or pre-ignite during compression, and it is depending on the composition of the fuel. Addition of alkylated lead components has been usual in order to increase the octane number, but due to environmental concerns more emphasis has been put on octane enhancement by catalytic reforming.

In 1930 thermal reforming was introduced to increase the octane number of gasoline. The process was performed at 540°C and 35 to 70 bar [2] and involved cracking of high molecular weight paraffins to lower molecular paraffins with higher octane numbers, production of olefins, and concentration of native aromatics by cracking of paraffins to gaseous fragments. As this was an inefficient process due to cracking and loss of products and the inability to produce aromatics, there was a need to develop a reforming process that could be more selective in producing the desired octane raising components. The first catalytic reforming process in the early 1940's involved the use of molybdenum and chromium oxide catalyst [3], but the major breakthrough came with the introduction of the Platforming process by UOP in 1949. The catalyst consisting of platinum supported on acidic alumina, was more active by an order of magnitude compared to the previous molybdenia and chromia

catalysts. Typical operation conditions were 450 to 510°C and 35 to 50 bar [3]. No regeneration facilities were provided, and the process was operated under conditions which minimised coke laydown. After the introduction of Platforming many new processes were announced and the catalytic reforming capacity grew rapidly.

The need to achieve increasingly higher octane numbers, i.e. operate at lower pressures to achieve higher aromatics yields, increased the rate of coke formation in catalytic reformer plants. In 1968 a significant improvement of the reformer catalyst was made by the introduction of the Pt-Re alumina catalyst by Chevron [4]. This catalyst was much more stable than those used previously and could be operated at much more severe conditions. By operating at lower pressures and higher temperatures thermodynamic limitations for the formation of aromatics can be minimised. Subsequently other bimetallic catalyst systems containing Ir, Sn, Ge and also multimetallics incorporating additional elements were also developed and came into the marked. The bi- and multimetallic catalyst systems have longer cycle lengths at high severity operations due to lower rates of coke deposition, ability to perform at high coke levels, and lower sintering rates of the metallic function [5].

New process design has been developed over the years and has accompanied new catalyst inventions. Bi- and multimetallic catalysts have made low pressure high-severity operation possible. A significant process innovation was the introduction of continuous catalytic reforming (CCR) by UOP where the Pt-Sn/Al_2O_3 catalyst is employed. In this process the catalyst is circulated through the reactors to contact and reform naphtha and then circulated through a regeneration zone, where the deactivated catalyst is restored to its initial activity. This allows steady-state reforming operation with fresh catalyst performance at optimum process conditions. Most new catalytic reforming plants are of this type.

1.2. Trends in catalytic reforming

Until 1974, almost all gasoline contained lead to improve the octane rating. The advent of catalytic devices in the exhaust system, which are rapidly deactivated by lead, of most 1975 model U.S. cars in fall 1974 [6] introduced unleaded gasoline to the marked. At the same time there was a lead phase out in gasoline driven by environmental legislation in the U.S. and Japan. Today, unleaded gasoline is becoming a reality also in Europe and is spreading to the rest of the world. It is expected that 84% of all gasoline sold will be unleaded in 2005 [7]. Through the use of catalytic reforming, unleaded gasoline was able to satisfy the octane demand. However, this led to an increased concentration of benzene and other aromatics in the fuel, which are good sources for octane, but are also highly toxic. Addition of other compounds such as oxygenates has also been done in order to compensate for the octane loss of the gasoline pool. In 1990s, the Clean Air Act Amendments (U.S.) resulted in new specification of gasoline and the introduction of Reformulated Gasoline (RFG). U.S.A. has taken the lead in the implementation of more stringent regulations, but other countries are following. Some present gasoline specifications and future trends are given in Table 1.1:

Table 1.1. *Present gasoline specifications and future trends [8-10]*

Specifications	U.S.A	EU		Japan
Max. values	2000	2000	2005	2000
RVP [kPa]		60		78
Sulphur [wppm]	50	150	50	100
Oxygenates [wppm]	2.2	2.7		
Benzene [vol.%]	1.0	1		1
Aromatics [vol.%]	35	45	35	
Olefins [vol.%]	15	18		
Lead (max.) [g/l]	-	0.005	-	

The reduction of the content of benzene and other aromatics in gasoline could make the future of catalytic reforming questionable. The high octane numbers of reformates are directly linked to the content of aromatics. If the content is to be reduced to 20% or even 10%, this would reduce the reformate contribution in gasoline to 24% and 11% [11]. This would create a need for additional capacities for isomerisation, alkylation, and etherification. However, as a consequence of a possible reduction of the reforming capacity as discussed here, the hydrogen production of a typical refinery would be reduced by 40% or even 80%. The refining industry would then not longer be in position to provide sufficient amounts of hydrogen to the hydrotreating and hydroprocessing units. Therefore, the main challenge for catalytic reforming is to achieve a high hydrogen production while maintaining the benzene production as low as possible. Thus, reforming has to adapt through new catalyst performance and improved technologies.

Even if the outlook for catalytic reforming for gasoline blending applications does not look too optimistic, it will remain the major source of feedstock for the aromatics petrochemical market.

1.3. Scope of the work

The $PtRe/Al_2O_3$ is the most widely used catalyst in catalytic reforming and has been studied extensively over the last few decades. The addition of rhenium to the monometallic Pt/Al_2O_3 reforming catalyst gave a much lower rate of deactivation. It is well known that coke deposition is the main cause of catalyst deactivation but in spite the scientific efforts so far the actual role of rhenium in bringing about the high catalyst stability is still not clear.

It has been explained that rhenium anchors the metal phase to the support [12] and stabilises the dispersion and thus preventing the formation of graphitic coke which demands large platinum ensembles. Others claim that rhenium acts independently by destroying coke precursors such as

cyclopentane [13,14]. It has also been proposed that rhenium induces effects on the dehydrogenation activity of Pt [15-17] or that it changes the electronic structure by formation of bimetallic particles (alloy) and the interaction of such particles with sulphur [18-20].

It appears that the final state of Pt-Re/Al2O3 catalysts is very sensitive to the conditions employed during preparation and pre-treatment [21-27]. This might explain some of the contradictory results found in the literature concerning platinum-rhenium interaction, the actual state of rhenium, and the catalytic role of rhenium.

Previously the effect of the pre-treatment conditions on bimetallic Pt-Re/Al_2O_3 has been studied at the Department of Industrial Chemistry, NTNU (Presently the Department of Chemical Engineering) [28,29]. The current work is aimed to follow up the previous work and to study further the metal function of bimetallic reforming catalysts with focus on the influence of pre-treatment conditions and the conditions employed during regeneration.

Pre-treatment of a commercial reforming catalyst involves first a drying step of the catalyst received from the manufacturer, then reduction, and finally sulphurisation before it is in its active state. When the catalyst activity is too low for economical use it is regenerated by coke combustion, oxychlorination in order to restore acidity and metal dispersion, calcination, reduction, and finally sulphurisation. The present study focuses on how the treatments listed below influences on the degree of bimetallic formation and the reduction degree of the second metal:

- Drying/heating temperature and atmosphere prior to reduction
- Reduction temperature, heating rate, and atmosphere
- Level of chlorine content prior to reduction

In order to perform model compound reaction studies, a dedicated pulse reactor was constructed. A major part of the work was devoted to build and test this experimental set-up. In addition to employ conventional analytical

techniques such as temperature-programmed reduction (TPR), hydrogen chemisorption, and model compound reactions for catalyst characterisation, it was also a goal to involve the use of more advanced techniques such as EXAFS and STEM/EDX in this study. This has been possible through collaboration with the Department of Physics and people highly skilled in the use of such instruments.

Part of this work has been published in the three papers listed on page VII. In addition, some of the results have been presented at ICAT, Technical University of Denmark (Denmark, 1999), Europacat-IV (Rimini, Italy 1999), and 12th ICC (Granada, Spain 2000).

This work was made possible through the financial support of the VISTA (Norwegian Scientific Foundation and Statoil), the Department of Chemical Engineering (NTNU), and SINTEF Catalysis and Kinetics group.

2. Literature

2.1. Catalyst reforming

2.1.1. Introduction

Catalytic reforming is a process where the molecular structure of hydrocarbons is changed. The feedstock to the process is naphtha, a refinery fraction of hydrocarbons in the C_5 - C_{12} range obtained from distillation of crude oil. The major objective of this process is to produce high-octane quality gasoline, but also aromatics to the petrochemical marked are produced. The octane number of gasoline is a measure of the tendency of the fuel to pre-ignite or knock in internal combustion engines. Gasoline is a complex mixture of paraffins, naphthenes, olefins and aromatics, and the components have different octane numbers. Normal paraffins have to lowest rating, whereas isomerised or more branched paraffins have higher octane numbers. The octane numbers of naphthenes are relative high, while aromatics have exceptionally high octane numbers. n-heptane, a paraffin that is particularly prone to knocking, has by definition octane number 0. One of the more highly branched hydrocarbons 2,2,4-trimethyl-pentane (iso-octane) is given the octane rating 100. The octane number of gasoline is then defined as volume % of iso-octane in blending with n-heptane that gives an equal strong knock as the gasoline under similar conditions.

In paper IV a more detailed description of catalytic reforming is given.

2.2. Catalytic reforming catalysts

2.2.1. The catalyst support

Alumina is the preferred support material for catalytic reforming catalysts, and the main types are the two transition aluminas γ-alumina and η-alumina. The preparation of these crystalline forms starts with precipitation from aqueous solutions containing Al^{3+} ions, which are aged at 20 - 80 °C, filtered, washed, and dried. The final operation in the preparation, where the Al_2O_3 passes through various states of hydration, consists of heating at temperatures up to 600°C. Fig. 2.1 shows how the various phases are formed from each other.

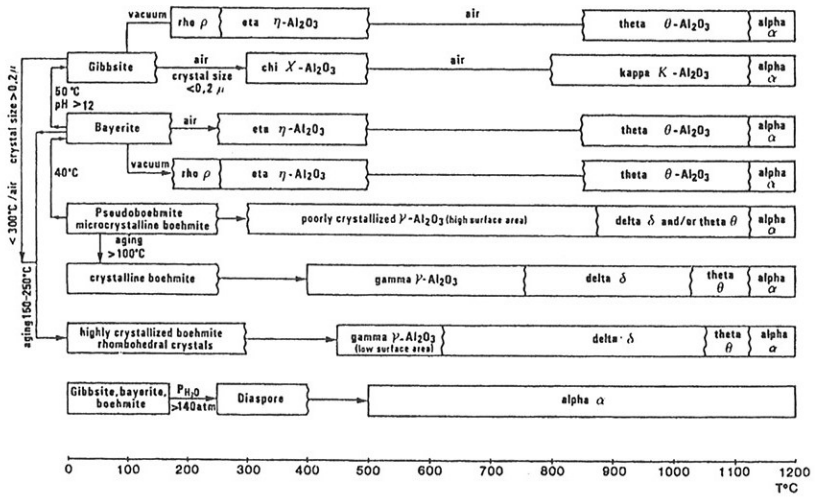

Fig 2.1. Schematic presentation of the formation of various Al_2O_3 hydrates [30].

γ-alumina and η-alumina are the important crystallites for reforming as they represent supports with high surface area and high thermal stability. Their surface acidity can be controlled, and depending on the degree of hydration

both Lewis and Brønstedt surface acidity is present. The origin of the Brønstedt acidity are OH^- groups attached to the tetrahedral Al^{3+} ions, and the acidity of these groups can be markedly enhanced by the proximity of Cl^- ions due to the electron affinity of the electronegative halogen atom. Thus it is possible to control the acidity of the alumina support with HCl or other chlorine compounds, which results in a replacement of OH^- groups with Cl^- ions leaving the remaining OH^- groups more acidic. Fig. 2.2 shows how the mechanism for the promotion of Brønstedt acidity is assumed to be [2]:

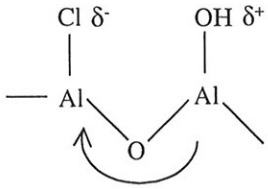

Fig. 2.2. Mechanism of acidity enhancement in alumina [2].

The most important reaction catalysed by the acidic alumina support is skeletal isomerisation of hydrocarbons. Approximately 1 wt% of chlorine is added to the support in order to optimise the catalyst for this reaction. A too high chlorine content will, however, lead to excessive unwanted hydrocracking.

2.2.2. The metal function

Because of both its high activity and its unique selectivity characteristics for dehydrogenation, platinum is the chosen catalyst for reforming. Ciapetta et al. [3] have compared the activities for dehydrogenation of benzene of various metal-oxide catalysts and other supported metals and the data are presented in Table 2.1.

Table 2.1. *Cyclohexane dehydrogenation activities of supported metal and metal oxide catalysts [3].*

Catalyst, wt%	Dehydrogenation activity (μmoles benzene/g catalyst s)
34% Cr_2O_3 cogelled with Al_2O_3	0.5
10% MoO_3 coprecipitated with Al_2O_3	3
5% Ni on Al_2O_3 or SiO_2-Al_2O_3	13
5% Co on Al_2O_3	13
0.5% Ir on Al_2O_3	190
1% Pd on Al_2O_3	200
5% Ni on SiO_2	320
1% Rh on Al_2O_3	890
0.5% Pt on Al_2O_3 or SiO_2-Al_2O_3	1400-4000

Differential flow reactor at 427°C, 6.8 atm, H_2/HC = 6 (mole ratio), activity determined after 30min on stream, pre-treated with H_2 at reaction conditions, LHSV varied to give differential operation

Both due to the costs of platinum and the importance of having the metal present in a highly dispersed form; 0.5 wt% Pt or less is used in commercial reforming catalysts. High dispersion ensures that as many metal sites as possible are exposed to the reactants in addition to providing very small metal clusters, which is desirable in order to obtain high selectivity for the desired reactions. The crystallites of reforming catalysts are usually as small as 10 Å or even smaller in diameter.

Crystallite size and structure sensitivity

Table 2.2 gives the fraction of total crystallite atoms that are surface atoms, the total number of atoms in the crystal, and the average coordination number of surface atoms for an octahedral crystallite of increasing size [31].

Table 2.2. *Properties of platinum crystals of different sizes with regular faces*

Length of crystal edge		Fractions of atoms on surface	Total number of atoms in the crystal	Average co-ordination number of surface atoms
Number of atoms	Å			
2	5.50	1	6	4.00
3	8.95	0.95	19	6.00
4	11.00	0.87	44	6.94
5	13.75	0.78	85	7.46
6	16.50	0.70	146	7.76
7	19.25	0.63	231	7.97
8	22.00	0.57	344	8.12
9	24.75	0.53	489	8.23
10	27.50	0.49	670	8.31
11	30.25	0.45	891	8.38
12	33.00	0.42	1156	8.44
13	35.75	0.39	1469	8.47
14	38.50	0.37	1834	8.53
15	41.25	0.35	2255	8.56
16	44.00	0.33	2736	8.59
17	46.75	0.31	3281	8.62
18	49.50	0.30	3894	8.64

In the size range 5.5 to 50 Å the average coordination number increases from 4 to 8.64, approaching a limit of 9. Corner atoms have a coordination number of 4, and edge atoms 6 or 7. Davis et al [32] have found that the atoms placed on the corners and terraces of platinum crystallites are more resistant to coking than the atoms situated at the faces. Barbier et al [33] have reported that the number of carbon atoms deposited per platinum atom surface site decreases

as the dispersion increases and various explanations for this structure sensitivity were discussed. The first was that the process of polymerisation of coke precursors to strongly adsorbed compounds demands large platinum crystal faces to occur. A second explanation was linked to the electron deficient nature of small platinum particles, thus that the catalytic properties of these atoms are different. If cyclopentadiene is the coke precursor leading to a non-desorbable compound, its dissociative adsorption will be more stabilised if the metal is more able to share its electrons and in that way increase the probability of adsorbed species to react with other unsaturated compounds to form coke. Thus a highly dispersed catalyst will be more resistant to deactivation by coke formation.

Generally reactions catalysed by Pt involving C-H bond breaking (hydrogenation/dehydrogenation) are structure insensitive. Boudard et al [34] have studied the hydrogenation of cyclopropane and found that the catalytic activity was independent of the metal dispersion (the reaction rate is proportional to the whole metal area). Poltorak et al [31] demonstrated that edges, faces and defects of the platinum surface had identical properties towards hydrogenation when studying various compounds. Somorjai at al [35] have reviewed studies of reactions on platinum single crystal catalysts and supported catalysts with respect to structure sensitivity. Here, it is explained that the formation of carbonaceous deposits may mask the catalyst surface and in this way making the reaction structure insensitive. The metal plays a secondary role providing atomic hydrogen to the molecule adsorbed on the carbonaceous layer.

Almost all reactions involving carbon-carbon bonds show structure sensitivity. This is due to the higher efficiency of the platinum atoms in kinks and steps for the breaking and formation of such bonds. Isomerisation of alkanes shows structure sensitivity depending on the number of carbon atoms in the molecule. This is due to two different mechanisms present. One mechanism involves an intramolecular carbon-carbon bond shift, whereas the other mechanism involves the formation of a cyclic intermediate. Light alkanes

containing fewer than five carbon atoms ($\leq C_4$), cannot form cyclic compounds and the only isomerisation mechanism possible is the structure sensitive reaction bond-shift mechanism. In the case of large alkanes the situation is more complicated as both the cyclic and bond shift mechanism may occur.

Table 2.3. *Dependence of several hydrocarbon reactions on the surface structure of supported and single-crystal Pt catalysts [35].*

Reaction	Single-crystal catalyst	Supported catalyst
	C-H bond formation and/or breaking	
Hydrogenation of olefins	Very little effect	Structure insensitive
Dehydrogenation of cyclohexane	Very little effect	Structure insensitive
	C-C bond formation and/or breaking	
Isomerisation of light alkanes ($\leq C_4$)	Strongly structure sensitive; rate enhanced by the presence of (100) sites; favoured by the presence of kinks and steps	Structure sensitive; activity increases with decrease in particle size
Isomerisation of large alkanes ($\geq C_6$)	Structure insensitive	Structure insensitive
Hydrogenolysis	Strongly enhanced by the presence of kinks; smaller effects in the presence of steps	Extremely structure sensitive; fivefold activity decrease with increase in particle size
Dehydrocylisation of n-haptane to toluene	Favoured by the presence of steps in (100) orientation, in the presence of kinks, formation of benzene (not toluene) favoured	Structure sensitive; activity increases with decrease in particle size

The cyclic mechanism is geometrically favoured on terraces and flat surfaces, and if both reactions are possible minimal structure sensitivity is expected. Table 2.3 gives an overview over the structure sensitivity of various

reactions of hydrocarbons on supported platinum catalysts and single crystal catalysts.

Impregnation

Platinum is usually impregnated on the catalyst support using a solution of chloroplatinic acid as the platinum precursor with the addition of hydrochloric acid as a competing agent. Platinum is rapidly fixed on the alumina surface, and the exchange equilibrium of Cl^- and $[PtCl_6]^{2-}$ occurs fast according to the equation [30]:

$$[PtCl_6]^{2-}{}_{Al} + 2Cl^-{}_{aq} = [PtCl_6]^{2-}{}_{aq} + 2Cl^-{}_{Al} \qquad (2.1)$$

The quantity of Cl^- ions added is usually adjusted to leave a sufficient amount of $[PtCl_6]^{2-}$ in the aqueous solution to ensure easy migration to the centre of the porous alumina particles. Various numbers of metal distribution profiles on the support surface between the periphery and grain centre may be obtained using different competitors, depending on their strength of their interaction with the support.

Drying and oxidation

Drying in air at 120°C eliminates most of the aqueous solution in the pores and modifies the adsorbed platinum complex. During oxidation (or calcination) the adsorbed $[PtCl_6]^{2-}$ ionic species are converted to mononuclear species of platinum whose complexation sphere contains oxygen and chloride ligands [36]. According to Lieske et al [37] these surface species have the general formula $[Pt^{IV}O_xCl_y]_s$ where the number of ligands x and y can vary. By oxidation (or calcination) at 500°C to 600°C, the chloride ligands are replaced by oxygen transforming the metal salt into a metal oxide.

Reduction

When the catalyst is reduced by hydrogen the platinum oxide is completely converted into zero-valent metal. The reduction step is typically conducted between 500°C to 550°C [30], and highly dispersed platinum is obtained. Several TPR studies involving the Pt/Al_2O_3 catalyst have shown that the catalyst, calcined in air at approximately 500 °C, is reduced at 250° to 300°C with an additional reduction near 450°C [21,22,24,27,28,37-39]. The reduction at 250°C to 300°C can be ascribed to the reduction of three dimensional PtO_2 species (Pt^{4+} to Pt^0), whereas the reduction at about 450°C can be attributed to the reduction of more stable two dimensional oxide species that interact strongly with the surface [40]. The Pt in this surface may be in the valence state 4+, 2+ or 0.

The variations in the reduction temperature of the different experiments performed may be due to different factors, but there seems to be a strong correlation with the calcination temperature. Low temperature calcination results in low temperature reduction of the platinum species [37]. The metal loading may also influence on the temperature of reduction. Chen et al [41] observed that the reduction temperature shifted from 435°C to 475°C when the platinum content decreased from 0.5 to 0.15 %. This indicates that the interaction of platinum is stronger when the content is lower.

Catalyst conditioning

The catalyst is often delivered in its oxidised form to the refinery, and the pre-treatment steps drying and reduction is then performed *in situ*. Drying is necessary in order to remove moisture adsorbed during transportation and storing of the catalyst as too much water may sinter the platinum particles.

2.2.3. Pt-Re catalysts

The first bimetallic catalyst was introduced by Chevron in 1969 [4] and was based on rhenium and platinum. This catalyst has become one of the most important industrial reforming catalysts due to the increased stability making it possible to run the reaction for longer periods without regeneration of the catalyst. Other bimetallic catalyst formulations are platinum-tin [42], platinum-iridium [43], and platinum-germanium [44]. The Pt-Sn catalyst is applied in modern continuous catalytic regeneration (CCR) units, and the major advantage of this catalyst is its increased selectivity to the desired products at low pressure.

2.2.3.1. Preparation

Impregnation

The impregnation of the metal on the surface is similar to the procedure employed when preparing the monometallic platinum catalyst. Rhenium precursors used are heptaoxide, perrhenates (especially NH_4ReO_4) and some halides ($ReCl_3$) [30]. Due to different affinities for the support, the platinum and rhenium precursors will not obtain similar distribution profiles. The metals are therefore often impregnated successively on the support in order to obtain the best Pt-Re interaction.

Drying and oxidation

After impregnation the catalyst is thermally treated in oxygen atmosphere (dried and calcined) to remove solvent from the support and to transform the precursors into oxidised species. Bulk rhenium precursors or oxides have a high volatility, but it decreases considerably by interaction with

the alumina support. Thermal treatment will also dehydrate the alumina and lead to a stronger interaction between Re_2O_7 and the support. Ammonium perrhenate, which according to Reyes et al [45] has the highest stability in oxygen, seems to be the best rhenium precursor.

The actual composition of oxidised rhenium formed upon drying and calcination (≈500°C) of the rhenium precursor NH_4ReO_4 has been discussed in several papers. Arnoldy et al [46] found that dried Re_2O_7 catalysts contained a mono-layer of a Re^{7+} surface phase as well as crystalline NH_4ReO_4. Calcination resulted in the formation of Re^{7+} surface face and Re_2O_7 clusters. Edreva-Kardjieva and Andreev [47] suggested the formation of a highly stable surface mesoperrhenate "$AlReO_5$" under oxidative conditions. Under ambient conditions the surface rhenium oxide resembles the ReO_4^- ion in an aqueous solution [48]. Upon dehydroxilation at elevated temperatures the surface compound interact with the oxide support by bridged oxygen to form stable surface Re^{7+} compound.

2.2.3.2. Reduction of Re supported on alumina

As stated previously, platinum is reduced to zero-valent metal during hydrogen reduction at temperatures typical for commercial reforming units. The reduction degree of rhenium at the same conditions has, however, been a matter of controversy. During oxidation most investigators assume that rhenium remains in the 7+ valence state [49,50].

By studying Re/Al_2O_3 by chemisorption and electron microscopy after reduction at 500-600 °C Freel [51] suggested that a 2-dimensional phase complexed with the alumina surface is formed. Using hydrogen consumption and XRD Johnson and LeRoy [50] finds that Re^{7+} is reduced to Re^{4+} both in monometallic and bimetallic samples. In a Pt-Re catalyst rhenium was supposed to exist as a lower oxide, probably ReO_2, distributed over the surface of alumina. However, these studies were conducted without continuous

removal of water formed during reduction, and Re^{4+} is thermodynamically favoured at these conditions [52]. Webb [53] conducted studies of the hydrogen consumption when reducing approximately 3.5 wt% Re supported on Al_2O_3 where the hydrogen was circulated over the catalyst. He found that the rhenium was completely reduced to zero-valent metal. However, the larger weight percent of rhenium means that the particles are larger and might be easier to reduce due to fewer interactions with the support. Yao and Shelef [49] discriminates between the reduction of the 2-dimensional dispersed phase and the 3-dimensional phase consisting of crystallites when examining the reduction degree of rhenium. A 1.2 wt% Re/Al_2O_3 was examined by chemisorption, ESR, and TPR, and the 3-dimensional phase was found to be easily reduced at 350 °C. Due to the strong interaction with the support, the dispersed phase can be reduced only at temperatures higher than 500 °C.

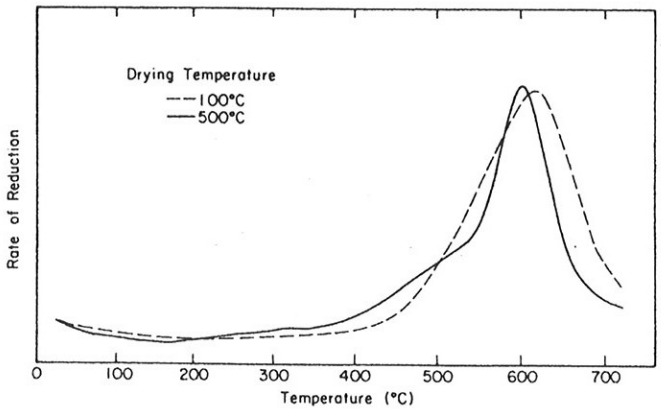

Fig. 2.3. TPR profile of 0.3 wt % Re/Al_2O_3 [24].

Isaacs and Petersen [24] have studied a 0.3 wt% Re/Al_2O_3 utilising TPR, and found that Re is reduced partly as a single peak at 600 °C (Fig. 2.3). Varying the drying temperature (and thus the degree of hydration) after calcination had no influence on the reduction temperature. However, an increase in the oxidation temperature will enhance the interaction with the support and increase the reduction temperature of rhenium. This is shown in Table 2.4, and

it is evident from these results that Re/Al_2O_3 will not be reduced under conditions employed during normal calcination and reduction of reforming catalysts.

Table 2.4. *Effect of Oxidation Temperature on TPR of Re/Al_2O_3.*

Catalyst	Oxidation temperature	Temperature corresponding to maximum reduction rate	Reference
0.2 wt% Re	525°C	550°C	[21]
0.7 wt% Re	525°C	525°C	[22]
1.2 wt% Re	500°C	550°C	[49]
0.4 wt% Re	500°C	560°C	[40]
1.2 wt% Re	300°C	360°C	[49]
0.7 wt% Re	300°C	360°C	[22]
0.4 wt% Re	100°C	275°C	[40]

2.2.3.3. Reduction of Re in the Pt-Re/Al_2O_3 catalyst system and alloy formation.

The above discussion of the oxidation state of Re is limited to studies of rhenium supported on alumina. Several reports show that rhenium is reduced at a lower temperature and more extensively when platinum is present. Broadbent et al [54] demonstrated, in a study of the hydrogenation activity of rhenium, that traces of PtO_2 catalysed the reduction of pure rhenium oxide Re_2O_3. Menon et al [55] showed by oxygen chemisorption that the dispersion and thus the reducibility of rhenium increased considerably in the presence of platinum. Hydrogen consumption studies of Pt-Re supported on alumina by Bolivar et al [56] demonstrated that platinum catalysed complete reduction of rhenium below 200°C. Due to the low melting point and high vapour pressure of Re_2O_3,

it was proposed that the component is able to migrate up to the surface of the metal particles via the gaseous phase or by surface migration on the Al_2O_3 support. Rhenium is then reduced by hydrogen activated by Pt.

Much of the studies of the Pt-Re system and focusing on the reduction degree and mechanism of Re reduction have mainly involved TPR as the experimental technique. To reveal the actual state of the metal particles chemisorption measurements and model compound reactions have also been employed, and more recent research has applied sophisticated physical characterisation techniques such as EXAFS, and TEM/STEM. Especially EXAFS has shown to be a powerful tool, as it can provide information about the interatomic distances and coordination numbers of the elements in the metal particles.

Characterisation with TPR and proposed reduction mechanisms

There has been conducted numerous TPR studies of the Pt-Re catalyst focusing on the catalytic effect of platinum on the reduction of rhenium. It has been demonstrated that the drying conditions prior to reduction have a profound effect on the TPR profile of the reduction of Pt-Re catalysts [22,24,27,38,40,57]. Simultaneous reduction of platinum and rhenium (one TPR peak) is observed when the catalyst is dried at ambient conditions ($\leq$ 250°C), whereas two or more TPR peaks are observed when the catalyst is pre-dried at higher temperatures (500°C).

Fig. 2.4 [24] shows the variation in the TPR profiles when drying the Pt-Re catalyst in argon at different temperatures. Mieville [38] found the same trends in the TPR profiles when drying the catalyst samples in air. The main origin for the different reduction behaviour of Re is ascribed to the different content of hydroxyl groups on the surface regulated by the drying temperature.

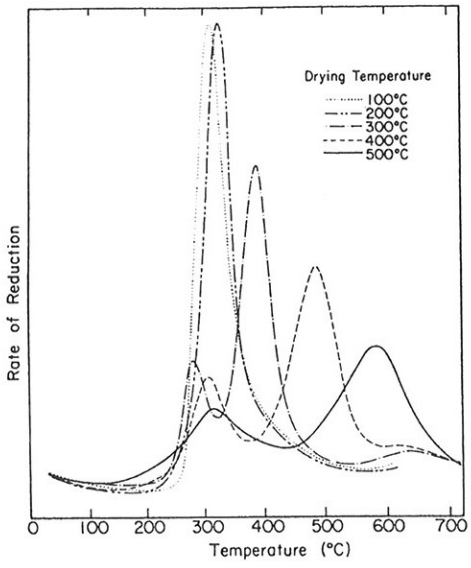

Fig. 2.4. TPR profiles of the 0.3-0.3 wt% Pt-Re/Al_2O_3 catalyst illustrating the effect of the drying temperature (Ar) on Re reduction [24].

Two mechanisms have been proposed to explain the effect of the hydration degree on the reduction of rhenium. As previously mentioned Bolivar et al [56] proposed a reduction mechanism where mobile Re_2O_7 surface species were involved. The increase in the reduction degree with increased degree of hydration was rationalised with the increased mobility of these species with increased surface concentration of hydroxyl groups. In this way rhenium comes in intimate contact with pre-reduced platinum atoms where hydrogen can be supplied for reduction. Bolivar et al [56] detected rhenium on the Pt/Al_2O_3 particles in physical mixtures of Pt/Al_2O_3 and Re/Al_2O_3 particles after reduction, whereas no platinum was found on the rhenium samples. However, these experiments have been conducted using low surface area α-alumina as supports. Studying Pt and Re supported on γ-Al_2O_3, which is the support applied in catalytic reforming, Bertolacini and Pellet [13] did not find any migration of Re to the Pt particles indicating that Re is more strongly

interacting with the γ-Al_2O_3 than the α-Al_2O_3 support. By studying a Pt-Re catalyst by TPR Wagstaff and Prins [22] suggested that platinum and rhenium are separated as oxides on the catalyst but during reduction reduced metal atoms (Pt) acts as nuclei for further reduction. Surface mobile species (Re_2O_3) migrate to these nuclei where they become reduced and alloyed. Thus, this mechanism is associated with the formation of bimetallic particles and intimate contact between the two metals. This mechanism has been supported by others [24,28,40]. As shown in Fig. 2.4, the reduction peak of Re is shifted to higher temperatures as the drying temperature is increased. It was thus concluded that the mobility of Re_2O_3 varies with the concentration of hydroxyl groups on the catalyst surface, and that all TPR peaks observed at temperatures observed for monometallic Re (<500°C) was attributed to Re reduction via the mechanism of Re oxide migration. This reduction mechanism is schematically shown in Fig. 2.5 [58].

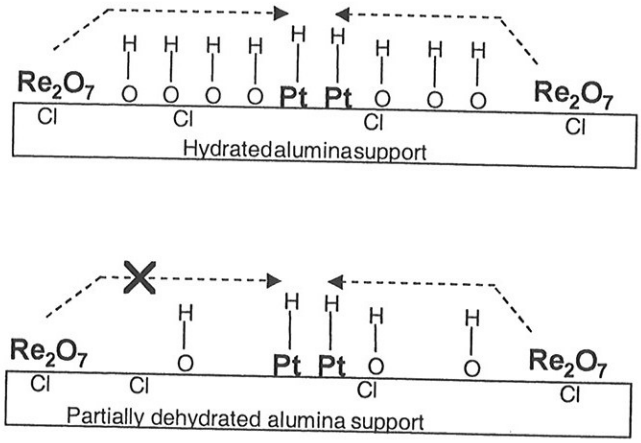

Fig. 2.5. Proposed mechanism for the Pt catalysed reduction of Re. The mobility of the Re oxides changes with catalyst hydration [58].

The other mechanism that has been proposed to explain the variation of reducibility with drying temperature involves diffusion of activated hydrogen

atoms to the Re oxides [38]. It is assumed that reduced platinum atoms on the Al_2O_3 support activates hydrogen which move to Re oxides sites via a spillover mechanism which is dependent on the degree of hydration of the alumina surface. Evidence for such a mechanism is that the TPR profiles of a catalyst upon reoxidation at 500 °C, after first have been oxidised at 300°C and reduced to give one TPR peak, displayed to separated peaks. It is assumed that it is not very likely that alloyed clusters would separate during oxidation to show this behaviour. It was also observed only a small temperature shift for the Re reduction when changing the Pt concentration from 0.35 to 0.01 wt%.

Model reaction studies

Reaction studies have been frequently used as a probe of alloy formation in the Pt-Re catalyst. Betizeau et al [59] reported the activity of benzene hydrogenation, benzene-deuterium exchange, cyclopentane and butane hydrogenolysis, and 1,1,3-trimethyl cyclohexane dehydrogenation as a function of the composition. The authors observed that the catalyst activity never changed linearly as a function of the percentage of Re as one would have expected if the catalysts were composed of Pt and Re crystallites without any interaction with each other. In the case of 1,2,3-trimethyl cyclohexane dehydrogenation the activity is always decreasing as the Re content increases and the specific activity of the bimetallic catalyst is always lower than the sum of the activities Pt and Re. The activity for benzene hydrogenation, cyclopentane hydrogenolysis, butane hydrogenolysis, and benzene-deuterium exchange has a maximum near 70% Re. This behaviour was explained as a combined effect of the monometallic activities and an electron interaction between the metals. The same investigators [23] later confirmed their findings for cyclopentane hydrogenolysis and showed that the activity was depending on the pre-treatment conditions of the catalyst. When the catalyst was directly reduced, and thus contained more moisture, more bimetallic particles were

formed and thus more rhenium was reduced leading to higher activity for hydrogenolysis.

Augustine and Sachtler [60] reported cyclopentane hydrogenolysis to be a highly ensemble specific reaction. The turnover frequency (TOF) for methane formation over Pt-Re was found to exceed that of the separate metals by a factor of 40. They therefore claimed that this reaction could be used to estimate the degree of alloy formation of supported bimetallic catalysts. The activity enhancement over bimetallic catalysts was explained by an intermediate heat of adsorption between pure Pt and Re. An ensemble consisting of only Pt atoms has a low heat of adsorption making C-C bond scission rate determining, while Re has a high heat of adsorption thus making product desorption the rate limiting step. From this, it follows that a mixed ensemble of Pt and Re atoms will have the highest activity. Fig. 2.6. shows the TOF for methane from the hydrogenolysis of cyclopentane as a function of the Pt-Re catalyst composition. The volcano shaped curve clearly demonstrates the beneficial effect of having mixed Pt-Re composition of the metal ensembles.

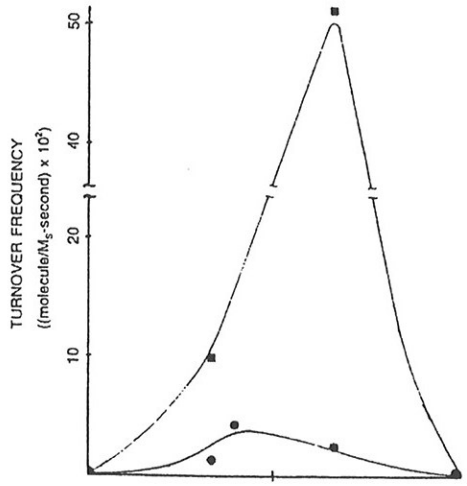

Fig. 2.6. Turnover frequency (TOF) for methane production from the hydrogenolysis of cyclopentane as a function of Pt-Re composition. Circles (●) and squares (■) represents drying temperatures at 100°C and 500°C respectively [25].

Augustine and Sachtler [25] demonstrated, using cyclopentane hydrogenolysis as the probe reaction, that the turnover frequency of methane and thus the degree of alloy formation was dependent on the drying temperature of the catalyst (Fig. 2.6). The beneficial effect of hydration prior to reduction using cyclopentane hydrogenolysis has later been demonstrated by Marecot et al [57]. Malet et al [27] employed n-butane hydrogenolysis to draw the same conclusion. Here, n-butane was used as a model component as coke deposition is not expected to occur. In contrast to Shum et al [61], which on the basis of experiments with n-hexane conversion suggested that there was a higher degree of alloy formation in the chlorinated catalysts, the authors further concluded that too much chlorine prior to reduction inhibited bimetallic formation. Pieck et al [62] supported the latter conclusion using hydrogenolysis of cylopentane and cyclohexane dehydrogenation. Later, they [63] investigated the effect of the preparation procedure on the degree of alloy formation employing hydrogenolysis of cylopentane. It was found that successive impregnation resulted in a higher degree of Pt – Re interaction than co-impregnation.

Characterisation by hydrogen chemisorption

Several authors have studied the Pt-Re catalyst by means of H_2 adsorption and H_2/O_2 titrations [18,23,51,55,64,65]. It is known that hydrogen is more strongly bond to Pt than Re, and that Re supported on alumina adsorbs negligible amounts of hydrogen at 25 °C [51]. Hydrogen chemisorption on the bimetallic catalyst is significantly less than on its mechanical mixture [51] indicating that Re modifies the adsorption characteristics of Pt. Isaacs and Petersen [66] explained the suppression of H_2 chemisorption by the reduction of number of pairs of Pt atoms necessary for the dissociative H_2 chemisorption. By studying the effect of the catalyst pre-treatment [64] they found that the amount of alloyed Pt-Re was independent of

the drying temperature in the range 100 to 500°C although the amount of unalloyed Re increased. In contrast Prestvik et al [28] demonstrated that the H/Pt ratio decreases as the drying temperature increases, indicating that the degree of alloying decreases. There is still, however, no consensus for the view that the H/Pt ratio is a mere measure of the alloy formation, and in a recent paper Fernández-Garcia et al [67] used hydrogen chemisorption to measure the number of exposed platinum atoms.

Characterisation by XAS

Short et al [68] examined the state of Re in reduced Pt-Re/Al_2O_3 catalyst by XAS and suggested that the Re is in the 4+ valence state after reduction at 480°C. Thus there is no alloy formation, and Re is present as a highly dispersed oxide. However, results obtained from TPR analysis indicate that it can not be expected to find Re reduced to zero-valent metal at conditions involving drying at 530°C and reduction at 480°C. The catalyst samples of Meitzner et al [69] were stored in containers after preparation and could therefore have adsorbed some moisture prior to reduction at 500 °C in the EXAFS apparatus. The analysis of the catalyst revealed that Re had an oxidation state of 0 and that Pt-Re bimetallic clusters were present after reduction. This conclusion was based on the intensity of the Re L_{III} edge as well as the EXAFS associated with the edge. Bimetallic clusters were also identified by Via et al [70]. EXAFS analysis revealed that both elements included atoms of both metals among their nearest neighbours. Hilbring et al [71] utilised XANES and TPR to follow the reduction of the individual metal components of a commercial 0.3-0.3 wt% Pt - Re/Al_2O_3 catalyst calcined at 180, 250, 400, and 580°C, respectively. Although they concluded that the white line intensity could not be used to determine the degree of reduction of Re and Pt, their analysis showed that Re is completely reducible if an extensive reduction treatment is performed on samples calcined at low temperature. Caballero et al [72] compared the effect of carbonaceous deposition on Pt/Al_2O_3 and Pt-Re/Al_2O_3 catalyst during n-heptane conversion

by investigating the metallic phase by EXAFS. The beneficial effect of Re was associated with the formation of an Pt-Re bimetallic phase which more efficiently removes carbonaceous residues deposited on the metallic phase. An oxidised rhenium phase partially incorporated within the subsurface layers of the alumina support was also detected. This phase can segregate to the surface to be reduced by the H_2 hydrocarbon mixture. Fung et al [73] prepared a Pt-Re/Al_2O_3 model catalyst from the $[Re_2Pt(CO)_{12}]$ precursor and examined it by EXAFS. On the basis of the data from the Re L_{III} and Pt L_{III} data, they proposed a structural model of the supported bimetallic species. Because the co-ordination numbers and distances are averaged, the structural model is simplified resulting in an average supported bimetallic cluster, which is represented as approximately Re_4Pt_2 (Fig. 2.7).

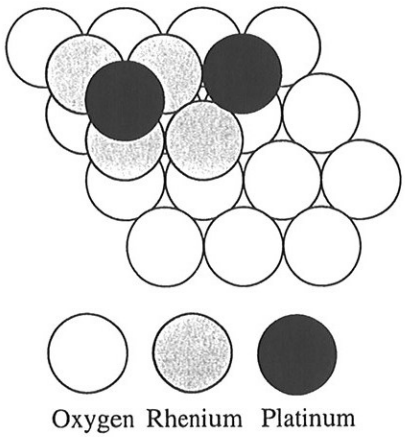

Fig. 2.7. Structural model of Re_4Pt_2 clusters on γ-Al_2O_3 based on the coordination parameters obtained from the Re L_{III} and Pt L_{III} edge EXAFS analysis [73].

The importance of a moderate drying pre-treatment was also stressed by Michel et al [26] employing combined XANES and TPR to study the reduction degree of Re. However, it was stated that an adjustment of the Cl content to 0.9-1.2 wt% was needed to maintain the bimetallic cluster formation as the concentration of water decreased. The authors claimed that mobile Pt oxychlorides and Re oxychlorides were responsible for the alloy formation at dry conditions. Fernandez-Garcia et al [67] have studied a 0.3-0.3 wt% Pt-Re/Al_2O_3 catalyst by XANES at different stages during oxychlorination/reduction cycles and revealed chemical characteristics of the Re intermediate and the alloyed phase. The authors proposed that a mobile Re specie with an oxidation state close to 1+ is responsible for the formation of an alloy phase during reduction. The XANES analysis shows that both metals do not interact significantly in the oxidised phase. They did not find, however, any evidence for the existence of Re oxychloride as proposed by Michel et al [26]. By observing the X-ray absorption of the close Pt L_{III} (11560 eV) and Re L_{II} (11957 eV) edges during reduction, and correlating this data to a detailed analysis of the EXAFS oscillations beyond the Pt edge, Bazin et al [74] was able to describe the bimetallic Pt-Re system. They observed that both Pt and Re were reduced, and for hydrated catalysts the reduction of the two oxides were simultaneous. Thus, it was concluded that hydrated Re_2O_7 mobile species are present migrating to the Pt reduction centres. At higher drying temperatures two distinct phases were formed, as the Re oxide was not longer able to migrate.

Characterisation by XPS

The valence state problem has been explored by XPS by studying the binding energy shift for the intense 4f shift. Biloen et al [19] characterised Pt-Re supported on SiO_2 by XPS and concluded that Pt-Re alloy was formed using the fact that the Pt_{4f} signal appears at a higher binding energy in PtRe/SiO_2 than in Pt/SiO_2 (Pt_{4f} signal is strongly overlapped by the Al 2p on

Al_2O_3 a supported catalysts). The proposed model of the working catalyst consisted of Pt-Re bimetallic particles where ReS_{ads} acted by dividing the surface into small ensembles (Similar to the model illustrated in Fig. 2.7)

XPS studies by Tysoe et al [75] of the oxidation and reduction of the Re-Pt system employing model systems indicated that Pt may catalyse the rhenium reduction step. The model system consists of rhenium either deposited onto or alloyed with a platinum metal film. Both these samples were oxidised to Re^{4+} and Re^{7+} after oxygen pre-treatment, although the process went faster on the alloy. In the case of the alloy, hydrogen treatment resulted in almost complete reduction, whereas the metal overlayer remained in a low oxidation state at a similar hydrogen exposure. It was therefore concluded that the degree of mixing between the platinum and rhenium affects the oxidation state of Re.

Onuferko et al [76] applied XPS and XAS to follow the *in situ* reduction of a Pt-Re/Al_2O_3 catalyst (0.9-0.9 wt%) and found that Pt^0 and Re^{4+} were the dominant species after reduction. However, others [77] have claimed that care must be taken when interpreting these results as the conclusion is mostly derived from the comparison of the L_{III} edge intensities of various Re species.

STEM/EDX

High spatial resolution STEM combined with EDX has been used by Kelley et al [78] to study reduced sulphided metal particles of 50 Å in size. Because of the absence of Re from groups of Pt-containing particles, it was concluded that no alloy formation had taken place. Huang et al [79] performed elemental analysis of particles of 2-3 nm in size calcined at 400°C and reduced at 400°C. No evidence of alloy formation was found, but the authors did, however, suggest that the platinum particles observed accounted for only a small amount of the total platinum in the catalyst, the majority of the platinum being TEM-unrecognisable. Rhenium was proposed to be present as a highly dispersed oxide. An extension of this work was done by Macleod et al [80], in which a variety of bimetallic reforming catalysts were analysed by employing

the combined TEM/EDX technique. Again it was concluded that the Re was present as a highly dispersed oxide after reduction, and the authors stated that the majority of the metal particles were too small to be analysed. Prestvik et al [29] conducted a study where the focus was put on the pre-treatment conditions. These authors claimed that they were able to analyse particles down to 5 Å, and found that rhenium was alloyed with platinum. The degree of Pt-Re interaction is highly dependent on the conditions employed during pre-treatment, and the highest degree of interaction is obtained if the catalyst contains sufficient amounts of moisture prior to catalyst reduction. The part of rhenium, which is not associated with platinum, was claimed to be present as submicroscopic particles. It was also suggested that only the smallest detectable particles were bimetallic.

Characterisation by IR

Peri [81] compared both industrial and laboratory monometallic and bimetallic catalysts by infrared studies of adsorbed NO and CO. No evidence for the formation of bimetallic particles was found as the metals together exhibited the same adsorptive properties as expected for the metals alone on an alumina support. In contrast, Bolivar at al [18] concluded that Pt and Re were alloyed when investigating a Pt-Re catalyst with a higher metal loading (2 wt%). The changes in the frequency of the Pt-CO and Re-CO bands against the percentage of Re was explained to be due to the electron transfer from Re to Pt. Due to the dilution of the Pt ensembles by Re, and thus less Pt-Pt neighbours, the optical density of bridged Pt_2CO decreased. In a later study [23] the same group confirmed their findings, and showed that the degree of alloy formation was highly dependent on the pre-treatment conditions. Anderson et al [82] found no influence of electronic effects on the metal atoms and hence the CO band position in a IR study of CO adsorption on the Pt-Re catalyst.

2.2.3.4 Role of rhenium and sulphur

Different theories have been proposed to explain the role of Re in modifying the catalytic performance of the Pt-Re system. Kluksdahl mentioned in the patent to Chevron [4] that the increased stability of the catalyst was due to the inhibiting effect of Re on the sintering of the metal particles. He related this to the formation of an alloy between Pt and Re with an increased melting point compared to Pt alone. Yermakov and Kuznetsov [12] claimed that the Re (ions bound to the support) was acting as an anchor for the Pt particles and thus impeding the migration of platinum over the support surface and the loss of active area.

Others have attributed the beneficial effect of Re as an active ingredient in the modification of the carbonaceous deposits formed during catalytic reforming. Coke formation is significantly reduced on bimetallic catalysts compared to Pt/Al_2O_3. However, it is not only the amount, but also the location [83] and nature [84] of the coke that leads to the better performance of bimetallic catalysts. The detailed mechanism of how Re participates in the reforming reactions has been controversial.

Bertolacini and Pellet [13] proposed, after obtaining data from physical mixtures, that Re was acting independently by converting coke precursors formed on Pt to harmless products. Similarly Margitfalvi et al [14] suggested that Re was hydrogenolysing potential coke precursors, whereas Burch and Michell [16] and Zhorov et al [15] found that the role of Re was to selectively hydrogenate dienes to alkenes, and thus avoiding the formation of coke precursors from this diene.

The most common view to explain the effect of Re on the catalytic properties of the Pt-Re catalyst is that Re is associated with Pt in bimetallic particles [59], and the interaction of such bimetallic particles or alloys with sulphur [19,20,26,85-88]. In the absence of sulphur, the mixed ensembles in the alloy are highly active in hydrogenolysis and the beneficial properties of $Pt-Re/Al_2O_3$ are observed only in the presence of adsorbed sulphur.

Biloen et al [19] proposed a model, shown schematically in Fig.2.8. where sulphur is chemisorbed on Re dividing the platinum surface into small (1-3 atoms) ensembles. Due to smaller ensembles the reorganisation of reversible coke to graphitic entities, the irreversible coke, will be inhibited.

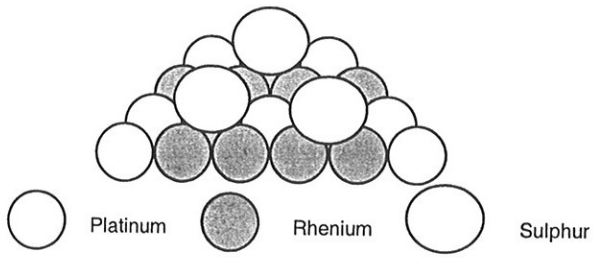

Fig. 2.8. A model for the active surface sites of Pt-Re/Al_2O_3.

In addition, the strongly chemisorbed sulphur will sterically hinder the formation of irreversible coke. In Table 2.5. the change in the nature and amount of the coke with the addition of Re and S is shown. The carbon deposition is reduced from 200 to 116 μmol/g cat, and the carbon species are much richer in hydrogen [86].

Table 2.5. *Carbon and hydrogen retained on the catalyst [86]*

Catalyst	Carbon retained (μmol/g cat)	Hydrogen retained (μmol/g cat)	H/C
Pt/Al_2O_3-Cl	342	126	0.37
PtRe/Al_2O_3-Cl	200	101	0.51
PtRe(S)/Al_2O_3-Cl	116	185	1.59

The hydrogen rich coke ("soft coke") probably only pose a mild hazard, if any, to catalyst activity.

Sulphur chemisorbed on the bimetallic surface will be bound preferentially to the Re atoms [19]. Michel [26] observed after sulphiding and hydrogen stripping that 10% of the Pt and all of the Re was covered with irreversibly adsorbed S. This has been attributed to the much lower electron affinity of Re [87], and that the Re-S bond is such that it increases the electron affinity of Pt. Thus electronic effects are responsible for the location of sulphur (adsorbed mainly on Re), whereas steric effects cause the modified reaction selectivity.

2.2.4. Platinum-tin catalysts

Tin increases the stability and the selectivity of the monometallic catalyst. In addition, it increases the resistance to agglomeration of the bimetallic crystallites during coke combustion. The Pt-Sn catalyst is preferred in CCR units due to better selectivity at low pressure and to the frequent regeneration and no need for pre-treatment with sulphur before use.

2.2.4.1 Preparation

Impregnation, drying, and oxidation

Tin precursors usually used industrially are chloro derivatives such as $SnCl_2$ and $SnCl_4$ [30]. Impregnation of Sn on the alumina support with the Sn precursor may either be the first step in the synthesis, or Pt is impregnated first. Pt and Sn may also be coimpregnated onto the support. Due to the high interaction with the alumina surface, high temperature treatment does not yield mobile Sn oxide species [30]. Therefore, the interaction between Pt and Sn has

to take place during the impregnation step if an intimate contact between the metals is desired.

2.2.4.2 *Reduction of Sn and alloy formation*

After reduction at temperatures higher than 400°C, it is generally accepted that Pt is in its metallic state. The oxidation state of Sn, however, is still a matter of discussion. It appears that the degree of reduction of Sn is highly dependent on the preparation procedure, metal precursors, Pt/Sn ratio, support, and pre-treatment procedures. Dautzenberg et al [89] concluded that Sn was present in the zero-valent state by studying Sn/Al_2O_3, Pt/Al_2O_3 and $PtSn/Al_2O_3$ by oxidation-reduction experiments and TPR experiments (Fig. 2.9.).

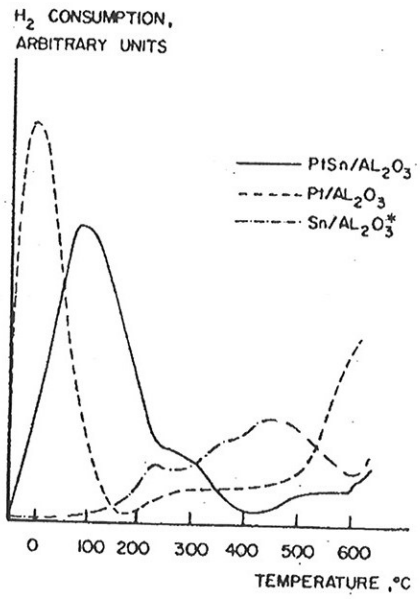

Fig. 2.9. TPR profiles of 0.4 – 0.4 wt% Pt-Sn/Al_2O_3, 0.4 wt% Pt/Al_2O_3, and 0.5 wt% Sn/Al_2O_3 after oxidation at 180°C [89]. The catalyst samples have been calcined at 500°C, and reduced at 500°C prior to oxidation and TPR analysis.

The TPR profile of the Pt-Sn catalyst differed considerably from what would be expected by superimposing the separate profiles for Pt/Al_2O_3 and Sn/Al_2O_3. A co-reduction at 100°C (one peak in the TPR profile) was observed after mild oxidation, and it was concluded that Pt and Sn are present as an alloy or bimetallic clusters in which Pt and Sn are in intimate contact with each other.

Burch [90] also states that Pt catalyses the reduction of Sn by studying $Pt\text{-}Sn/Al_2O_3$ with different wt% Sn by TPR after calcination at 500°C. However, the lowest oxidation state was found to be Sn(II) and no alloy formation was detected. Lieske and Völter [91] employed the same methods of characterisation, and concluded that a minor part of the Sn was reduced to Sn(0). This part was catalytic reduced by Pt and forms bimetallic particles or alloys with Pt. As the alloy formation is a result of the catalytic reduction by Pt, it was stated that the degree of alloy formation was dependent on the pre-treatment conditions. Contact between Pt and Sn is obtained during high temperature calcination by mobile Pt(IV) and/or Sn(IV) species. Reduction results in the formation of bimetallic clusters consisting of Pt(0) and Sn(0), surrounded by Sn(IV).

The state of the metals has also been investigated by Sn Mössbauer spectroscopy of the $Pt\text{-}Sn/Al_2O_3$ reforming catalyst enriched with ^{119}Sn [92-94]. Bacaud et al [93] found ionic species of Sn(IV) and Sn(II) together with Pt-Sn alloys. In addition, large amounts of unalloyed Pt were detected. Using the same technique another group [94] confirmed the complex nature of the Pt-Sn catalyst where Sn is present both in an alloy form and in oxidised forms. The only significant alloy phase present is Pt:Sn = 1:1. Kappenstein et al [95] investigated Pt-Sn interactions in the catalyst using two preparation techniques by Mössbauer spectroscopy in addition to other characterisation methods. It was found that the catalyst prepared from $[Pt(NH_3)_4][SnCl_6]$ contained more phases of Pt and Sn in intimate contact compared with the samples prepared by conventional coimpregnation of H_2PtCl_6 and $SnCl_4$.

Several XPS studies [96,97] reveal that Sn in the $PtSn/\gamma\text{-}Al_2O_3$ catalyst is primarily present as Sn(II) after reduction at 500°C and no substantial amount of Sn(0) was found. Alloy formation was observed when Pt and Sn supported on silica were reduced under the same conditions. Adkins et al [97] proposed a model where Sn is present as an eggshell of Sn aluminate surrounding the alumina support with the Pt(0) supported on the Sn aluminate. However, by investigating Pt-Sn catalysts prepared by special preparation procedures Li et al [98] found zero-valent Sn and the formation of bimetallic particles.

A number of investigations of the Pt-Sn catalyst using XANES and EXAFS have been performed. Meitzner et al [99] suggested that Sn primarily is present as Sn(II) after reduction. It was proposed that Pt is present as highly dispersed clusters on alumina that has Sn(II) present on the surface. It was also conducted comparative studies of the $PtSn/SiO_2$ system where Sn(0) was found to be present on the support in bimetallic clusters. It was thus concluded that the nature of the Pt-Sn system is highly dependent on the support employed. Young Xi-Li [100] conducted similar experiments reducing different Pt-Sn catalysts *in situ* and approached the same conclusions. The same authors [98] have obtained Sn in the zero-valent state using the solvated metal atom dispersion (SMAD) method to deposit the metal atoms on to the support. It was shown that Sn(0) within and on Pt particles had significant effect on the catalyst performance. El Abed et al [101] tried different preparation techniques in order to obtain higher interaction between Pt and Sn. EXAFS investigations showed that by employing the compound $[Pt(NH_3)_4][SnCl_6]$ as precursor Sn brought about a better distribution of Pt in this catalyst. During reduction the Pt clusters increases in size with Sn in the core. The following reduction of Sn leads to the formation of Pt-Sn alloys.

Arteaga et al [102] have performed CO chemisorption and FTIR analysis of the adsorbed CO on Pt-Sn catalysts of various metal loading during oxychlorination-reduction cycles. After reduction of chlorine free samples it was found that they consisted of reduced Pt crystallites with Sn(II) spread over

the alumina surface. The presence of Sn oxide on the catalyst surface inhibited the formation of oxychloro-Pt complexes, and thus increased dispersion of Pt during oxychlorination treatment.

2.2.4.3 Role of Sn

To explain the advantageous effect of Sn in the Pt-Sn system two different mechanisms have been proposed. Either is Pt modified by an "ensemble effect" where Sn decreases the number of contiguous Pt atoms, or Sn changes the electronic environment of the Pt atoms.

Dautzenberg et al [89] favoured for the formation of an alloy and that the beneficial effect of Sn is due to the "ensemble" effect. Bacaud et al [93] suggest that alloying accounts for the decrease in catalytic activity related to Pt. In addition it was also suggested that if part of the Pt was unalloyed, its activity would also be inhibited due to an electronic effect of Sn ions. Coq and Figueras [103] studied the conversion of methyl cyclopentane on the Pt-Sn system. It was observed that the addition of Sn had a stabilisation effect on the catalytic activity and resulted in a decrease of hydrogenolysis. Thus it was concluded that the main role of Sn is to dilute the Pt surface. Li et al [98] concluded that the Sn oxides improve the stability of the catalyst by blocking Pt particle sintering and that the presence of Pt-Sn bimetallic particles significantly depresses hydrogenolysis. Paál et al [104] rationalised the changes in activity and selectivity brought about by Sn in terms of geometric effects with Sn as a solid solution in Pt or as an alloy dilution of multiatomic Pt sites.

Burch [90] suggested that the special properties of Pt-Sn catalysts could not be due to a geometrical effect in which Sn divide the surface into small clusters of Pt atoms as little metallic Sn was found. The beneficial effect of Sn was attributed to the change in the electronic properties of small Pt crystallites and the modification of the acidic properties of the support [105]. As a result self-poisoning (poisoning that occurs when dehydrogenated hydrocarbons are

adsorbed very strongly on metal sites) is reduced and the selectivity for non-destructive reactions is increased. Sexton et al [96] support the conclusions made by Burch suggesting that Sn(II) is a surface modifier of γ-Al_2O_3 and that the reactivity changes are most likely due to the changes in the electronic interaction between Pt and Sn(II)-γ-Al_2O_3. Parera et al [17] stated that the alloying of Pt with Sn could result in an electron transfer from Pt to Sn, creating electron deficient Pt atoms, which influences markedly the adsorption-desorption steps of the catalytic reaction. It was also suggested that both electronic and geometric effects act together to yield the great decrease in hydrogenolysis.

The exact role of Sn in the Pt-Sn system is closely related to the chemical state of Sn in the system, and the diverging results from the literature may be due to different catalyst preparation, pre-treatment and experimental techniques applied.

2.2.5. Other bimetallic systems

After the successful introduction of the Pt-Re catalyst, a number of other combinations with Pt have been reported. Of these catalysts Pt-Ir/Al_2O_3 [43] appears to be the most widely studied and is used in commercial operation [106]. Another catalyst system that has been frequently studied is Pt-Ge. Germanium have the same characteristics as tin, but is substantially more expensive.

3. Experimental methods

3.1. Catalysts

3.1.1. Standard catalysts

Pt/Al_2O_3 (CK 303) and $PtRe/Al_2O_3$ (CK433) standard reforming catalysts, received from Akzo Chemie Nederland BV, have been employed in this study. These catalysts are referred to as EUROPT-3 and EUROPT-4, respectively, and they utilise the same γ-Al_2O_3 support called CK 300 (BET surface area of 188 m^2/g and a pore volume of 0.50 cm^3/g). The metal content of the monometallic catalyst is 0.3 percent by weight of platinum, whereas the bimetallic catalyst contains 0.3 wt% of both platinum and rhenium. As received the catalyst contains approximately 1.0 wt% Cl. Prior to use, the pre-calcined catalyst has been grounded and sieved to particles of 0.25 - 0.075 mm in size and stored in sealed bottles at ambient temperature. These bottles have again been placed in a sealed vessel containing a drying agent. By moisture measurement the water content was estimated to 5 wt%.

3.1.2. Catalyst preparation

In addition to the standard catalysts used in this work, some catalyst samples were prepared in the laboratory. In order to have comparative samples either CK 300 (γ-Al_2O_3) or CK 303 (0.3wt% Pt/γ-Al_2O_3) were employed as supports. All catalysts have been prepared by incipient wetness impregnation of the metals. The support was dried at 120 °C overnight prior to impregnation.

In order to obtain 0.9 wt% Pt/Al_2O_3 and 0.9-0.9 wt% $PtRe/Al_2O_3$ the alumina support was first impregnated with a controlled amount of $H_2PtCl_6 \cdot 6H_2O$ dissolved in 0.2 M HCl and dried at 120 °C overnight. After

calcination at 450 °C for 4 hours, part of the catalyst was impregnated with an aqueous solution of $(NH_4)ReO_4$ to yield 0.9 wt% Re. Finally the catalyst was again dried over night at 120 °C and subjected to calcination at 450 °C for 4 h.

0.3-0.3 wt% $PtSn/Al_2O_3$ catalysts were prepared by impregnation the 0.3 wt% Pt/Al_2O_3 catalyst (CK 303) with a certain amount of $SnCl_2 \cdot 2H_2O$ dissolved in 0.2 M HCl. The same procedure with drying over night at 120°C and calcination at 450 °C for 4 h was also applied for this catalyst.

Table 3.1. *Characteristic data for the standard catalysts from AKZO Chemie and the catalysts synthesised in this work.*

Catalyst	wt% Cl	wt% Pt	wt% Re	wt% Sn	S_a [m^2/g]
γ-Al_2O_3 (CK 300)	0.04	-	-	-	188
Pt/Al_2O_3 (CK 303)	1.00	0.296	-	-	183
$PtRe/Al_2O_3$ (CK 433)	0.95	0.296	0.311	-	187
$PtRe/Al_2O_3$	-	~ 0.9	~ 0.9	-	-
$PtSn/Al_2O_3$	0.65	0.296	-	~ 0.3	-

3.1.3. Catalyst pre-treatment

3.1.3.1 Oxychlorination

To adjust the chlorine level, the catalyst was subjected to an oxychlorination treatment. This was performed in a dedicated apparatus where chlorine was supplied to the catalyst by air saturated with hydrochloric acid. The tubes and fittings of the saturator flask and corresponding lines were made of Nylon in order to avoid corrosion problems. The flask, which was submerged in a water bath having a temperature of 15 °C, was filled with hydrochloric acid of different concentrations in order to tune the chlorine

content to the desired level. Approximately 1 g of catalyst was loaded in a tubular quartz reactor, which was situated in a Kanthal type furnace, and the flow of air was adjusted to 10 ml/min using a calibrated rotameter. A programmed Eurotherm 818 temperature controller connected to the thermocouple regulated the temperature. After heating the sample to 500°C with a heating rate of 1°C/min, and keeping it at this temperature for 3 days, the catalyst was treated in a flow of dry air at 510 °C for 1 h. Mr. Helge Semb at SINTEF Applied Chemistry measured the chlorine content of the samples by Escha dissolution of the sample and silver nitrate titration using chromate as indicator (Mohr method). The linear relationship between hydrochloric acid concentration and chlorine content at the conditions described is shown in Fig. 3.1.

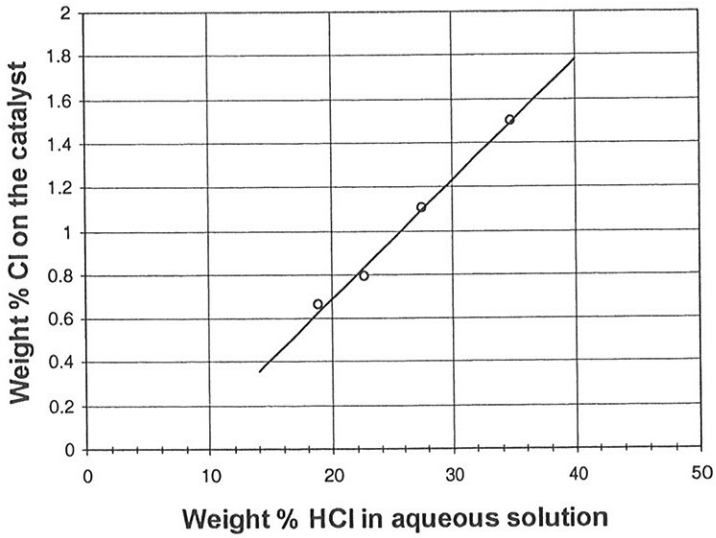

Fig. 3.1. Chlorine content of the catalyst support as a function of the wt% HCl when treated in air at 500°C for three days with air saturated with aqueous solution of HCl at 15°C.

3.1.3.2. Drying and reduction

The catalyst samples were slowly heated (0.8°C/min) in air or N_2 to various temperatures (240°C, 550°C, 680°C) and held at this temperature for 4 hours. The temperature was then lowered (10°C/min) to 200 °C and the sample was flushed with N_2 (30 ml/min) for 5 minutes prior to reduction. Reduction was performed in dry or moist (5000 ppm H_2O) hydrogen by heating the sample slowly (0.8°C/min) to 480°C and held at this temperature for 1 hour. Pre-treatment was usually done *in situ*, except for the samples investigated by STEM/EDX and XAS.

3.2. Pulse apparatus and model reactions

3.2.1. Experimental set-up

A major part of this work has been focused on constructing a pulse-reactor apparatus for activity and selectivity measurements. The basic idea was to pulse small amounts of feed over the catalyst bed in order to avoid rapid deactivation of the catalyst. In this way, initial activity values could be obtained. The outline of the experimental set-up is shown in Fig 3.2. The carrier gas (He) was flowing via the loop attached to the 6 port valve through the catalyst bed and to the GC column and FID detector. At certain intervals, the valve was switched directing the hydrocarbon/hydrogen feed mixture through the loop. By switching the valve back in position after 30 seconds, a small pulse of feed was introduced to the carrier gas leading it through the reactor. The resulting product mixture was directly analysed using a HP 5890 Series II gas chromatograph equipped with a flame ionisation detector (FID). The hydrocarbons were separated using a 50 m GS Alumina column (J&W Scientific).

Liquid hydrocarbon feed was dosed using a Bronkhorst Hi-Tech liquid flow controller (LFC). The feed was vaporised and mixed with hydrogen in an evaporator (a furnace equipped with a gas mixer). Heated lines kept the mixture in gas phase to the reactor and analysis section. By tuning the fine metering valve the pressure was kept slightly above atmospheric (1.75 bar abs.) in order to minimise the pressure difference between the carrier gas and the feed mixture.

Gas phase hydrocarbons (i.e. n-butane) were purified by an oxygen trap and a gas drier (4 Å molecular sieve) and the flow was tuned using a Bronchorst Hi-Tech mass flow controller (MFC) before it was mixed with hydrogen. Oxygen traps and gas dryers purified both hydrogen and nitrogen, whereas a gas drier purified the air. Bronkhorst Hi-Tech mass flow controllers (MFC) controlled the gas flows.

Depending on the kind of model reaction and thus the catalyst loading, fixed bed quartz reactors with two different bed sizes were used. As the $PtRe/Al_2O_3$ catalyst is highly active for dehydrogenation reaction, the reactor was designed for a smaller catalyst bed (Fig. 3.3a)). When performing hydrocarbon hydrogenolysis experiments, the reactor shown in Fig. 3.3b) allowing a higher catalyst loading was employed. Both reactors were 40 cm long and 6 mm in outer diameter. In order to ensure high quality analysis, the volume of the reactor and the tubing in the analysis section was minimised. The reactor was constructed using two connected quartz tubes of different inner diameter. Above the catalyst bed the inner diameter of the reactor tube was 3.0 mm. The lower part of the reactor consisted of a capillary quartz tube with an inner diameter of 0.6 mm. After catalyst loading, a thermocouple was placed close to the catalyst bed outside the reactor wall. A Kanthal type furnace provided heating of the reactor, and a programmable Eurotherm 818 temperature controller connected to the thermocouple regulated the temperature. The overall system is made of stainless steel. The tube dimension of the gas supply lines was 1/4", whereas all lines involving the carrier gas were made of 1/16" tubes in order to minimise the system volume.

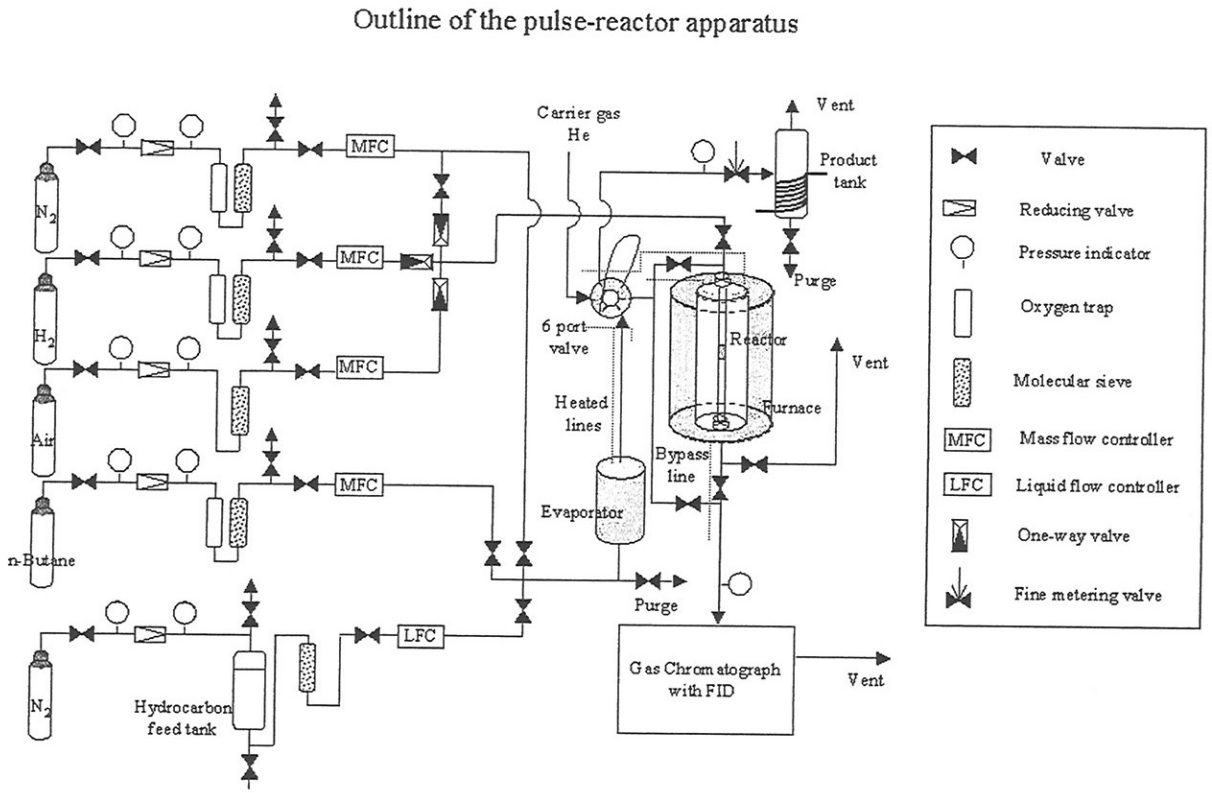

Fig. 3.2. Outline of the pulse apparatus employed for activity and selectivity measurements.

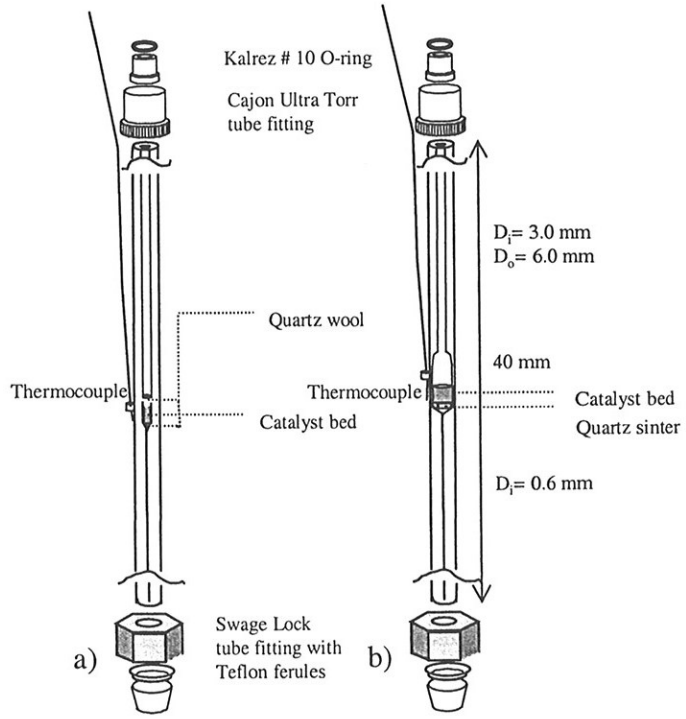

Fig. 3.3. The fixed bed quartz reactor used for a) hydrocarbon dehydrogenation studies and b) hydrocarbon hydrogenolysis studies.

3.2.2. Procedures

3.2.2.1. Methylcyclohexane dehydrogenation

The reaction conditions for methylcyclohexane (MCH) dehydrogenation are shown in Table 2.1. Quartz wool was used to support the bed where 10 mg of catalyst was loaded. Pre-treatment and reduction was done as previously described. After reduction at 480°C, the temperature was lowered to 270 °C. The carrier gas was switched from the bypass line to the reactor inlet, and the

H_2 flow was raised to 164 ml/min. When the pressure was stabilised, a MCH flow of 0.024 ml/min was introduced to the hydrogen at the inlet of the evaporator and the total pressure was set to 1.75 bar abs. After stabilising the hydrocarbon/hydrogen mixture the 6 port valve was automatic switched every 25 min, introducing a pulse of 0.74 ml to the catalyst. The experiment was terminated after 60 pulses.

Table 3.2. *Reaction conditions during methylcyclohexane dehydrogenation*

Temperature	270 °C
Pressure	1.75 bar abs.
Pulse	0.74 ml
Carrier Gas Flow (He)	250 ml/min
H_2/MCH	35 mol/mol
Catalyst loading	10 mg

3.2.2.2. Cyclopentane (CP) hydrogenolysis

Table 3.3 shows the reaction conditions employed during experiments involving cyclopentane hydrogenolysis. After heating and reduction of the catalyst, the temperature was set to 250 °C. The carrier gas (He) was then switched from the by-pass line to the reactor, while the H_2 flow was adjusted to 164 ml/min. When the pressure of the feed line was stabilised, 0.05 ml/min CP was mixed with the H_2 and the pressure was set to 1.75 bara. Every 40 minutes a pulse of 1.20 ml was introduced to the carrier gas, and the pulse sequence consisted of totally15 pulses.

Table 3.3. *Reaction conditions during cyclopentane hydrogenolysis*

Temperature	250 °C
Pressure	1.75 bar abs.
Pulse	1.20 ml
Carrier Gas Flow (He)	250 ml/min
H_2/CP	12 mol/mol
Catalyst loading	150 mg

3.2.2.3. n-butane hydrogenolysis

The reaction conditions given in Table 3.4 for n-butane hydrogenolysis were basically the same as for CP hydrogenolysis except for the H_2/hydrocarbon ratio. After switching of the carrier gas over the reactor, a flow of 164 ml/min of H_2 was adjusted. When the pressure of the feed stream had stabilised, a flow of 9.4 ml/min of n-butane was mixed with the H_2. The reaction mixture pressure was set to 1.75 bar abs., and after 30 minutes of stabilisation, it was pulsed (1.2 ml) over the catalyst bed (0.15 g) with regular intervals in the He flow (250 ml/min) at a reactor temperature of 250 °C.

Table 3.4. *Reaction conditions during n-butane hydrogenolysis*

Temperature	250 °C
Pressure	1.75 bara
Pulse	1.20 ml
Carrier Gas Flow (He)	250 ml/min
H_2/CP	17 mol/mol
Catalyst loading	150 mg

3.3. Temperature Programmed Reduction

3.3.1. Principles

Temperature Programmed Reduction (TPR) is a simple experimental technique that characterises heterogeneous catalysts by monitoring the consumption of hydrogen when submitting an oxidic catalyst precursor to a programmed temperature rise while a reducing gas mixture, usually hydrogen diluted in some inert gas, is passed over it. Since the gas flow is kept constant, the change in hydrogen concentration is proportional to the rate of reduction. Peaks appear when the reduction passes through a maximum.

The TPR profiles are interpreted by observing the peak maximum temperature, the number of peaks, and the hydrogen consumption. The chemical nature and the environment of the reducible species will determine the position of the peaks appearing in the TPR profile. Hydrogen consumption yields information about the extent of reduction.

Experimental parameters will also influence on the TPR profile, the most important being the heating rate and the gas flow rate. Increased heating rate generally results in sharper peaks shifted to higher temperatures, but with lower resolution [107]. An increase in the flow rate results in a lowering of the degree of conversion, thus increasing the concentration of the reactant, and the peaks are shifted to lower temperatures. Increasing the sample mass of the metal oxide leads to reduced resolution, which may give difficulties in separating two reduction processes. In too large catalyst beds temperature gradients may exist and cause bad resolution due to non-homogeneous reduction.

3.3.2. Apparatus

The experimental unit consists of a gas feed section with Alltech molsieves and oxytraps for gas purification and with Bronkhorst Hi-Tech mass flow controllers. 0.5 g catalyst was placed on a quartz sinter in a quartz glass sample holder. A cold trap was installed in order to remove water formed during reduction. The detection unit consisted of a TC detector in a Shimadzu GC-8A gas chromatograph connected to a Shimadzu C-R5A Chromatopac integrator. The heat source was an electrical Kanthal type furnace controlled by a Eurotherm 818P temperature controller. One thermocouple was placed in the sample holder immediately above the sample measuring the temperature of the incoming gas, whereas another thermocouple was placed outside the sample holder and used for furnace control.

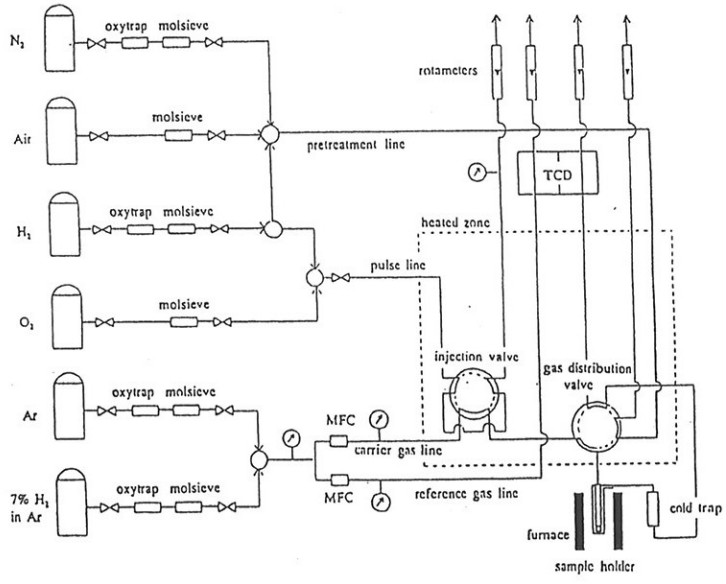

Fig. 3.4. Outline of the apparatus used for catalyst characterisation by TPR and pulse chemisorption [108].

3.3.3. Procedure

3.3.3.1. Variation of the drying temperature

The heating of the catalyst sample (0.5-1.0 g) was performed *in situ* as previously described. After heating for 4 hours, the temperature was lowered to 25°C and flushed with N_2 for 5 minutes. The TPR involved heating at a rate of 10 °C/min in a 7% H_2 in Ar mixture (30 ml/min) to 900 °C and held at this temperature for 20 minutes.

3.3.3.3.2 Variation of the chlorine content

The chlorine content of the catalyst samples was adjusted *ex situ* as previously described. After being placed in the sample holder the sample was heated slowly at 0.8°C/min, and dried at 510°C for 4 h. The TPR procedure was performed as previously described.

3.4. Hydrogen chemisorption

3.4.1. Volumetric chemisorption

3.4.1.1. Principle

Volumetric chemisorption of hydrogen is a technique where the amount of hydrogen adsorbed is measured at increasing pressures while the catalyst sample is maintained at a constant temperature. A Langmuir-type adsorption isotherm is obtained and the linear part of the isotherm is extrapolated to zero pressure. The intercept with the ordinate is taken as the gas required to form a

monolayer on the surface. After evacuation, a second isotherm may be obtained which only measures the physisorbed amount of hydrogen. By subtracting the second isotherm from the first, the chemisorbed amount of gas can be calculated.

3.4.1.2. Apparatus and procedure

Volumetric hydrogen chemisorption was measured at 25°C using a Micromeretics ASAP 2010 Chemi instrument. The samples were heated, reduced, and analysed in the chemisorption apparatus. Oxychlorination treatment was performed *ex situ*. The dispersion, or hydrogen to platinum ratio (H/Pt), is calculated based on the volume of hydrogen chemisorbed on the sample. The volume adsorbed was obtained by making two subsequent isotherms with evacuation to 10^{-5} torr for 30 minutes in between. The values reported were obtained by subtracting the second isotherm from the first isotherm. It is assumed that the adsorption stoichiometry for H_2 on Pt is H/Pt =1, and that Re does not chemisorb H_2 at 25°C [51,66]. Approximately 1.0 g of catalyst was used in each experiment.

3.4.2. Pulse chemisorption

3.4.2.1. Principle

Small gas pulses of hydrogen are sent into a carrier gas flow from a pulse valve and passes a reduced catalyst. A thermal conductivity detector monitors the composition of the gas exiting the sample and the pulsing is continued until the hydrogen peaks on the chromatogram are identical. Knowing the pulse volume, pulse pressure, pulse temperature and the number

of pulses adsorbed, the amount of gas chemisorbed and thus the dispersion can be calculated.

3.4.2.2. Apparatus and procedure

Pulse chemisorption experiments were performed in the same apparatus as the TPR experiments (Fig. 3.4), and the same sample holder was used. An adsorbate loop (50μl) for pulse injections was connected to the carrier gas stream before the sample holder. The samples were either slowly (0.8 °C/min) heated to 500 °C and held at this temperature for 4 h or not heated prior to reduction, and the reduction was varied according to the descriptions in Appendix 1. If the sample was heated, it was flushed with N_2 for 5 minutes at ambient temperature before reduction was performed.

3.5. STEM/EDX particle analysis

3.5.1. Principles

Analytical Electron Microscopy (AEM) is used to detect small amounts of an element in a sample at high resolution. The instrumentation consists of a Transmission Electron Microscope (TEM) or a Scanning Transmission Electron Microscope (STEM) interfaced to energy-dispersive X-ray spectrometer (EDS) systems. AEMs which employ field-emission guns (FEGs) provide small electron probes with high currents capable of generating high X-ray fluxes in thin specimens. X-ray detectors collect the emitted X-ray flux, and a detection of small amounts of elements even at sub-10 nm resolution is possible. The principle of the instrumentation is shown in Fig.3.5.

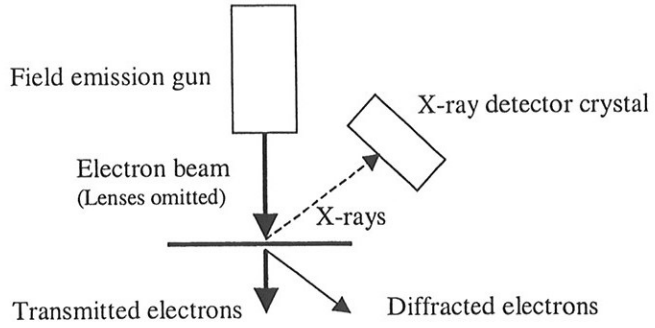

Fig. 3.5. Schematic diagram showing the interaction of the primary electron beam and the sample in the electron microscope.

3.5.2. Instrument and procedure

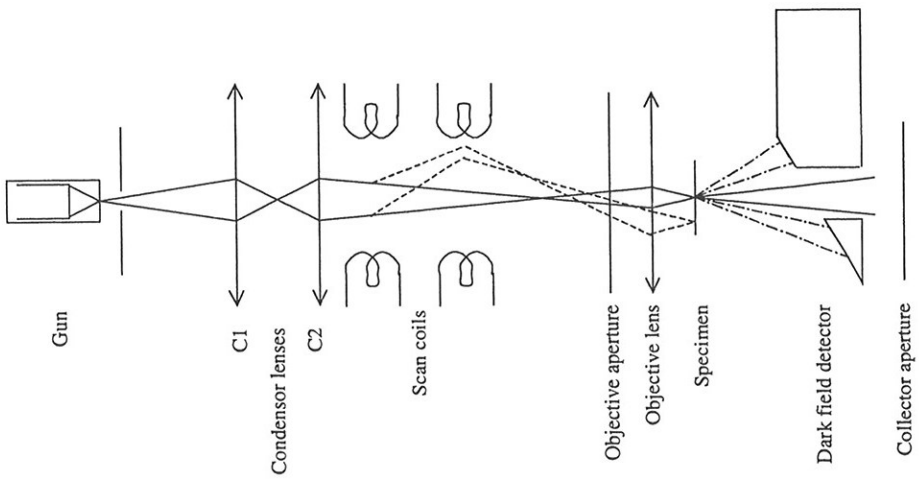

Fig. 3.6. Ray diagram for bright and annular dark field imaging.

Combined STEM/EDX particle analysis was performed at Lehigh University by Professor Charles E. Lyman and Associate Professor Bård

Tøtdal, Department of Physics, NTNU. The instrument was a Vacuum Generators Microscopes HB-603 field-emission dedicated STEM equipped with a windowless Si(Li) detector (Oxford Instruments EDS X-ray detector) and was operated at 300 kV. Fig. 3.6 shows the ray diagram of the instrument for bright-field and annular dark-field imaging.

The detailed analysis procedure which is being referred to here has been described previously [29] The samples, which were pre-treated *ex situ*, were crushed in a mortar and the powder was dispersed dry onto a Ti grid coated with a holey carbon film. In order to minimise hydrocarbon contamination the specimens were kept in the microscope overnight before being investigated. Images were obtained in STEM mode with the annular dark-field detector, generally at a magnification of 2Mx-5Mx. The size of the particles was assessed by measuring with a ruler on the screen. EDX signals of the particles were obtained by focusing the electron beam on the particles and accumulating the spectra. Every 10 s the EDX accumulation was stopped and the microscope returned to imaging mode in order to keep track of the particle position. When it was no longer possible to detect a clear increase of the Pt or Re peaks, the EDX counting was stopped and the spectrum stored. The spectra were later processed with the SIMPLEX procedure of the DTSA spectrum analysis program of National Institute of Standards and Technology (NIST). The number of counts in the ReLα and PtLα peaks were then used as net intensities I_X in the formula:

$$\frac{C_{Pt}}{C_{\mathrm{Re}}} = k_{Pt,\mathrm{Re}} \frac{I_{Pt}}{I_{\mathrm{Re}}} \qquad (3.1)$$

where C is the mass fraction and k is the sensitivity factor. It is assumed that the particles consisted of Pt and Re only giving:

$$C_{Pt} = \frac{k \cdot I_{Pt}}{I_{\mathrm{Re}} + k \cdot I_{Pt}} \qquad (3.2)$$

In the absence of a suitable Pt-Re standard, the *k*-factor was calculated as k=1.05 for analysis at 300 kV and at an X-ray take-off angle of 20°.

3.6. EXAFS/XANES spectroscopy

3.6.1. Principles

XAS is based on the absorption of X-rays and the creation of photoelectrons that are scattered by nearby atoms in the lattice. Interference effects due to this scattering result in a fine structure in the absorption edge spectrum. The fine structures of the absorption edge is designated XANES (X-ray absorption near edge structure) and EXAFS (Extended X-ray absorption fine structure). XANES contains information about the electronic structure and the geometric structure of the absorbing atom, whereas the information yielded from EXAFS reveals interatomic distances, co-ordination numbers, and degrees of order and disorder. The analysis is performed at synchrotrons where tuneable sources of X-rays are accessible.

3.6.2. Instrument and procedure

The samples for XAS analysis were heated and reduced in a quartz sample holder similar to the one used for TPR experiments, and the same instrumentation and pre-treatment gases were used. In order to transport the catalyst sample without exposing it to the atmosphere, the sample holder was equipped with small capillary quartz tubes. When the pre-treatment and reduction was finished, the catalyst sample was flushed with He and the catalyst particles were transferred to the capillary tubes. The glassblower then sealed these tubes before transport to the synchrotron radiation facility.

XAS data were collected by doctoral student Magnus Rønning, Department of Chemical Engineering, and Professor David G. Nicholson, Department of Chemistry, at the Swiss-Norwegian Beamline (SNBL) at the

ESRF, France and at Beamline X11-A at the National Synchrotron Light Source, NSLS, Brookhaven National Laboratory, USA. At SNBL, spectra were recorded in the fluorescence mode at both the Pt L_{III} edge (11 564 eV) and the Re L_{III} edge (10 535 eV). A channel-cut Si(111) monochromator was used to scan the X-ray spectra. The beam currents ranged from 130 - 200 mA at 6.0 GeV. Higher-order harmonics were rejected by means of a chromium-coated mirror. At NSLS, the station was equipped with a double crystal Si(111) monochromator and the storage ring operated at 2.5 GeV, with a ring current of 180-350 mA. Higher order harmonics were suppressed by tuning the monochromator crystals to 50% of maximum intensity.

Magnus Rønning performed data analysis and parameter refinement. A description of the procedure is given in Paper II. The mathematical expression for the EXAFS signal employed is given by Stern [109]. A more comprehensive treatment of the data reduction procedure and data analysis is given elsewhere [110].

4. Results and discussion

The first part of this chapter deals with the influence of the pre-treatment conditions on the formation of bimetallic particles in the $PtRe/Al_2O_3$ catalyst system. The second part focuses on the influence of the chlorine content prior to reduction, whereas the studies of another reforming catalyst system are introduced in the third part.

All the activity tests have been performed using the specially designed pulse apparatus described in Chapter 3.2. The objective was to avoid fast initial deactivation of the catalyst and thus obtain data from the catalyst as fresh as possible.

4.1. The effect of the pre-treatment conditions on the $PtRe/Al_2O_3$ catalyst

The $PtRe/Al_2O_3$ catalyst investigated has been pre-calcined at the manufacturer, but has adsorbed some moisture even during storage in sealed bottles. The average content of adsorbed water on the catalyst is approximately 5 wt% (Defined here as the water desorbing from the catalyst during vacuum treatment at 150°C). Prior to reduction the catalyst is dried in air in order to reduce the moisture level. As previously discussed the content of water prior to reduction influences the final state of the catalyst after reduction, and one of the objectives of this work was to further investigate the alloy formation of the Pt-Re catalyst as a function of the drying temperature.

In addition the effect of varying the conditions during reduction was also studied. The purpose of this study is to investigate whether the variations of the partial pressure of water formed during reduction have any influence on the formation of bimetallic particles.

4.1.1. The effect of water

4.1.1.1. Hydrogenolysis of n-butane and cyclopentane

Hydrogenolysis of certain hydrocarbons can be taken as an indirect measure of the degree of bimetallic formation. Assuming that the active sites consist of small bimetallic particles, a higher rate of methane production has been explained by the synergetic effect of Pt and Re metal atoms in intimate contact [60]. Hydrocarbons adsorb strongly on Re, but weaker on Pt. In such bimetallic clusters an intermediate heat of adsorption will result in a higher rate of reaction and methane formation. Reaction on the acid support such as cracking will also occur but the hydrogenolysis reaction resulting in the formation of methane is catalysed by the metal sites.

Two different hydrogenolysis reactions were employed in order to investigate the metal function. Hydrogenolysis of n-butane was chosen as a probe reaction both because this light hydrocarbon is well suited for pulse apparatus experiments and because little coke formation is expected. In this study, where a pulse reactor is used, it is very important to produce pulses of equal composition in order to obtain reproducible results. Efforts were therefore also made to ensure homogeneous mixing of the vaporised liquid and incoming gas when performing hydrogenolysis of cyclopentane. Others have successfully employed this test reaction in continuos mode for investigations of the alloy formation in $PtRe/Al_2O_3$ catalyst [60,62]. However, more coke formation and thus more rapid deactivation of the catalyst is expected here.

The conversion of n-butane over $PtRe/Al_2O_3$ catalyst samples dried at 240°C and 550°C are plotted in Fig. 4.1 and the selectivity to methane is displayed in Fig. 4.2.

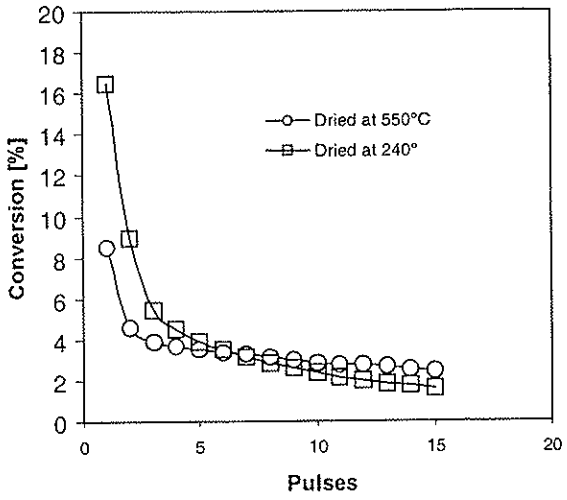

Fig. 4.1 Effect of drying temperature on n-butane conversion over $PtRe/Al_2O_3$ catalyst. Reaction conditions: 250°C, 1.75 bar abs., pulse 1.20ml, H_2/CP=12, and carrier gas flow 250ml/min

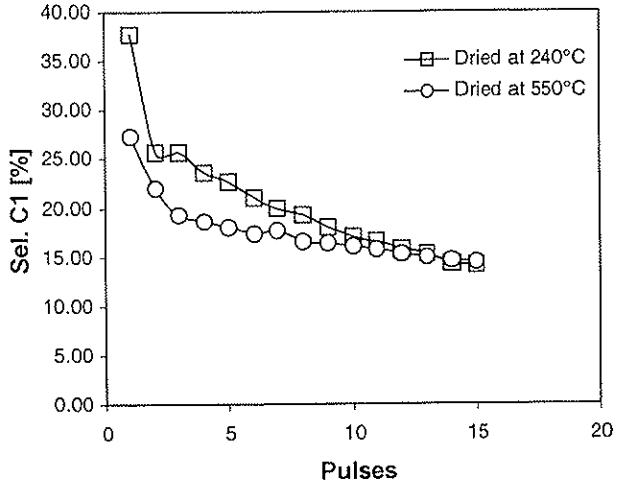

Fig. 4.2 Effect of drying temperature on the selectivity to methane in n-butane conversion over $PtRe/Al_2O_3$ catalyst. Reaction conditions: 250°C, 1.75 bar abs., pulse 1.20ml, H_2/CP=12, and carrier gas flow 250ml/min

The sample dried at 240°C prior to reduction clearly displays the highest initial conversion of n-butane and the highest selectivity to methane. This is taken as an indication of a higher degree of bimetallic formation on the sample being most hydrated prior to reduction. Such findings are consistent with a reduction mechanism that involves mobile Re oxide species on hydrated alumina [22]. These species are able to migrate to Pt particles where they are reduced forming an alloy with Pt.

The fast decrease in hydrogenolysis activity of the catalysts means that there must be some deactivation due to coke formation during the short traverse of the pulse through the catalyst bed. However, the conversion of the first pulse is still taken as a measure of the initial activity of the catalyst revealing information about the state of the metal particles. The initial activities of the various samples that are reported in paper I and III are averages of several experiments using the values of the first pulse. Fig. 4.2 shows that the selectivity to methane is highest for the sample dried at 240°C, which is obvious as long as the hydrogenolysis activity is also highest and it is assumed that this is the main reaction occurring.

Figures 4.3 and 4.4 show the results from the conversion of cyclopentane. The samples have either been heated in air at 240 °C, and 550 °C, or not dried at all. It can be observed that the catalyst samples display differences in catalytic performance. Similar to the n-butane experiments the sample treated at 240°C clearly shows the highest conversion of cyclopentane and the highest selectivity to methane. This is an indication that moderate treatment in air yields most bimetallic particles. If the catalyst is reduced without any pre-treatment it shows a very low conversion of cyclopentane and low selectivity to methane compared to the other samples. The positive effect of water therefore seems to be limited to a certain hydration degree controlled by treatment in air at elevated temperatures. If the catalyst is heated to 550°C the catalyst is much less active in the hydrogenolysis reaction than the catalyst

heated to 240°C, showing that removal of too much moisture reduces alloy formation and thus hydrogenolysis activity.

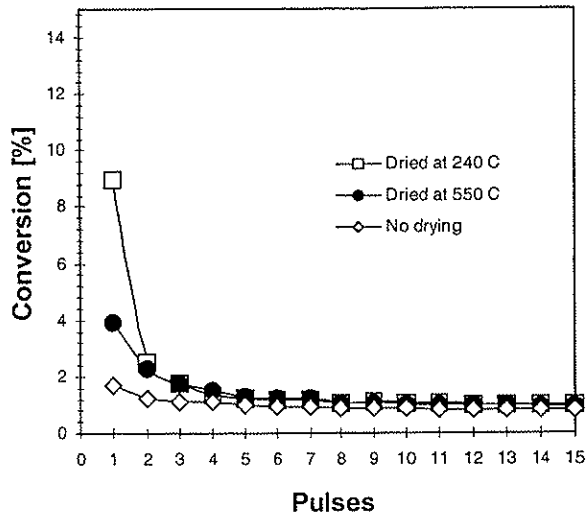

Fig. 4.3 Effect of drying temperature on cyclopentane conversion over $PtRe/Al_2O_3$ catalyst. Reaction conditions: 250°C, 1.75 bar abs., pulse 1.20ml, H_2/CP=17, and carrier gas flow 250ml/min

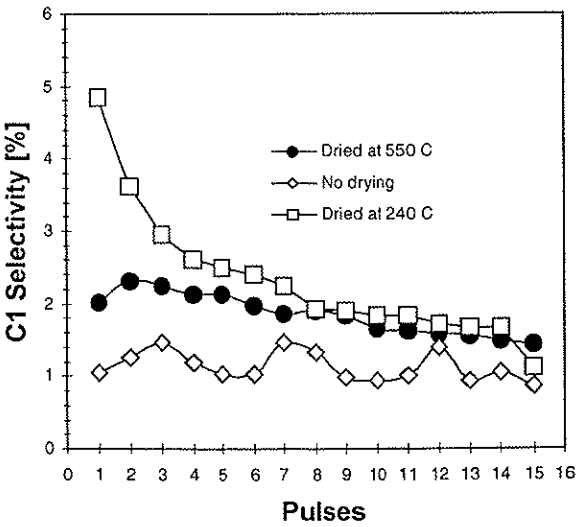

Fig. 4.4 Effect of drying temperature on the selectivity to methane in cyclopentane conversion over $PtRe/Al_2O_3$ catalyst. Reaction conditions: 250°C, 1.75bar abs., pulse 1.20ml, H_2/CP=12, and carrier gas flow 250ml/min

4.1.1.2. Dehydrogenation of methylcyclohexane

Dehydrogenation of methylcyclohexane has been reported to be a structure insensitive reaction not influenced by Re [111]. Dehydrogenation of cyclohexane uses only the metallic function of the bifunctional catalyst [112], and the activity for dehydrogenation is therefore a measure of the dispersion of Pt on the catalyst. Although is has been shown that the dehydrogenation of methylcyclohexane is Pt particle size dependent, the reaction is regarded insensitive over highly dispersed systems such as $PtRe/Al_2O_3$ as the particle size is smaller than 20 Å [113].

Compared to hydrogenolysis that involves C-C bond scission, dehydrogenation occurs much more readily on supported Pt. In order to avoid equilibrium conditions a small amount of catalyst was used and the H_2 to MCH ratio was kept high. The first run was performed with a catalyst not heated prior to reduction yielding about 28 % initial conversion. This was well below equilibrium conversion that was calculated to be 73 % (Appendix 2) Tests with various particle sizes were performed in order to find any possible internal diffusion limitations present. As shown in appendix 3 no such limitations were found under the conditions employed in these studies. Thus it is assumed that the variations in dehydrogenation activity reflect the Pt dispersion of the catalyst.

The results obtained from the methyl cyclohexane dehydrogenation are shown in Fig. 4.5. By pulsing small amounts of feed over a catalyst preheated at 240°C and 550°C prior to reduction no trends where found with regard to the dehydrogenation activity. However, the activity was surprisingly low for the catalyst not heated prior to reduction. Comparing the results from what was found from the hydrogenolysis of cyclopentane, this sample displays particular low activity for both model reactions. There might be different explanations for this low activity. As the dehydrogenation reaction is a measure of the catalyst dispersion, the lower dehydrogenation activity might be due to the sintering effect of water on the Pt particles. Too much water present might also suppress

the reduction of the metals, particularly Re. As this catalyst show low hydrogenolysis activity, too much water could result in less reduced Re and thus less formation of bimetallic particles. Pre-treating the catalyst samples at 240°C and 550°C results in much higher dehydrogenation activity (approximately 50% conversion). As both samples show the same dehydrogenation activity, it is an indication that the Pt dispersion is the same. This is as expected, and the different activity with regard to hydrogenolysis can be explained with different degrees of alloy formation due to different degrees of hydration.

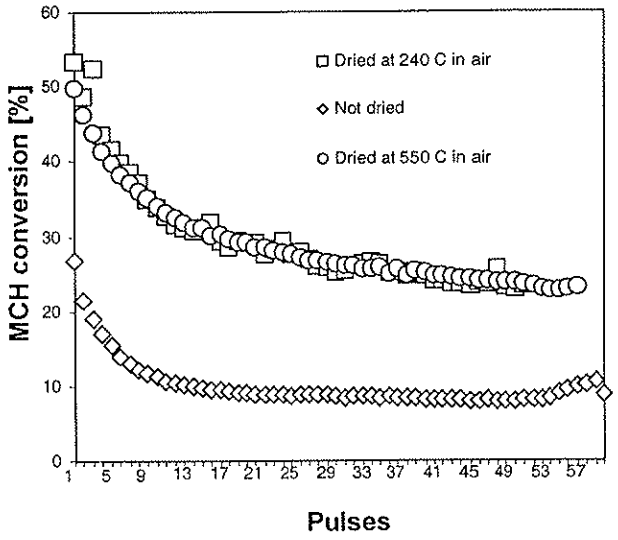

Fig. 4.5. Effect of drying temperature on the conversion of methylcyclohexane (MCH) over $PtRe/Al_2O_3$ catalyst. Reaction conditions: 270°C, 1.75 bar abs., pulse 0.74ml, H_2/MCH=35, and carrier gas flow 250ml/min.

4.1.1.3. Volumetric chemisorption of hydrogen on Pt-Re/Al_2O_3

There are numerous of investigations showing that Re does not chemisorb H_2 at room temperature [18,51,65,66]. It is therefore assumed when performing H_2 chemisorption on $PtRe/Al_2O_3$, that the H_2 adsorption only reflects the uptake by Pt particles. It has also been demonstrated that the H_2 chemisorption capacity is much lower for $PtRe/Al_2O_3$ compared to that of Pt/Al_2O_3 [51,66]. It is suggested that this is due to the formation of alloys and that such alloys contain fewer contiguous Pt atoms than a pure Pt crystalline. Since Pt chemisorbs H_2 dissociatively and Re does not chemisorb H_2, this means that the number of Pt pairs required for dissociative chemisorption is reduced when Re is alloyed with Pt.

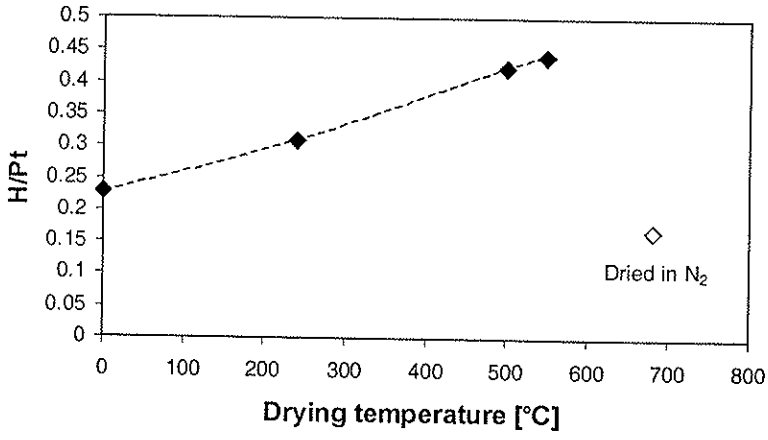

Fig. 4.6. Effect of drying temperature on the H_2 chemisorption on $PtRe/Al_2O_3$ catalyst. The samples have been dried in air if nothing else is stated.

Fig. 4.6 shows the H_2 uptakes (H/Pt) on the $PtRe/Al_2O_3$ catalyst as a function of the drying temperature. No drying gives a H/Pt value of 0.23 whereas drying in air at 240°C gives a value of 0.31. The increase in the H/Pt ratio can be interpreted in two ways. Either the dispersion increases, or the degree of alloying decreases. Based on the results from the model reaction studies, it seems that an increase in the H/Pt ratio is due to a larger Pt dispersion when dried at 240°C prior to reduction. The dehydrogenation activity is much lower for the sample not dried, indicating lower dispersion. In addition, the hydrogenolysis activity is low, reflecting less bimetallic particle formation. The latter result should have resulted in a higher H_2 uptake than the dried samples if the dispersion was equal. It is therefore suggested that the sample not dried prior to reduction have both a low Pt dispersion and a low degree of alloy formation. Increasing the drying temperature from 240°C to 500°C and 550°C increases the H/Pt ratio from 0.31 to 0.42. As the dehydrogenation activity of both catalyst samples (dried to 240°C and 550°C) is equal, the difference in H_2 uptake is an indication of different degrees of alloy formation. A certain amount of water is apparently beneficial for the formation of bimetallic particles during reduction.

One sample was treated at 680°C in N_2 in order to sinter the Pt particles and thus have a reference sample where the dispersion was expected to be low [28]. A H/Pt ratio of 0.17 was found, a ratio even lower than for the sample not dried prior to reduction. Reproduction of the volumetric measurements confirmed the trends in the data.

4.1.1.4. XAS experiments

In order to obtain direct measurements of the metal particle composition the X-ray absorption spectroscopy (XAS) technique was employed. This is a powerful technique for obtaining detailed information about the metal containing species in highly dispersed systems lacking long range order. As XAS experiments involves the use of synchrotron radiation at special facilities and that special data analysis tools have to be utilised in order to extract data from the obtained X-ray spectra this work has been performed in close collaboration with experts at NTNU. A number of XAS studies on $PtRe/Al_2O_3$ have been reported dealing with the reduction degree of Re and the degree of bimetallic particle formation [67-69,71,72,74,114,115]. Recent studies have made use of the combination of TPR and XAS in order to investigate the effect of hydration prior to reduction on the degree of reduction of the metals [71,74]. It would thus be interesting to employ similar techniques in combination with the model reactions and hydrogen chemisorption.

EXAFS analysis

Fig. 4.7 and Fig 4.8 show the EXAFS spectrum (upper) and the corresponding Fourier transform (lower) of the Pt L_{III} and Re L_{III} of the sample heated at 240°C prior to reduction. The results from the Pt L_{III} and Re L_{III} EXAFS analysis are summarised in Table 4.1. A detailed treatment of the EXAFS analysis is given in Paper II.

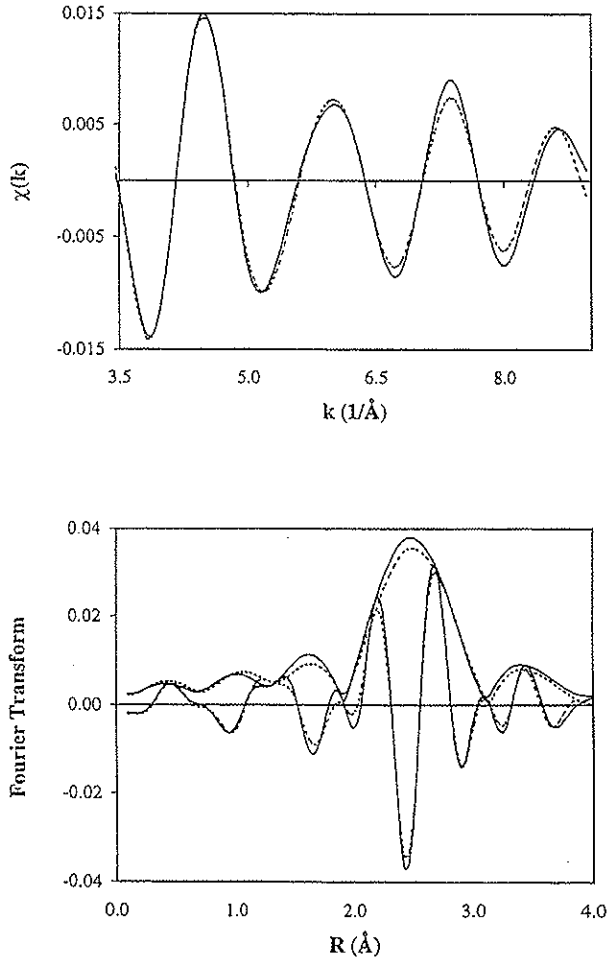

Fig. 4.7. Pt L_{III} EXAFS spectrum (upper) and corresponding Fourier transform (lower) of $PtRe/Al_2O_3$ catalyst dried at 240°C, using Δk = 3.5 – 9.0 $Å^{-1}$ and ΔR = 1.3 – 3.4 Å. Experiment is shown in solid lines, and k^0 fit in dotted lines.

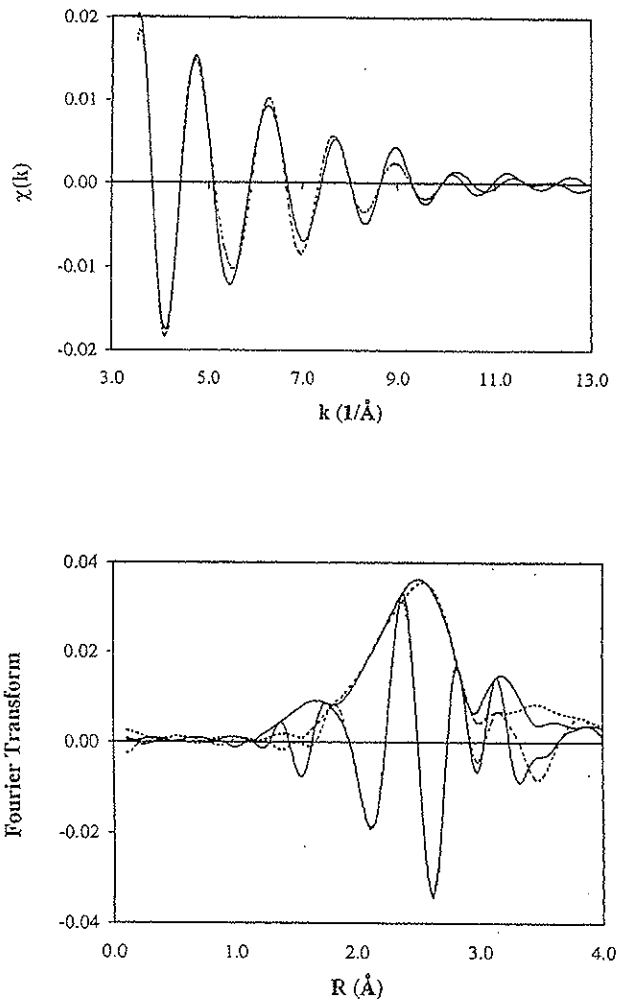

Fig. 4.8. Re L_{III} EXAFS spectrum (upper) and corresponding Fourier transform (lower) of $PtRe/Al_2O_3$ catalyst dried at 240°C, using Δk = 3.5 – 9.0 $Å^{-1}$ and ΔR = 1.3 – 3.4 Å. Experiment is shown in solid lines, and k^0 fit in dotted lines.

Table 4.1. *Changes in Re neighbours as a function of drying temperature. Results from the EXAFS analysis of data from the Re L_{III} edge.*

Drying temperature	Co-ordination shell	Number of neighbours N	Interatomic distance R(Å)
No drying	Re-Pt	2.0	2.75
	Re-Re	4.1	2.56
	Re-O	1.5	1.72
	$Re\text{-}O_{Support}$	1.3	2.02
240 °C	Re-Pt	4.8	2.75
	Re-Re	5.2	2.59
	Re-O	0.4	1.93
	$Re\text{-}O_{Support}$	1.1	2.13
500 °C	Re-Pt	5.2	2.75
	Re-Re	3.3	2.55
	Re-O	1.5	1.76
	$Re\text{-}O_{Support}$	2.4	2.05

The Re EXAFS analysis involves a structural model including four shells, Re-Pt, Re-Re, and two different Re-O distances associated with Re(+VII) oxide species and support interaction. This resulted in good fit to the fine structure and realistic structural parameters where found. From the EXAFS analysis it seems that the samples dried at 240°C and 500°C have the highest Re-Pt coordination and thus the highest degree of alloy formation. The sample not dried prior to reduction shows a significantly lower bimetallic coordination than the other samples. This is an interesting result as both the model reaction and chemisorption studies indicate that this catalyst contains much less bimetallic particles. Previous studies involving $PtRe/Al_2O_3$ catalyst samples have shown that no pre-treatment prior to reduction is beneficial with regard to alloy formation [40]. However, as the preparation of the samples probably is

different from those delivered from AKZO the results are not comparable. The samples (reported in [40]) were only dried, not calcined after impregnation and were then allowed to adsorb moisture from the atmosphere for one week. The samples involved in this EXAFS analysis have probably been prepared and calcined at high temperature by the manufacturer. In the laboratory the catalyst has been stored for many months in sealed containers situated in exicators containing a drying agent. The moisture content has been measured to be approximately 5 wt%. From Table 4.1 it can be seen that the sample treated at 240°C exhibits the most balanced coordination towards platinum and rhenium (4.8 and 5.2, respectively). In addition, this sample also contains a larger fraction of reduced Re than the sample treated at 500°C. It can therefore be suggested, in accordance with results presented in Chapter 4.1.1.1. -3., that treatment in air at low temperatures (i.e. much less than 500°C) provides the most suitable conditions for the formation of bimetallic particles. A certain amount of moisture has to be present on the catalyst surface prior to reduction in order to provide mobility for Re oxide species allowing transport to reduced Pt.

The results from the Pt EXAFS analysis show only minor differences between the three samples. All samples have a Pt-Pt coordination of ca. 3 and a Pt-Re coordination close to 1. The platinum atoms are thus present as highly dispersed and coordinated to both Pt and Re. Both the low coordination number of Pt and the short Pt-Pt bond distance (2.67 Å) compared to that of bulk (2.77 Å) indicate that all samples contain platinum particles of average particle diameter less than 10 Å and that the dispersion is close to 100%.

The atomic fraction of Re (C_{Re}) was calculated by dividing the Re-Re coordination number by the total Re-metal coordination number. The atomic fraction of Pt (C_{Pt}) was found in the same way. Only negligible differences were found in the C_{Pt} values for all three samples, whereas C_{Re} indicates that the sample dried at 240°C has got the highest bimetallic interaction (C_{Re}=0.52).

Table 4.2. *Changes in Pt neighbours as a function of drying temperature. Results from the EXAFS analysis of data from the Pt L_{III} edge.*

Drying temperature	Co-ordination shell	Number of neighbours N	Interatomic distance R(Å)
No drying	Pt-Re	1.1	2.75
	Pt-Pt	2.9	2.66
	Pt-$O_{Support}$	0.2	2.69
240 °C	Pt-Re	1.1	2.75
	Pt-Pt	2.5	2.67
	Pt-$O_{Support}$	0.5	2.70
500 °C	Pt-Re	1.3	2.75
	Pt-Pt	2.9	2.67
	Pt-$O_{Support}$	0	-

Linear combination of XANES

Figures 4.9 and 4.10 show the XANES spectra of the Re L_{III} and Pt L_{III} edge, respectively. The shape of the absorption edge and the white line intensity contains information about the oxidation state and the chemical environment of the element in question. By comparison with the reference compounds in Fig. 4.9 it is clear that Re is not completely reduced in any of the samples. The fraction of unreduced Re can be determined from linear combination of XANES profiles by using the Re foil and the unreduced sample as reference compounds. Only approximately 45% of the total Re content was reduced in the samples directly reduced or dried at 240 °C prior to reduction, whereas the sample dried at 500 °C contained only 11% of reduced Re.

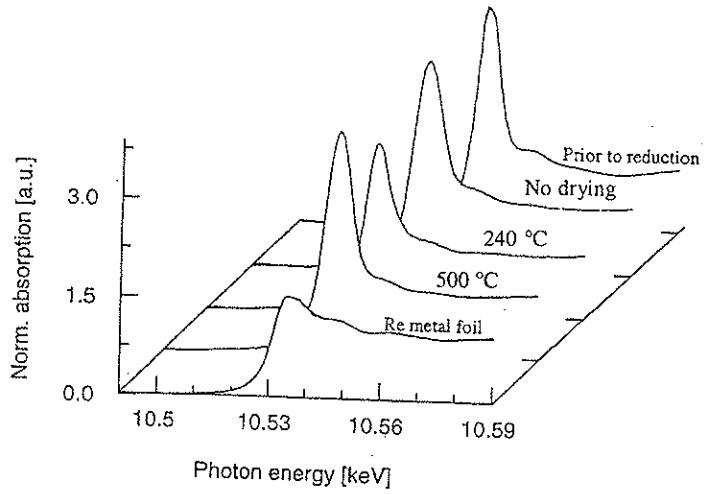

Fig. 4.9. Normalised Re L_{III} edge profiles and white lines intensities of catalyst pre-treated at different temperatures shown together with the profiles of the Re foil and the unreduced sample as reference.

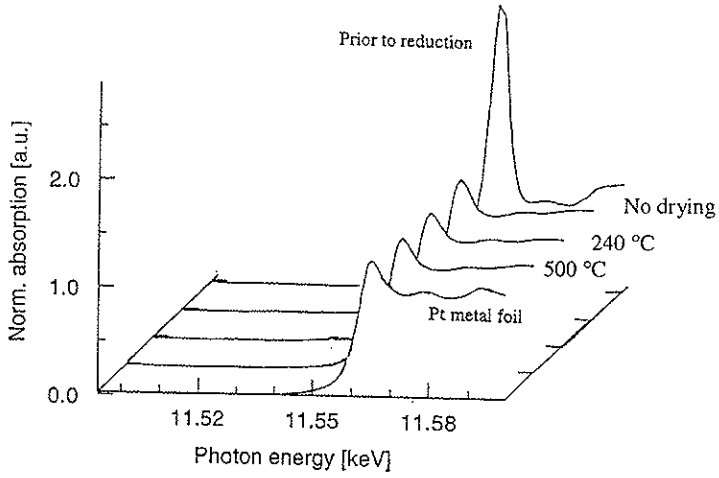

Fig. 4.10. Normalised Pt L_{III} edge profiles and white lines intensities of catalyst pre-treated at different temperatures shown together with the profiles of the Pt foil and the unreduced sample as reference.

The fraction of reduced Re can also be calculated using the data obtained from the EXAFS analysis. This is obtained by dividing the Re-O coordination number by the Re-O coordination number for the unreduced sample. In this case the Re-$O_{Support}$ interaction is not included, and the reduction degree of the sample not dried, dried at 240°C, and 500°C is 63%, 90%, and 63%, respectively. If the Re-$O_{support}$ is included the results from the EXAFS and XANES converge to agreement. As the sample dried at 240°C contains the highest amount of reduced Re, it can be suggested that this sample contain more alloyed Re catalytically reduced by Pt.

The XANES analysis of the Pt L_{III} edge shows that practically all Pt is reduced, which is in agreement with the EXAFS data. The white line intensities of the catalyst samples presented in Figure 4.8 are all very similar to the profile of the Pt metal foil.

4.1.2. The effect of the reduction procedure

In addition to the effect of water prior to reduction on the alloy formation the effect of the heating rate during reduction and the reduction temperature was also studied. During reduction water is produced and the partial pressure of water is a function of the rate of reduction (controlled by the heating rate). As a heating rate of 0.8°C/min was employed in all other experiments, rates of 0.2°C/min and 3.3°C/min were used here in order to see the effects of slower and faster reduction rates. The reduction temperature varied either 480°C, 510°, or 530°C and the partial pressure of water in the incoming reduction gas adjusted to either 0 or 1500 ppm. All investigations involved catalyst either dried at 500°C or reduced directly as these samples represent the extremes with respect to the level of hydration.

4.1.2.1. Hydrogen chemisorption

A number of pulse hydrogen chemisorption measurements were performed. Figs. 4.11, 4.12, and 4.13 show the results from these experiments.

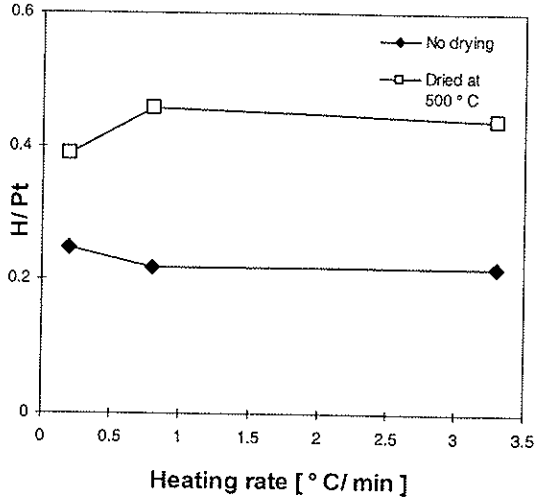

Fig. 4.11. The influence of the heating rate on the H/Pt ratio of the $PtRe/Al_2O_3$ catalyst either reduced directly or dried at 500°C prior to reduction.

From Fig. 4.11 it can be observed that the heating rate during reduction has a much less impact on the H/Pt ratio than pre-treatment of the catalyst prior to reduction. As discussed previously the hydrogen uptake of the catalyst not dried prior to reduction is lower than the catalyst heated at 500°C (Fig. 4.6). This was explained by a possible lower Pt dispersion. The catalytic activity of this sample was low for dehydrogenation of methylcyclohexane as well as for hydrogenolysis of cyclopentane, indicating low dispersion of Pt and a low degree of alloy formation. It was suggested that too much water present on the catalyst prior to reduction could result in sintering of Pt. A very slow reduction

rate would be beneficial in order to decrease the partial pressure of water during reduction, but the rate has hardly any influence. The sample dried at 500°C is also virtually unaffected by the reduction rate.

After drying at 500°C the reduction was started at 20°C, 200°C, and 400°C in order to see whether the reduction interval could be critical to the degree of bimetallic particle formation. If the reduction is performed over a short period of time or a short temperature interval a higher partial pressure of water would result, which could have an influence on the reduction mechanism of Re. The H/Pt values presented in Fig. 4.12 do not indicate any influence of the reduction interval.

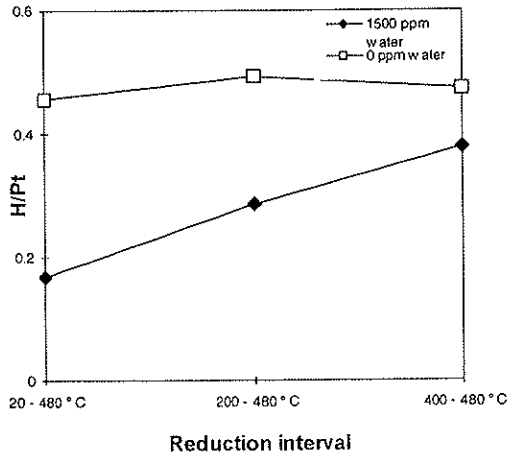

Fig. 4.12. The influence of the reduction interval and the addition of 1500ppm of water on the H/Pt ratio of the $PtRe/Al_2O_3$ catalyst dried at 500°C prior to reduction.

1500 ppm of water was introduced to the reduction gas in order to investigate the influence of moisture added during reduction. It is clear that the samples treated with water during reduction have a lower H/Pt ratio than the samples reduced in dry hydrogen. If the reduction with moist gas is started at a

higher temperature the H/Pt ratio increases. The interpretation of the H/Pt ratio has previously been related to the degree of alloy formation [28]. A low ratio has been ascribed to a high degree of alloy formation. Augustine et al [40] suggest that rhenium oxide that has been immobilised by the formation of a surface compound with Al_2O_3 regains its mobility upon hydrolysis. Thus, mobile Re oxide can be reduced at a lower temperature by the catalytic action of Pt yielding more bimetallic particles. However, it can not be ruled out that changes in the H/Pt can be ascribed to changes in the Pt dispersion. Similar hydrolysis of immobilised Pt compounds might also lead to sintering of Pt particles. Comparing the H/Pt values with those of the sample not dried prior to reduction it can be observed that they are at the same level and even lower when reduced from 20°C. The increase in the H/Pt ratio when starting the reduction at a higher temperature can be attributed to less influence of the moisture level at higher temperatures.

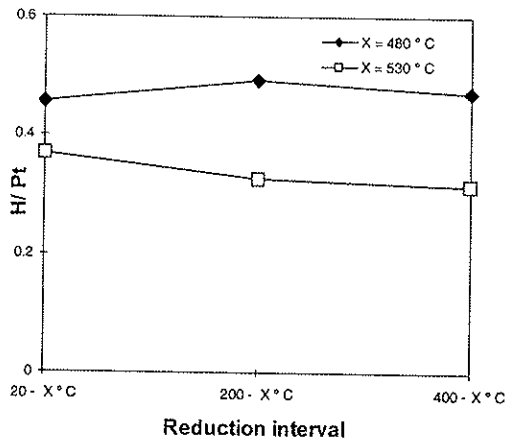

Fig. 4.13. The influence of the reduction interval and final reduction temperature on the H/Pt ratio of the $PtRe/Al_2O_3$ catalyst dried at 500°C prior to reduction.

Fig. 4.13 shows the effect of increasing the final reduction temperature. The H/Pt ratios of the sample reduced at 530°C are compared to data taken from Fig. 4.12. Catalyst reduced at 480°C, which is the standard reduction temperature, have higher H/Pt ratios than the samples reduced at 530°C. It therefore seems that a higher reduction temperature yields more alloy formation. A higher reduction temperature should not result in a lower dispersion, as Pt does not sinter under these conditions. However, the Re oxide species might gain increased mobility. Re is also reduced to a larger degree at a higher temperature.

4.1.2.2. STEM/EDX analysis

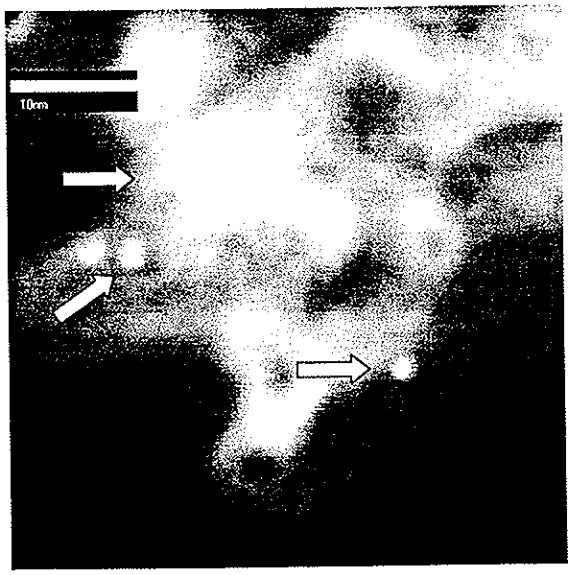

Fig. 4.14. Annular dark field image of a singular alumina particle containing many metal particles (Sample containing 1.5 wt% Cl). The metal particles appear as white dots and are indicated by arrows.

The catalyst samples were also studied with combined STEM and EDX. The metal particles can be observed as white spots on the annular dark-field STEM micrograph as indicated in Fig. 4.14.

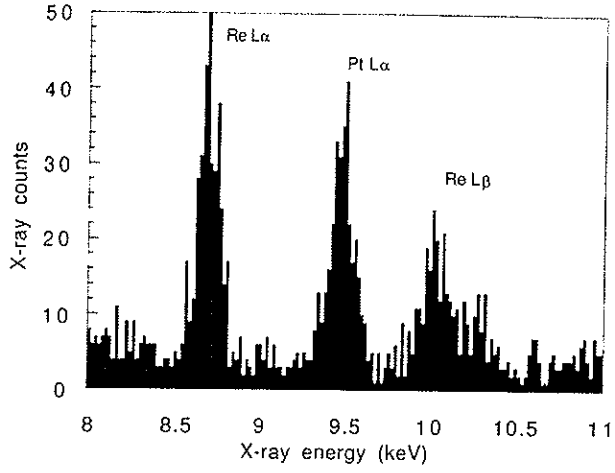

Fig. 4.15. X-ray spectrum obtained from a particle of approximately 1 nm in diameter.

The STEM analysis was performed by observing only thin layers (10-50 nm) of the supporting alumina as shown in Fig. 4.14, thus simplifying metal particle detection. The smallest particles observed were approximately 0.5 nm in diameter. Fig. 4.15 shows an example of an EDX-spectrum of collected X-rays emitted from a single metal particle. The Pt and Re signals detected clearly show that the metal particle is bimetallic.

Information about the composition of the particles was obtained by collecting EDX-spectra of 100-120 particles for each sample. The data obtained were used to plot particle composition-size diagrams of each sample providing a "fingerprint" of the catalyst. The metal particles of the $PtRe/Al_2O_3$ catalyst are very small ($\leq$ 2nm) and this makes direct studies difficult due to the resolution limitation of conventional instruments. Previous studies [79] using

combined STEM and EDX to describe the Pt-Re alloy formation for the same catalyst system have indicated that Re was not alloyed with Pt. However, it seems that the particles studied in this case were too large (2-3 nm) to represent the system. The instrument used here (VG Microscope HB 603) has been specially designed for high spatial resolution [116] and studies of particles smaller than 1 nm are possible.

As the hydrogen chemisorption studies did not reveal any significant difference in alloy formation by varying the reduction rate in the range 0.2 – 3.3 °C/min more severe reduction conditions were employed here. As drying at 240°C has proved to be the most beneficial treatment prior to reduction regarding bimetallic particle formation all samples were dried at this temperature. A sample was also reduced at 480°C for 100 h to see if a higher degree of alloy formation could be obtained under such conditions. Fig. 4.16 through 4.18 shows the composition-size diagrams of the different samples. Even if small variations may be detected, it can be observed from these diagrams that the particle size and composition of all samples are virtually identical. As a limited number of particles have been analysed it can not be ruled out that the differences in particle size and composition are actually larger. The major disadvantage of the STEM/EDX technique compared to chemical characterisation techniques is the inability to map the whole system. Analysis is only performed on particles situated on the edge of the alumina particles in order to avoid background contribution from the bulk. Due to a time consuming analysis procedure it was possible to analyse only 100 –150 particles.

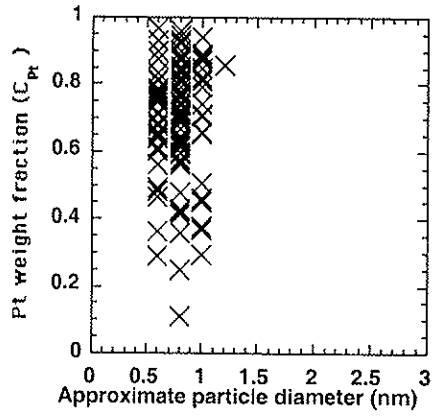

Fig. 4.16. Approximate particle diameter and measured Pt fraction of individual metal particles on the catalyst reduced at 480°C for 100 h using a heating rate of 0.8°C/min from 20°C to 480°C.

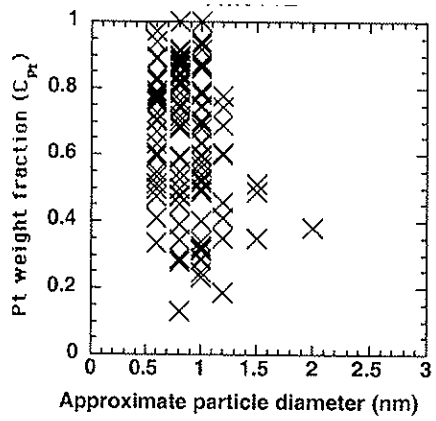

Fig. 4.17. Approximate particle diameter and measured Pt fraction of individual metal particles on the catalyst reduced at 530°C for 1 h using a heating rate of 0.8°C/min from 20°C to 480°C.

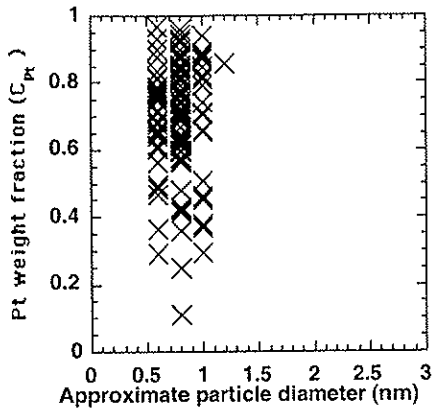

Fig. 4.18. Approximate particle diameter and measured Pt fraction of individual metal particles on the catalyst reduced at 480°C for 1 h using a heating rate of 24°C/min from 20°C to 480°C.

4.2. The effect of the chlorine content on the $PtRe/Al_2O_3$ catalyst

During regeneration $PtRe/Al_2O_3$ is oxychlorinated in order to re-establish the Pt dispersion and to restore acidity. One of the objectives of this work has been to investigate whether the chlorine level prior to reduction (after oxychlorination) has any effect on the formation of bimetallic particles. It has been reported that the chlorine content is critical, but the conclusions are diverse. Michel et al [26] suggest that there is a mobile oxychloride compound involved in the reduction mechanism, whereas others [27,62] claim that chlorine inhibits Pt-Re interaction. In commercial practice approximately 1.0 wt% of Cl is added. This amount is, however, set to optimise acidity during

reforming and not necessarily to optimise the conditions for bimetallic formation.

4.2.1. Hydrogenolysis of n-butane

The results from the n-butane hydrogenolysis experiments, shown in Figs. 4.19 and 4.20, do not reveal any significant differences in alloy formation when increasing the chlorine content from 0.65 wt% to 1.1 wt%. These samples show all the same conversion of n-butane. It is important to bear in mind that reactions on the acid support, such as cracking, also will occur. Differences in n-butane conversion could therefore be due to differences in the chlorine content. However, the conversion of the sample containing 0.65 wt% Cl is approximately equal to the sample containing 1.10 wt% and even higher than the sample of 1.5 wt% Cl. The difference in catalytic activity is therefore attributed to differences in the metal particle characteristics. The conversion of n-butane and the selectivity to methane is lowest for the sample containing 1.5 wt% Cl indicating that too much chlorine inhibits alloy formation during reduction. Chlorine may therefore behave as obstacles to the migrating Re oxide species.

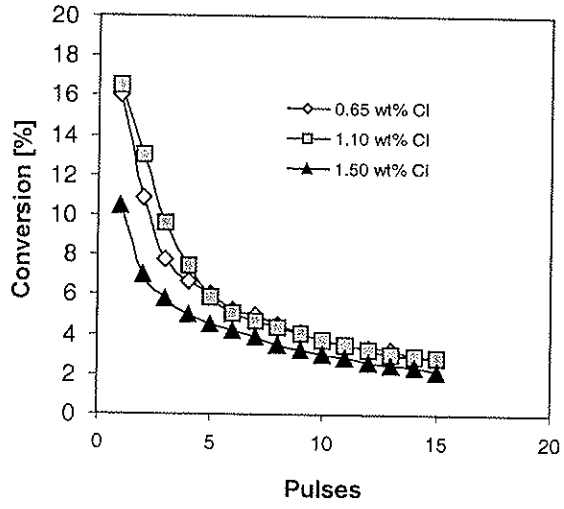

Fig. 4.19. Effect of chlorine content prior to reduction on n-butane conversion over $PtRe/Al_2O_3$ catalyst. Reaction conditions: 250°C, 1.75bara, pulse 1.20ml, H_2/CP=17, and carrier gas flow 250ml/min

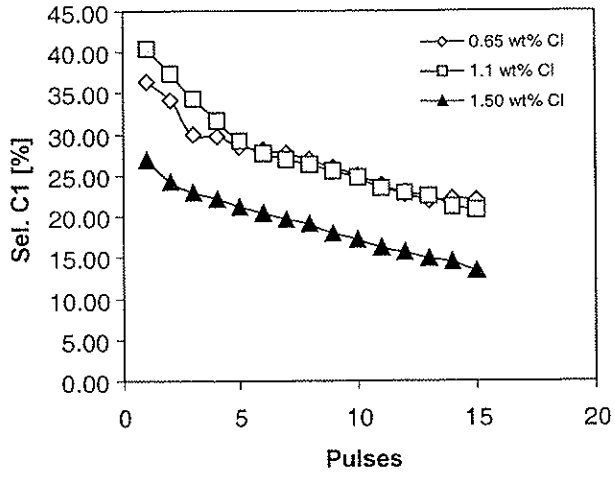

Fig. 4.20. Effect of chlorine content prior to reduction on methane selectivity over $PtRe/Al_2O_3$ catalyst during conversion of n-butane. Reaction conditions: 250°C, 1.75bara, pulse 1.20ml, H_2/CP=17, and carrier gas flow 250ml/min

4.2.1. Hydrogenolysis of cyclopentane

4.2.1.1. Dry reduction

Figure 4.21 and 4.22 show the results from the hydrogenolysis of cyclopentane over catalysts over different chlorine levels prior to reduction in dry hydrogen. Although the differences are small the conversion of cyclopentane seem to increase with increasing chlorine content. As previously discussed this may be due to higher cracking activity as the acidity of the support increases. Bearing the Figure 4.17 in mind it is interesting to observe the differences in selectivity to methane for the three samples. The selectivity plots presented here are three different experiments, whereas the values presented in Paper I and III are averages of several experiments.

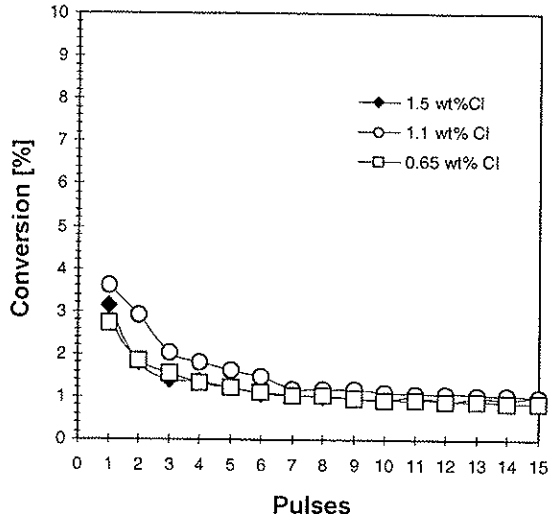

Fig. 4.21. Effect of chlorine content prior to reduction on conversion of cyclopentane over $PtRe/Al_2O_3$ catalyst. Reaction conditions: 250°C, 1.75bara, pulse 1.20ml, H_2/CP=12, and carrier gas flow 250ml/min

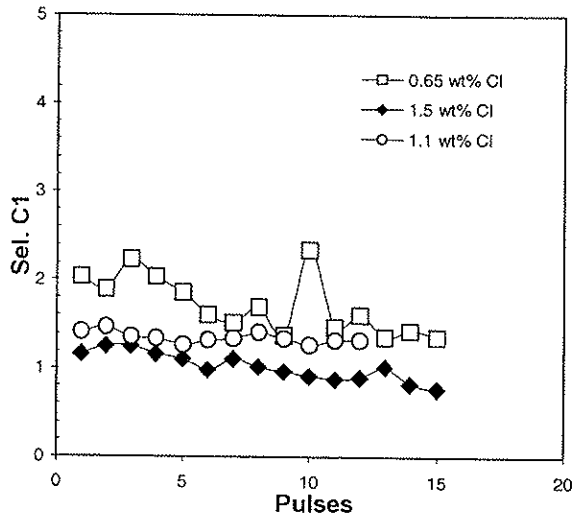

Fig. 4.22. Effect of chlorine content prior to reduction on the selectivity to methane over $PtRe/Al_2O_3$ catalyst during conversion of cyclopentane. Reaction conditions: 250°C, 1.75bara, pulse 1.20ml, H_2/CP=12, and carrier gas flow 250ml/min

The selectivity to methane is highest for the sample containing 0.65 wt% Cl even if the conversion of cyclopentane is lowest. Even if the differences are small this is an indication that the sample with the lowest chlorine content has the highest degree of Pt-Re interaction. The samples containing more chlorine show lower selectivity to methane even when the conversion of cyclopentane is somewhat higher. This behaviour can be attributed to higher acid cracking activity and poorer hydrogenolysis activity. It has to be stressed that the differences are small and data from other characterisation techniques have to be considered in order to make decisive conclusions.

4.2.1.2. Reduction in moist atmosphere

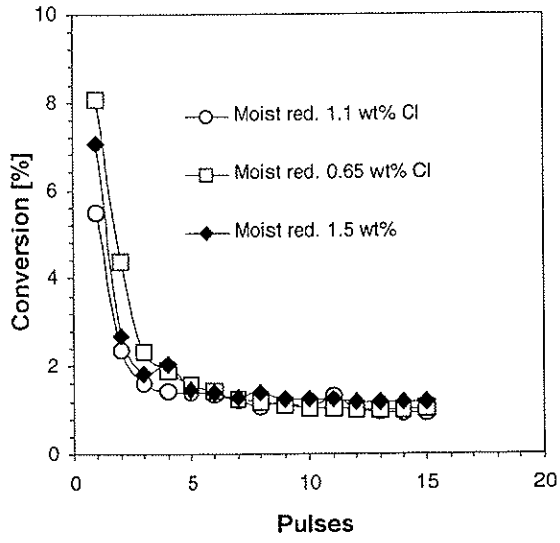

Fig. 4.23. Effect of chlorine content prior to reduction in moist atmosphere on the conversion of cyclopentane over $PtRe/Al_2O_3$. Reaction conditions: 250°C, 1.75bara, pulse 1.20ml, H_2/CP=12, and carrier gas flow 250ml/min

In the previous chapters the effect of water on the bimetallic particle formation has been demonstrated. After adjusting the chlorine level of the catalyst samples they were subjected to reduction in moist atmosphere in order to investigate the combined effect of water and chlorine.

From Fig. 4.23 it is clear that the conversion for all samples has increased (compared to the results reported in Fig. 4.21) when treated with 5000 ppm water during reduction. Although the sample with the lowest chlorine content shows the highest conversion of cyclopentane it is, however, no clear correlation between the chlorine content and the cyclopentane hydrogenolysis activity. When discussing the effect of chlorine on alloy formation under these conditions it has to be beard in mind that high temperature treatment in moist atmosphere introduces stripping of chlorine. Hydroxyl groups will replace the surface chlorine atoms and thus enhance the mobility of rhenium oxide by ensuring a higher level of surface hydration and reducing the inhibiting effect of chlorine. The sample with the lowest chlorine level will in this case also contain most bimetallic particles after reduction. The catalytic performance of all samples should be affected by the removal of chlorine due to changes in support acidity. In spite of this the conversion of cyclopentane is higher after reduction in moist hydrogen and this increased conversion must therefore be attributed to a higher degree of alloy formation. Water in the reduction gas could also lead to sintering of platinum, but as the structure sensitive hydrogenolysis reaction is favoured on small metal particles this effect is not significant.

Figure 4.24 shows the selectivity to methane for the three samples, and the catalyst containing 0.65 wt% Cl displays the highest selectivity to methane. As the production of methane is measure of the hydrogenolysis activity, it can be suggested that the metal particles of this sample have the highest degree of alloy formation. The two other samples show approximately the same selectivity.

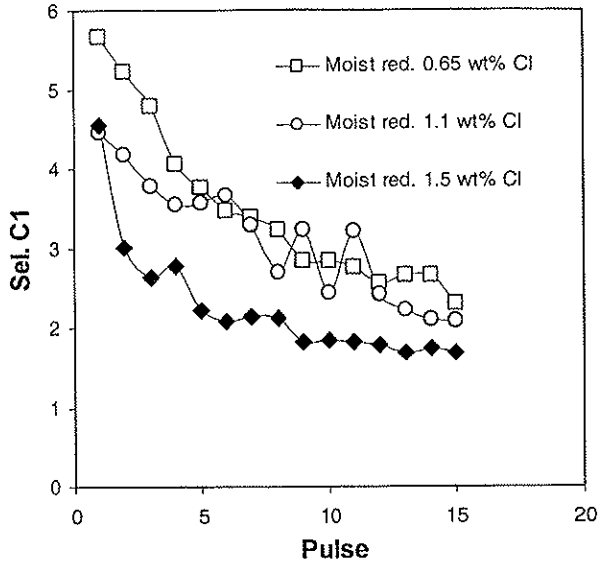

Fig. 4.24. **Effect of chlorine content prior to reduction in moist atmosphere on the selectivity to methane over $PtRe/Al_2O_3$ catalyst during conversion of cyclopentane. Reaction conditions: 250°C, 1.75bara, Pulse 1.20ml, H_2/CP=12, and carrier gas flow 250ml/min**

4.2.2. STEM/EDX analysis

The oxychlorinated samples were also subjected to combined STEM/EDX analysis in order to obtain direct physical information of the metal particles. Figs. 4.25 and 4.26 show composition-size diagrams of a sample containing 0.65 wt% Cl and 1.50 wt% Cl prior to reduction, respectively.

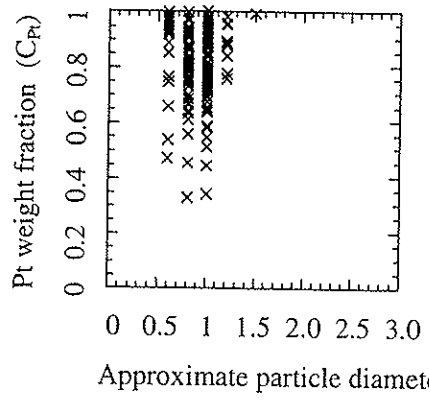

Fig. 4.25. Approximate particle diameter and measured Pt fraction of individual metal particles in the sample containing 0.65 wt% Cl, dry reduction

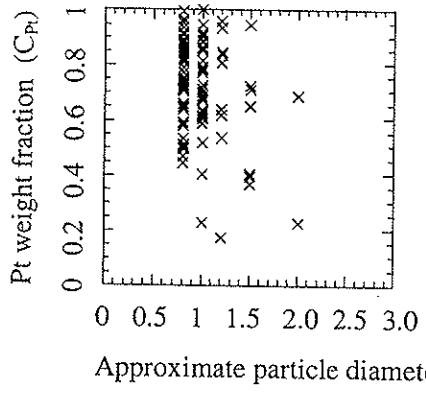

Fig. 4.26. Approximate particle diameter and measured Pt fraction of individual metal particles in the sample containing 1.50 wt% Cl, dry reduction

The average particle size and the average metal composition were calculated for each sample based on the data collected from the STEM/EDX analysis, and is given in Table 4.3. These results give an indication of the state of the metal particles on the catalyst after reduction. The average particle size and composition is only approximate values as indicated by the broad distribution of the parameters. It is therefore not obvious to find any trends from these data. From Figs. 4.25 and 4.26 and Table 4.3 it can be concluded that the effect of the chlorine level on the bimetallic particle formation is limited and therefore difficult to observe from this technique. The lack of significant results can also be attributed to various factors such as a limitation in the number of particles analysed.

Table 4.3. *Average platinum compositions (C_{Pt}) and particle diameters ($D_{Particle}$) obtained from combined EDX/STEM analysis of the $PtRe/Al_2O_3$ catalyst containing different levels of chlorine. Reduction in dry H_2.*

Chlorine level	EDX C_{Pt}	STEM $D_{Particle}$ [nm]
0.65	0.8	0.9
1.10	0.8	1.0
1.50	0.7	1.0

Figs. 4.27 and 4.28 show the particle composition-size diagrams of the samples containing 0.65 wt% Cl and 1.50 wt% Cl prior to reduction in *moist* hydrogen. From these diagrams and the average composition and average size presented in Table 4.4 no differences in alloy formation can be found when varying the chlorine level in the range 0.65 wt% to 1.50 wt% Cl. However, it can be observed that the metal particles are somewhat larger and more alloyed when water is added to the reducing gas. As previously discussed water ensures Re oxide mobility and Pt sintering which results in larger particles. It can therefore be speculated that the effect of moisture in the reduction gas is the formation of larger particles.

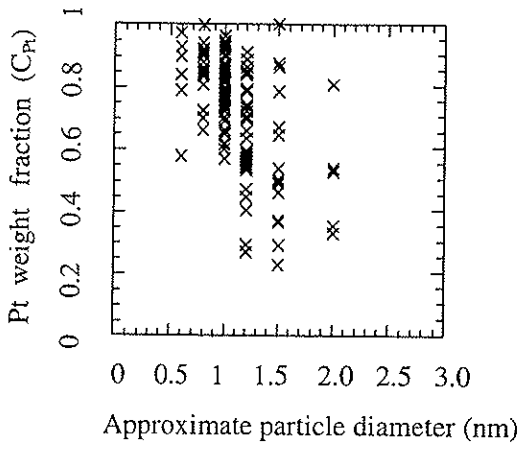

Fig. 4.27. Approximate particle diameter and measured Pt fraction of individual metal particles in the sample containing 0.65 wt% Cl, reduction with moist hydrogen.

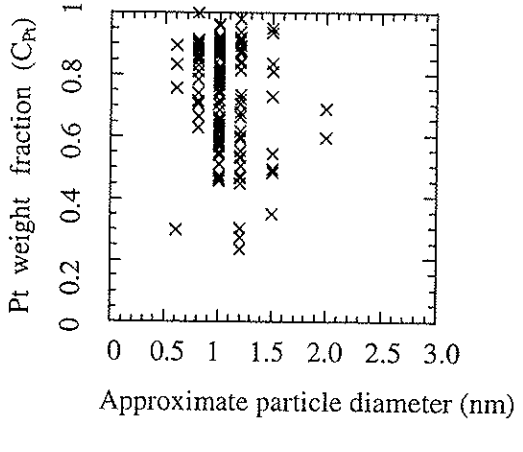

Fig. 4.28 Approximate particle diameter and measured Pt fraction of individual metal particles in the sample containing 1.50 wt% Cl, reduction in moist hydrogen.

Table 4.4. *Average platinum compositions (C_{Pt}) and particle sizes ($D_{Particle}$) obtained from combined EDX/STEM analysis of the $PtRe/Al_2O_3$ catalyst containing different levels of chlorine. Reduction in moist H_2.*

Chlorine level	EDX C_{Pt}	STEM $D_{Particle}$ [nm]
0.65	0.7	1.1
1.10	0.7	1.2
1.50	0.7	1.1

The introduction of water may result in stripping of chlorine and this will also effect the formation of bimetallic clusters during reduction. The influence of water can thus be attributed to the removal of chlorine as well as to the introduction of more hydroxyl groups on the catalyst surface.

4.2.3. TPR experiments

Figure 4.29 shows the TPR profiles of the $PtRe/Al_2O_3$ catalyst containing 0.65, 1.10, and 1.50 wt% Cl dried at 510°C prior to the experiment. As seen from the TPR profile of the monometallic Pt/Al_2O_3 catalyst shown in Figure 4.30, the first peak observed at about 250°C can be assigned to the reduction of Pt. At 350°C the next peak emerges which is characteristic of further reduction of Pt and the catalytic reduction of Re oxide by metallic Pt. The last peak observed at 610°C can be attributed to reduction of isolated Re oxide. The shape of the peak in the 250 - 350°C range is similar for Pt/Al_2O_3 and the $PtRe/Al_2O_3$ catalyst sample containing 0.65 wt% Cl. The narrow peak in the low temperature region can be taken as an indication of co-reduction of Pt and Re and thus alloy formation. The samples containing 1.10 wt% Cl and 1.50 wt% Cl have a lower H_2 consumption is this area reflected by the smaller peaks. Measurements of the H_2 consumption and calculation of the degree of

reduction of the metals are complicated by the fact that there might be some reduction and removal of chlorine. However, according to Barbier et al [117] at such low concentrations (1.5 – 0.65 wt% Cl) the chlorine level is relatively unaltered during reduction. The degree of reduction of Re can be calculated by using the monometallic Pt catalyst (CK 300) as a standard and assuming 100% reduction. The amount of Re both co-reduced with Pt and reduced at 610°C is found by subtracting the hydrogen consumed by Pt. In the sample containing 0.65 wt % Cl Re is reduced to approximately 80% in the temperature range 20-450°C, whereas the reduction degree of the sample containing 1.10 wt% Cl and 1.50 wt% Cl is as low as 30% in the same temperature interval.

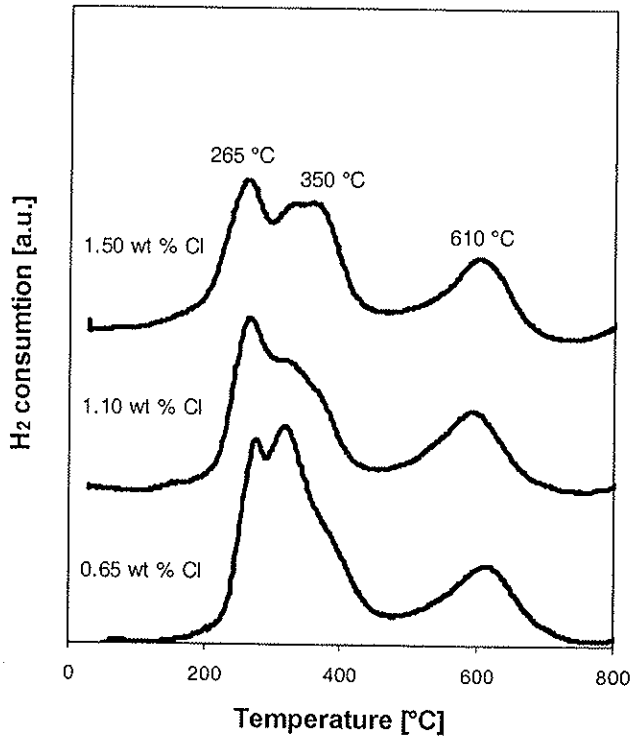

Fig. 4.29. Temperature Programmed Reduction (TPR) profiles of $PtRe/Al_2O_3$ catalyst with different chlorine content: 0.65 wt%, 1.10 wt%, and 1.50 wt% Cl.

The difference in reduction degree is reflected in the different sizes of the first peaks in the low temperature region. A higher degree of reduction of Re in the low temperature region of the sample containing 0.65 wt% Cl can be interpreted such that this catalyst contains more alloyed particles than the other samples.

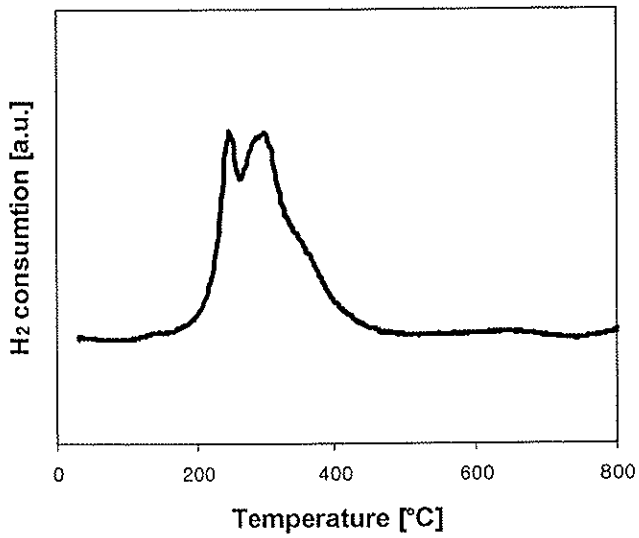

Fig. 4.30. Temperature Programmed Reduction (TPR) profile of Pt/Al_2O_3 catalyst dried at 510°C.

4.3. The effect of the pre-treatment conditions on the $PtSn/Al_2O_3$ catalyst

The $PtSn/Al_2O_3$ catalyst studied has been synthesised in the laboratory as described in Chapter 3.1.2. Preliminary experiments involving TPR and hydrogen chemisorption were conducted in order to investigate the effect of the pre-treatment conditions on the metal function of the Pt-Sn system.

In case of the Pt-Re system the degree of hydration prior to reduction has been found to be crucial with respect to alloy formation. Previous studies [90,91,105] have shown that the calcination temperature or the drying temperature is also crucial for the degree of Sn reduction in the Pt-Sn system. It was therefore of interest to conduct measurements of the Pt-Sn catalyst employing the same conditions as for the Pt-Re catalyst.

4.3.1. TPR experiments

The catalyst samples, which have been stored in sealed containers after synthesis and calcination, were dried at either 240°C or 550°C or not dried prior to reduction. Figs. 4.31 and 4.32 display the TPR profiles of the 0.3-0.3 wt% $PtSn/Al_2O_3$, 0.3 wt% Pt/Al_2O_3, and 0.3 wt% Sn/Al_2O_3 dried at 240°C and 550°C, respectively. Virtually no hydrogen is consumed when the Sn/Al_2O_3 sample, dried at 240°C or 550°C, is reduced from 20°C to approximately 600°C. At such low concentrations it seems that the supported Sn oxide is very stable and similar TPR profiles are obtained by other authors [91,96,118,119]. The TPR profile of the $PtSn/Al_2O_3$ catalyst is quite similar to the Pt/Al_2O_3 profile. Investigation of the hydrogen consumption reveals the catalytic effect of Pt on the reducibility of Sn.

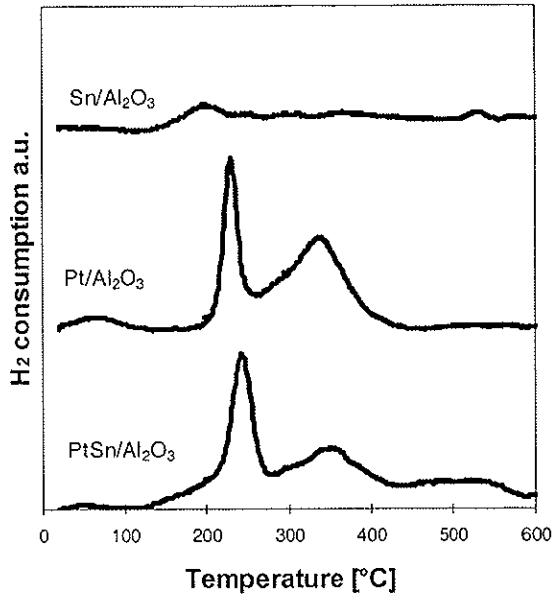

Fig. 4.31. Temperature Programmed Reduction (TPR) profiles of Sn/Al_2O_3, Pt/Al_2O_3, and $PtSn/Al_2O_3$ catalyst dried at 240°C.

Increasing the drying temperature from 240 °C to 550°C results in larger and different peaks from those shown in Fig. 4.31. The drying temperature has no influence on the Sn/Al_2O_3 profile, but more Sn is being reduced in the PtSn catalyst. Simultaneously the TPR profile of the Pt/Al_2O_3 catalyst changes and more hydrogen is consumed during reduction as shown in Table 4.5. As 100 % reduction of Pt is expected for drying temperatures of 240°C and 550°C this increase in consumption cannot be due to more reduction of Pt oxide. Previously Isaacs and Petersen [24] found small differences when drying the Pt/Al_2O_3 catalyst in Ar at 100°C and 500°C although a higher drying temperature resulted in a broader TPR peak. Mieville [38] found that the peak was broader when the Pt sample was dried in air at 300°C than at 500°C, reaching an opposite conclusion. Burch et al [90] related the differences in the

TPR profile of the Pt/Al_2O_3 catalyst to the conversion of the chloro-ligands into HCl. However, with such an explanation the TPR peak will decrease with higher temperatures (Reactive Cl ions will be removed at high temperature treatment in air). Because virtually no hydrogen was consumed during reduction of the 0.3 wt% Sn/Al_2O_3 catalyst any large contributions from surface chlorine removal or hydrogenation of impurities can be neglected. Other explanations for the different TPR profiles of Pt/Al_2O_3 catalysts dried at 550°C, 240°C and not dried (DR) prior to reduction as shown in Fig. 4.33 can be that drying at different temperatures might result in more or less oxygen rich Pt oxide species. It can not be ruled out that the fresh Pt/Al_2O_3 catalyst is partially reduced after calcination at the manufacturer. From Table 4.5 it is obvious that there is a discrepancy between the theoretical assumptions and the experimental findings regarding the reduction degree of the catalyst samples. However, no further investigations were performed in order to reveal the composition of the Pt surface compounds.

Lieske and Völter [91] observed that the reduction degree of Sn in the 0.5-1.2 wt% $PtSn/Al_2O_3$ catalyst system increased when increasing the calcination temperature from 250°C to 550°. The authors explained this effect in more intimate contact between Pt and Sn due to mobile surface oxide species at high temperatures and thus catalytic reduction of Sn oxide by reduced Pt clusters. On the other hand Dautzenberg et al [89] reported that oxidation at high temperatures resulted in segregation of Pt and Sn. Comparing the TPR profiles of $PtSn/Al_2O_3$ and Pt/Al_2O_3 presented in Fig. 4.32, it can be observed that they have similar peaks in the 250°C to 350°C range (although the peaks of the PtSn catalyst appear at somewhat higher temperatures.) The large peak at approximately 375°C in the TPR profile of the PtSn catalyst can be ascribed to the reduction of Sn. As this peak is superimposed on the characteristic reduction profile of the Pt catalyst the reduction of Sn is probably catalysed by Pt. Fig. 4.31 show the TPR profiles of the samples dried at 240°C and the close similarity of the profiles of Pt and PtSn catalyst indicates that less Sn is being

reduced. It can therefore be concluded that less bimetallic particles are formed when the catalyst is pre-treated at 240°C.

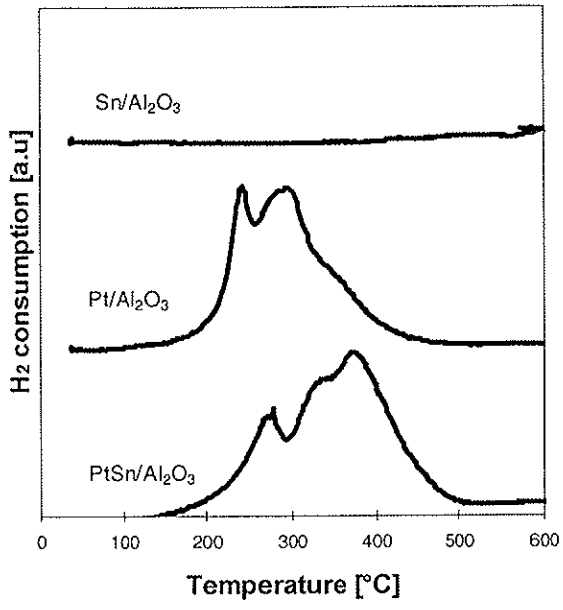

Fig. 4.32. Temperature Programmed Reduction (TPR) profiles of Sn/Al_2O_3, Pt/Al_2O_3, and $PtSn/Al_2O_3$ catalyst dried at 550°C.

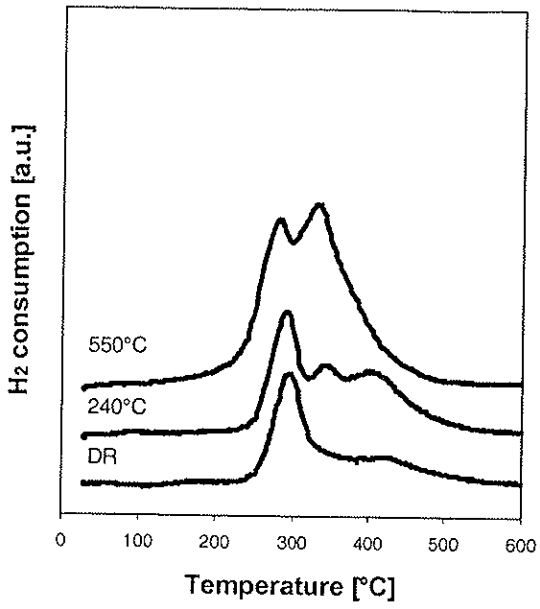

Fig. 4.33 Temperature Programmed Reduction (TPR) profiles of Pt/Al_2O_3 catalyst dried at 550°C, 240°C, and no drying (DR).

The hydrogen uptake was calculated based on a calibration factor found from TPR of Ag_2O. The experimental obtained hydrogen uptake was compared with the theoretical consumption based on the stoichiometric equations:

$$PtO_2 + 2H_2 \rightarrow Pt + 2H_2O \quad (4.1)$$

$$SnO_2 + 2H_2 \rightarrow Sn + 2H_2O \quad (4.2)$$

Table 4.5. *Quantitative analysis of the TPR profiles. The degree of reduction of the different samples*

Catalyst	Drying temperature in air [°C]	Degree of reduction [%][a]
Pt/Al_2O_3	DR	130
Pt/Al_2O_3	240°C	180
Pt/Al_2O_3	550°C	320
Sn/Al_2O_3	240°C	10
Sn/Al_2O_3	550°C	10
$PtSn/Al_2O_3$	DR	100
$PtSn/Al_2O_3$	240°C	100
$PtSn/Al_2O_3$	550°C	160
Ref. Catalyst[b]	240°C	60
Ref. Catalyst[b]	550°C	160

a = Average values based on 2-3 TPR experiments

b = Commercial $PtSn/Al_3O_3$ catalyst. Assumed weight fraction of Pt and Sn is 0.3 %

DR = Direct reduction (i.e. no drying prior to reduction)

4.3.2. Volumetric chemisorption of hydrogen

Table 4.6. *H/Pt ratios of Pt-Sn/Al_2O_3 catalyst measured by volumetric chemisorption.*

Catalyst	Drying temperature in air [°C]	H/Pt ratio
Pt-Sn/Al_2O_3	240°C	53
Pt-Sn/Al_2O_3	550°C	47

The Pt-Sn/Al_2O_3 catalysts dried at 240°C and 550°C were subjected to studies by H_2 chemisorption. The results are presented in Table 4.6. It can be observed that the hydrogen uptake for the catalyst dried at 550°C is slightly lower than for the catalyst dried at 240°C. If the same reasoning as for the bimetallic Pt-Re/Al_2O_3 catalyst is used, it can be suggested that the catalyst

dried at the highest temperature has the highest degree of alloy formation. This is in accordance with Lieske et al [91] which also suggest that a decrease in the H/Pt ratio is indicative of alloy formation in the Pt-Sn system.

4.3.3. Final remarks on the studies of the Pt-Sn/γ–Al_2O_3 catalysts and suggestions for further work.

As discussed in Chapter 4.3.1. reduction degrees exceeding 100% as shown in Table 4.5 does not make sense physically. A possible explanation for these values could be that it has been made erroneous assumptions regarding the stoichometry of the reduction or the composition of the catalyst. There may also have been problems with the measuring of the hydrogen consumption, but to our knowledge the TC detector in the TPR apparatus was correctly calibrated.

In this work only preliminary studies of the Pt-Sn/Al_2O_3 catalyst were made. It has been suggested that high temperature treatment in air prior to reduction results in more alloyed particles. There has not, however, been performed any activity experiments to reveal what should be the most beneficial state of Sn in the catalyst. In order gain more insight about the effect of the pre-treatment effects on the final states of the metal particles a more elaborate study must be conducted involving activity measurements and more advanced characterisation techniques.

5. Conclusions

The metal particles of bimetallic reforming catalysts have been investigated employing various experimental techniques. The results and findings from this work can be summarised in the following conclusions:

1. A pulse apparatus has been developed and employed for model reaction studies. It has been possible to measure the initial activity for model reactions on a Pt-Re/Al_2O_3 catalyst and thus obtain indirect information of the state of the metal particles after reduction.

2. Drying the Pt-Re/Al_2O_3 catalyst at moderate temperatures (around 240°C) in air prior to reduction yields the most alloyed particles. A certain degree of hydration is beneficial in order to provide mobility for the rhenium oxide species during reduction. The surface migration of rhenium oxide species results in contact with reduced platinum particles and thus the formation of alloys through catalytic reduction by platinum.

However, the results obtained from model reactions, H_2 chemisorption, and XAS analysis also indicate that direct reduction (no drying prior to reduction) of the catalyst results in low catalyst dispersion and less bimetallic particle formation. Thus, too much water is not beneficial, as this seems to promote sintering of platinum particles.

Drying the catalyst at high temperatures in air (above 500°C) yields less bimetallic particles than drying at lower temperatures. The catalyst becomes more dehydrated and the rhenium oxide mobility is inhibited.

3. Variations of the heating rate in the range 0.2 °C – 3.3 °C during reduction did not have any significant influence on the alloy formation.

4. Increasing the reduction temperature of the catalyst from 480°C to 530°C after drying at 500°C resulted in a higher degree of bimetallic formation.

5. Addition of moisture (1500 ppm) during reduction has a significant effect on alloy formation. This effect can be ascribed to the beneficial effect of water on the Re oxide mobility.

6. The chlorine level of the Pt-Re catalyst samples was varied in the range 0.65 to 1.50 wt % by oxychlorination. Only limited influence of the chlorine content was found when analysing with techniques such as STEM/EDX, model reactions, TPR, and H_2 chemisorption. The sample with the lowest chlorine content seems to have the highest degree of alloy formation indicating that chlorine atoms may act as obstacles for the rhenium oxide species. Addition of moisture during reduction of the chlorinated catalysts probably results in more alloyed catalyst. This is both due to stripping of chlorine and increased hydration of the surface.

5. Investigations of bimetallic reforming catalyst containing Pt and Sn showed that the drying temperature prior to reduction is an important factor for the final state of this catalyst system. Drying at 550°C prior to reduction seems to yield more reduced Sn than drying at 240°C. High temperature treatment in air probably results in increased contact between Sn and Pt oxide species and thus catalytic reduction of Sn by Pt. This mechanism is different from what is found from the Pt-Re system.

References

1. International Petroleum Encyclopedia Vol 32 (Penn Well Publishing Co, Tulsa, OK 1999)

2. M.J. Sterba and V. Haensel, Ind. Eng. Chem. Prod. Res. Dev. 15, 1 (1976)

3. P.H. Emmet: *Catalysis. Alkylation, Isomerization, Polymerization, Cracking and Hydroreforming* Vol VI (Reinhold Publishing Corporation, New York 1958)

4. H.E. Kluksdahl: U.S. Patent US 3415737 (1968)

5. S. Sivasanker and P. Ratnasamy: Reforming for Gasoline and Aromatics. Recent Developments, in *Catalytic Reforming of Naphtha*, G.J. Antos, A.M. Aitani and J.M.Parera (Marcel Dekker, INC., New York 1995)

6. D.M. Little: *Catalytic reforming* (PennWell Publishing Company, Tulsa 1985)

7. M. Walsh : The Global Phaseout of Leaded Gasoline: A Successful Initiative (1999) http://earthsummitwatch.org/gasoline.html. (Earth Summit Watch Program)

8. G. Martino: Catalysis for oil refining and petrochemistry, recent developments and future trends, Proceedings of the 12th ICC, Granada, Spain, July 9-14 2000 in *Studies in Surface Science and Catalysis*, A. Corma, F.V. Melo, S. Mendioroz and J.L.G. Fierro Vol 130a (Elsevier, Amsterdam 2000)

9. E.L. Hartman, D.W. Hanson and B. Weber, Hydrocarbon Processing 77, (1998)

10. Petroleum Association of Japan: Annual Review 1999 (1999) http://www.paj.gr.jp/html/english/index.html.

11. O. Clause, L. Mank and G. Martino, Proc. World Pet. Congr. 2, 695 (1998)

12. Y.I. Yermakov and B.N. Kuznetsov, J. Mol. Catal. 9, 13 (1980)

13. R.J. Bertolacini and R.J. Pellet: The function of Rhenium in Bimetallic Reforming Catalysts, *in Catalyst Deactivation*, B. Delmon and G.F. Froment (Eds.) Elsevier Scientific Publishing Company, Amsterdam 1980) pp. 73-77

14. J. Margitfalvi, S. Göbölös, E. Kwaysser, M. Hegedüs, F. Nagy and L. Koltai, React. Kinet. Catal. Lett. 24, 315 (1984)

15. Y.M. Zhorov and G.M. Panchenkov, Kinet. Catal. 22, 1058 (1981)

16. R. Burch and A.J. Mitchell, Appl. Catal. 6, 121 (1983)

17. J.M. Parera, J.N. Beltramini, C.A. Querini, E.E. Martinelli, E.J. Churin, P.E. Aloe and N.S. Figoli, J. Catal. 99, 39 (1986)

18. C. Bolivar, H. Charcosset, R. Frety, M. Primet and L. Tournayan, J. Catal. 45, 163 (1976)

19. P. Biloen, J.N. Helle, H. Verbeek, F.M. Dautzenberg and W.M.H. Sachtler, J. Catal. 63, 112 (1980)

20. V.K. Shum, J.B. Butt and W.H. Sachtler, J. Catal. 96, 371 (1985)

21. B.D. McNicol, J. Catal. 46, 438 (1977)

22. N. Wagstaff and R. Prins, J. Catal. 59, 434 (1979)

23. H. Charcosset, R. Frety, G. Leclercq, E. Mendes, M. Primet and L. Tournayan, J. Catal. 56, 468 (1979)

24. B.H. Isaacs and E.E. Petersen, J. Catal. 77, 43 (1982)

25. S.M. Augustine and W.M.H. Sachtler, J. Phys. Chem. 91, 5953 (1987)

26. C.G. Michel, W.E. Bambrick and R.H. Ebel, Fuel Processing Technol. 35, 159 (1993)

27. P. Malet, G. Munuera and A. Caballero, J. Catal. 115, 567 (1989)

28. R. Prestvik, K. Moljord, K. Grande and A. Holmen, J. Catal. 174, 119 (1998)

29. R. Prestvik, B. Tøtdal, C.E. Lyman and A. Holmen, J. Catal. 176, 246 (1998)

30. J.P. Boitiaux, J.M. Devés, B. Didillon and C.R. Marcilly: Catalyst Preparation *in Catalytic Reforming of Naphtha*, G.J. Antos, A.M. Aitani and J.M. Parera (Marcel Dekker, Inc., New York 1995)

31. O.M. Poltorak and V.S. Boronin, Russ. J. Phys. Chem. 40, 1436 (1966)

32. S.M. Davis, F. Zaera and G.A. Somorjai, J. Catal. 77, 439 (1982)

33. J. Barbier, G. Corro, Y. Zhang, J.P. Bournonville and J.P. Franck, Appl. Catal. 13, 245 (1985)

34. M. Boudard, A. Aldag, J.E. Benson, N.A. Dougharty and C.G. Harkins, J. Catal. 6, 92 (1966)

35. G.A. Somorjai and J. Carrazza, Ind. Eng. Chem. Fundam. 25, 23 (1986)

36. G. Lietz, H. Lieske, H. Spindler, W. Hanke and J. Völter, J. Catal. 81, 17 (1983)

37. H. Lieske, G. Lietz, H. Spindler and J. Völter, J. Catal. 81, 8 (1983)

38. R.L. Mieville, J. Catal. 87, 437 (1984)

39. K. Ebitani and H. Hattori, Bull.Chem.Soc.Jpn. 64, 2422 (1991)

40. S.M. Augustine and W.M.H. Sachtler, J. Catal. 116, 184 (1989)

41. L. Chen, Y. Ni, J. Zang, L. Lin, X. Luo and S. Cheng, J. Catal. 145, 132 (1994)

42. R.E. Rausch: U.S. Patent US 4016068 (1977)

43. J.H. Sinfelt: U.S. Patent US 3953368 (1976)

44. G.J. Antos: U.S. Patent US 4101418 (1978)

45. J. Reyes, G. Pecchi and P. Reyes, J.Chem.Research, 318 (1983)

46. P. Arnoldy, E.M. van Oers, O.S.L. Bruinsma, V.H.J. Beer and J.A. Moulun, J. Catal. 93, 231 (1985)

47. R.M. Edreva-Kardjieva and A.A. Andreev, J. Catal. 94, 97 (1985)

48. D.S. Kim and I.E. Wachs, J. Catal. 141, 419 (1993)

49. H.C. Yao and M. Shelef, J. Catal. 44, 392 (1976)

50. M.F.L. Johnson and V.M. LeRoy, J. Catal. 35, 434 (1974)

51. J. Freel, Prepr. Amer. Chem. Soc. Div. Petro. Chem. 18, 10 (1973)

52. M.F.L. Johnson, J. Catal. 39, 487 (1975)

53. A.N. Webb, J. Catal. 39, 485 (1975)

54. H.S. Broadbent, G.C. Campbell, W.J. Bartley and J.H. Johnson, J.Org.Chem. 24, 1847 (1959)

55. P.G. Menon, J. Sieders, F.J. Streefkerk and G.J.M. Van Keulen, J. Catal. 29, 188 (1973)

56. C. Bolivar, H. Charcosset, R. Frety, M. Primet, L. Tournayan, C. Betizeau, G. Leclercq and R. Maurel, J. Catal. 39, 249 (1975)

57. P. Marecot, M. Peyrovi and J. Barbier, C. R. Acad. Sci. Paris 307, 1509 (1988)

58. R. Prestvik : *Characterization of the metal function of a Pt-Re/Al2O3 reforming catalyst*, Doctoral Thesis, The Norwegian Institute of Technology (1995)

59. C. Betizeau, G. Leclercq, R. Maurel, C. Bolivar, H. Charcosset, R. Frety and L. Tournayan, J. Catal. 45, 179 (1976)

60. S.M. Augustine and W.M.H. Sachtler, J. Catal. 106, 417 (1987)

61. V.K. Shum, J.B. Butt and W.M.H. Sachtler, J. Catal. 99, 126 (1986)

62. C.L. Piek, P. Marecot, J.M. Parera and J. Barbier, Appl. Catal. 126, 153 (1995)

63. C.L. Pieck, P. Marecot, C.A. Querini, J.M. Parera and J. Barbier, Appl. Catal. 133, 281 (1995)

64. B.H. Isaacs and E.E. Petersen, J. Catal. 85, 8 (1984)

65. J. Barbier, H. Charcosset, G. Periera and J. Riviere, Appl. Catal. 1, 71 (1981)

66. B.H. Isaacs and E.E. Petersen, J. Catal. 85, 1 (1984)

67. M. Fernández-García, F.K. Chong, J.A. Anderson, C.H. Rochester and G.L. Haller, J. Catal. 182, 199 (1999)

68. D.R. Short, S.M. Khalid and J.R. Katzer, J. Catal. 72, 288 (1981)

69. G. Meitzner, G.H. Via, F.W. Lytle and J.H. Sinfelt, J. Chem. Phys. 87, 6354 (1987)

70. G.H. Via, J.H. Sinfelt, G. Meitzner and F.W. Lytle, Mat. Res. Soc. Symp. Proc. 143, 111 (1989)

71. F. Hilbrig, C. Michel and G.L. Haller, J. Phys. Chem. 96, 9893 (1992)

72. A. Caballero, F. Villain, H. Dexpert, F. LePeltier and J. Lynch, J. Chem. Soc. Faraday. Trans. 89, 159 (1993)

73. A.S. Fung, M.J. Kelley, D.C. Koningsberger and B.C. Gates, J. Am. Chem. Soc 119, 5877 (1997)

74. D. Bazin, H. Dexpert, J. Lynch and J.P. Bournonville, J. Synchrotron Rad. 6, 465 (1999)

75. W.T. Tysoe, F. Zaera and G.A. Somorjai, Surface Sci. 200, 1 (1988)

76. J.H. Onuferko, D.R. Short and M.J. Kelley, Appl. Surf. Sci. 19, 227 (1984)

77. J. Xiao and R.J. Phuddephatt, Coordination Chemistry Reviews 143, 457 (1995)

78. M.J. Kelley, R.L. Freed and D.G. Swartzfager, J. Catal. 78, 445 (1982)

79. Z. Huang, J.R. Fryer, C. Park, D. Stirling and G. Webb, J. Catal. 148, 478 (1994)

80. N. Macleod, J.R. Fryer, D. Stirling and G. Webb, Catal.Today 46, 37 (1998)

81. J.B. Peri, J. Catal. 52, 144 (1978)

82. J.A. Anderson, F.K. Chong and C.H. Rochester, J.Mol.Catal. 140, 65 (1999)

83. J. Beltramini and D.L. Trimm, Appl. Catal. 32, 71 (1987)

84. W.M.H. Sachtler, J.Mol.Catal. 25, 1 (1984)

85. F.H. Ribeiro, A.L. Bonivardi and G.A. Somorjai, Catal. Lett. 27, 1 (1994)

86. S.M. Augustine, G.N. Alameddin and W.H.M. Sachtler, J. Catal. 115, 217 (1989)

87. J. Biswas, G.M. Bickle, P.G. Gray, D.D. Do and J. Barbier, Catal.Rev.-Sci.Eng. 30, 161 (1988)

88. A. Bensaddik, A. Caballero, D. Bazin, H. Dexpert, B. Didillon and J. Lynch, Appl. Catal. 162, 171 (1997)

89. F.M. Dautzenberg, J.N. Helle, P. Biloen and W.M.H. Sachtler, J. Catal. 63, 119 (1979)

90. R. Burch, J. Catal. 71, 348 (1981)

91. H. Lieske and J. Volter, J. Catal. 90, 96 (1984)

92. C. Kappenstein, M. Guerin, K. Lazar, K. Matusek and Z. Paak, J. Chem. Soc. Faraday. Trans. 94, 2463 (1998)

93. R. Bacaud, P. Bussiere and F. Figueras, J. Catal. 69, 399 (1981)

94. Y.-X. Li, K.J. Klabunde and B.H. Davis, J. Catal. 128, 1 (1991)

95. R.E. Lakis, C.E. Lyman and H.G. Stenger, J. Catal. 134, 261 (1995)

96. B.A. Sexton, A.E. Hughes and K. Foger, J. Catal. 88, 466 (1984)

97. S.R. Adkins and B.H. Davis, J. Catal. 89, 371 (1984)

98. Y.-X. Li and K.J. Klaubunde, J. Catal. 126, 173 (1990)

99. C. Meitzner, G.H. Via, F.W. Lytle, S.C. Fung and J.H. Sinfelt, J. Phys. Chem. 92, 2925 (1988)

100. Y.-X. Li, N.S. Chiu, W.H. Lee, S.H. Bauer and B.H. Davis, ACS Symp. Ser. 411, 328 (1989)

101. A. El Abed, S.E. El Qebbaj, M. Guérin, C. Kappenstein, H. Dexpert and F. Villain, J., Chim. Phys. 94, 54 (1997)

102. G.J. Arteaga, J.A. Anderson and C.H. Rochester, J. Catal. 184, 268 (1999)

103. B. Coq and F. Figureras, J. Catal. 85, 197 (1984)

104. Z. Paál, A. Györy, I. Uszkurat, S. Olivier, M. Guérin and C. Kappenstein, J. Catal. 168, 164 (1997)

105. R. Burch and L.C. Garla, J. Catal. 71, 360 (1981)

106. J.H. Sinfelt: Bimetallic Catalysts Discoveries, Concepts, and Applications (Wiley, New York 1983)

107. S. Bhatia, J.N. Beltramini and D.D. Do, Catal.Today 7, 305 (1990)

108. E.A. Blekkan, A. Holmen and S. Vada, Acta.Chem.Scand. 47, 275 (1993)

109. E.A. Stern, Phys.Rev. 10, 3027 (1974)

110. M. Rønning : *Bimetallic Catalysts and Platinum Surfaces Studied by X-ray Absorption Spectroscopy and Scanning Tunneling Microscopy*, Doctoral Thesis, NTNU, Trondheim (2000)

111. L.W. Jossens and E.E. Petersen, J. Catal. 76, 265 (1982)

112. J.A. Cusumano, G.W. Dembinski and J.H. Sinfelt, J. Catal. 5, 471 (1966)

113. F. Frusteri, A. Parmaliana, A. Mezzapica, A.L. Chuvilin, P. Tsiakaras and N. Giordano, Reaction Kinetics Catalysis Letters 1, 315 (1992)

114. C.G. Michel, W.E. Bambrick, R.H. Ebel, G. Larsen and G.L. Haller, J. Catal. 154, 222 (1995)

115. A. Bensaddik, D. Bazin, H. Dexpert, A. Caballero, J. Lynch and B. Didillon, J.Phys. 6, C4 (1996)

116. C.E. Lyman, J.I. Goldstein, D.B. Williams, D.W. Ackland, S. von Harrach, A.W. Nicholls and P.J. Statham, Journal of microscopy 176, 85 (1994)

117. J. Barbier, D. Bahloul and P. Marecot, J. Catal. 137, 377 (1992)

118. S.R. Bajaj, P. Pal, J.K. Gupta, L.D. Sharma and G.M. Dhar, Stud.Surf.Sci.Catal. 113, 365 (1998)

119. F.B. Passos, A.G.A. Donato and M. Schmal, J. Catal. 178, 478 (1998)

Appendices

Appendix 1: Reduction program

Appendix 2: Calculation of the equilibrium conversion of dehydrogenation of MCH

Appendix 3: Effect of the temperature and catalyst particle size on the conversion of MCH

Appendix 4: Paper I

Appendix 5: Paper II

Appendix 6: Paper III

Appendix 7: Paper IV

Appendix 1

Table A.1. *Reduction program for samples heated at 500 °C or not heated prior to reduction*

Reduction temperature interval	Heating rate	H_2O in H_2
25 - 480 °C	0.2 °C/min	
25 - 480 °C	0.8 °C/min	
25 - 480 °C	3.3 °C/min	
25 - 480 °C	0.8 °C/min	500 ppm
25 - 480 °C	0.8 °C/min	1000 ppm
25 - 480 °C	0.8 °C/min	1500 ppm
200 - 480 °C	0.2 °C/min	
200 - 480 °C	0.8 °C/min	
200 - 480 °C	3.3 °C/min	
400 - 480 °C	0.2 °C/min	
400 - 480 °C	0.8 °C/min	
400 - 480 °C	3.3 °C/min	
200 - 480 °C	0.8 °C/min	1500 ppm
400 - 480 °C	0.8 °C/min	1500 ppm
25 - 510 °C	0.8 °C/min	
25 - 530 °C	0.8 °C/min	
200 - 530 °C	0.8 °C/min	
400 - 530 °C	0.8 °C/min	

Appendix 2

Calculation of MCH equilibrium conversion $MCH \Leftrightarrow Toluene + 3H_2$

Reaction conditions: T = 543 K, P_{tot} = 1.75 bar , H_2/MCH = 35 mol/mol

At equilibrium:

$\Delta G_r = 0 \quad \Rightarrow \Delta G_f^0 = -RT \ln K$

Basis:

$n_{i,MCH} = 1$

$n_{i,H2} = 35$

Equilibrium composition:

$n_{2,MCH} = 1 - x$

$n_{2,Tol} = x$

$n_{2,H2} = 3x + 35$

Total amount of components at equilibrium:

$n_{tot} = 3x + 36$

Equilibrium constant expression:

$$K = \frac{(x)(3x+35)^3}{(1-x)(3x+36)^3} \cdot \left(\frac{P^{tot}}{P^0}\right)^3 \qquad K \approx 5{,}12\frac{x}{1-x}$$

Calculation of ΔG^0

$\Delta G^0 = \Delta G^0_{f(Tol)} + 3\Delta G^0_{f(H2)} - \Delta G^0_{f(MCH)} = 194{,}5$ kJ/mol + 0 – 206,4 kJ/mol

$\Delta G^0 = -11{,}9$ kJ/mol

Calculation of K

$K = e^{(-\Delta G/RT)} \qquad K = e^{(11900/8{,}314\cdot 543)} = 13{,}96 \qquad \Rightarrow$

$x \approx 0{,}73$

Appendix 3

Effect of the temperature on the MCH conversion

Table A.2. *Conversion of MCH at different temperatures*

Reaction temperature [°C]	Initial conversion (1st pulse) [%][a]
255	31
270	47
285	60

Effect of the catalyst particle size on the MCH conversion

Table A.3. *Conversion of MCH at different catalyst particles sizes*

Particle diameter [mm]	Initial conversion (1st pulse) [%][a]
<0.075	50
0.25-0.075	52

a= average values (± 4 %)

Paper I

Studies in Surface Science and Catalysis 130
A. Corma, F.V. Melo, S. Mendioroz and J.L.G. Fierro (Editors)

Bimetallic nano-particle formation in the Pt-Re reforming catalysts revealed by STEM/EDX, XANES/EXAFS and chemical characterization techniques. Effects of water and chlorine.

T. Gjervan [a], M. Rønning [a], R. Prestvik [b], B. Tøtdal [c], C.E. Lyman [d] and A. Holmen [a]

[a]Dept. of Chemical Engineering, Norwegian University of Science and Technology (NTNU), 7491 Trondheim, Norway

[b]SINTEF Applied Chemistry, 7465 Trondheim, Norway

[c]Dept. of Physics, NTNU, 7491 Trondheim, Norway

[d]Dept. of Materials Science and Engineering, Lehigh University, Bethlehem, PA 18015, USA.

The effect of various concentrations of water and chlorine on the formation of bimetallic particles on commercial Pt-Re/Al_2O_3 reforming catalysts has been investigated. STEM combined with EDX has been used to directly measure the degree of "alloy" formation in the metal particles. XANES/EXAFS analysis was employed to further elaborate the effect of drying prior to reduction. As an indirect measure of bimetallic particles, chemical characterization techniques such as cyclopentane hydrogenolysis and hydrogen chemisorption were used. The beneficial effect of water on the formation of bimetallic particles has been confirmed. No significant effect of the level of chlorine content prior to reduction was found.

1. INTRODUCTION

Pt-Re/γ-Al_2O_3 catalysts are widely used commercially in semi-regenerative reforming units for upgrading refinery naphtha streams. Rhenium is not active in the main reforming reactions, but markedly improves the long-term stability of the catalyst. The most common view for explaining the effect of rhenium has been that of Pt-Re alloy formation and interaction of rhenium in such a bimetallic structure with sulfur. It has been proposed that the formation of bimetallic particles occurs when the catalyst surface is hydrated prior to or during the reduction step. On a hydroxylated alumina surface the rhenium oxide species are mobile and can migrate to prereduced platinum atoms where atomic hydrogen is supplied for its reduction. If the catalyst is dehydrated prior to reduction, the rhenium oxide is immobilized and is reduced at higher temperatures typical of monometallic rhenium. Consequently, less bimetallic interaction is achieved. In addition to water, the chlorine content of the catalyst has also been regarded as critical for the formation of alloy (bimetallic) particles although the conclusions are diverse (1,2). Hydrogenolysis has been used as a probe reaction to distinguish between different degrees of alloy formation in catalyst samples (3). Previous results also indicate that alloying affects the hydrogen chemisorption capacity (4,5). Due to the very high metal dispersions and small particle sizes (typically $\leq$1nm) in these catalysts and the limited sensitivity of conventional instruments, direct evidence for alloy formation has been difficult

to obtain. Until recently no method existed for direct elemental analysis of such individual particles. However, in a recent study (6) it was possible for the first time to obtain such evidence using a STEM/EDX instrumentation specifically designed for high spatial resolution elemental analysis by x-ray emission spectrometry.

In the present work, STEM/EDX and EXAFS/XANES have been used together with chemical characterization techniques such as hydrogen chemisorption and cyclopentane hydrogenolysis to further elaborate the effects of water and chlorine on the metal function of a Pt-Re/γ-Al_2O_3 catalyst.

2. EXPERIMENTAL

2.1 Catalyst pretreatment

The catalyst examined was the EUROPT-4 (Akzo) 0.3-0.3 wt.% Pt-Re/γ-Al_2O_3. As received, it contains 1.0 wt.% chlorine. Samples with 0.65, 1.10 and 1.50 wt.% chlorine were made by oxychlorination at 500°C using air with different H_2O/Cl ratios. All oxychlorinated samples were dried at 510 °C before a standard reduction from 200 to 480°C in dry or moist (5000 ppm H_2O) hydrogen. Drying at different temperatures (240°C or 550°C) before the reduction varied the water content of the fresh samples (not oxychlorinated). One sample was reduced without drying, and to investigate sintered particles a sample was dried at 680 °C in nitrogen (N_2).

2.2 Test reaction

Cyclopentane hydrogenolysis was performed at 250°C and low conversions (<10%) where the cyclopentane (CP) and hydrogen feed was pulsed (1.2 ml) with regular intervals in a Helium flow (250 ml/min) over the catalyst bed (0.15 g) using a H_2/CP ratio of 12.

2.3 Hydrogen chemisorption measurements

Hydrogen chemisorption was measured using a Micromeretics ASAP 2010 instrument. The hydrogen to platinum ratio (H/Pt) is used both as a measure of the platinum dispersion and the number of platinum-platinum neighbors. The chemisorption measurements were performed at 25 °C.

2.4 STEM/EDX particle analysis

The STEM/EDX particle analysis was performed at Lehigh University with a VG microscope HB-603. The particle sizes were found from the STEM images, whereas the EDX data yielded information on the composition. Detailed description of the analysis procedure is given elsewhere (6).

2.5 EXAFS/XANES spectroscopy

The samples for EXAFS analysis were dried and reduced in a quartz flow-through reactor, flushed with He and sealed in quartz capillary tubes before transported to the synchrotron radiation facility. XAS data were collected at the Swiss-Norwegian Beamline (SNBL) at the ESRF, France and at Beamline X11-A at the National Synchrotron Light Source, NSLS, Brookhaven National Laboratory, USA. At SNBL, spectra were recorded in the fluorescence mode at both the Pt L_{III} edge (11 564 eV) and the Re L_{III} edge (10 535 eV). A channel-cut Si(111) monochromator was used to scan the X-ray spectra. The beam currents ranged from 130 - 200 mA at 6.0 GeV. Higher-order harmonics were rejected by means of a chromium-coated mirror. At NSLS, the station was equipped with a double crystal Si(111)

monochromator and the storage ring operated at 2.5 GeV, with a ring current of 180-350 mA. Higher order harmonics were suppressed by tuning the monochromator crystals to 50% of maximum intensity. Details on the data analysis are given elsewhere (7).

3. RESULTS AND DISCUSSION

3.1 Influence of the drying temperature

Previously obtained STEM/EDX and EXAFS data (6,7) shown in Table 1, strongly suggest that the amount of water (as given by the drying temperature) on the catalyst before reduction at 480°C markedly changes the degree of alloy formation The degree of alloying, given by the average weight fraction of platinum (C_{Pt}) in the metal particles, increases with decreasing drying temperatures. A possible mechanism for this alloy formation is that water, in form of hydroxyl groups on the surface, provides mobility for rhenium oxide species that may be catalytically reduced when coming into intimate contact with metallic platinum.

Table 1
Effect of drying conditions

Sample	Pre-treatment/ Drying temperature	STEM/ EDX C_{Pt}	STEM $D_{Particle}$ [nm]	EXAFS C_{Pt}	EXAFS $D_{Particle}$ [nm]	CP conv. [%]	C_1 sel.	H/Pt
1	None/ Direct reduction	0.7	0.9	0.7	<1.0	1.7	1.1	0.23
2	240 °C, air	0.7	1.0	0.7	<1.0	9.0	4.9	0.31
3	550 °C, air	0.9	1.0	0.7	<1.0	3.9	2.0	0.44
4	680 °C, N_2	1.0	2.3	1.0	<1.0	*	*	0.16

Cyclopentane (CP) hydrogenolysis experiments confirm this trend, as well as the hydrogen chemisorption data. An increase of the H/Pt ratio of sample 1, 2, and 3 is interpreted as an indication of less intimate contact between Pt and Re, and thus less alloy formation. However, sample 1 (not dried) shows low CP conversion and low methane (C_1) selectivity which accounts for the lower degree of alloy formation compared to sample 2 (dried at 240 °C). The catalyst samples have been stored in sealed bottles after calcination at the manufacturer, but they have nevertheless adsorbed some water from the atmosphere (~5 wt.%). The results from the Re L_{III} EXAFS analysis of sample 1 (7) indicate that a smaller fraction of rhenium is completely reduced when the sample is not dried before reduction. The beneficial effect of water in bimetallic particle formation seems clear, allthough *too much* water may suppress the reduction of rhenium as stated earlier (2). From the STEM/EDX analysis and hydrogen chemisorption measurements on this sample, it is clear that the metal particles are very small and contain platinum and rhenium in intimate contact. The difference in catalytic performance between sample 1 and sample 2 is therefore attributed to the degree of reduced rhenium.

There is a difference in average particle diameter of sample 4 when measured by the two techniques EDX and EXAFS. This difference may be due to the fact that EXAFS is able to discriminate between metal and metal oxide particles, and that the outermost surface of large platinum particles is being easily passivated leading to smaller metal particles (7).

3.2 Influence of the chlorine content

The role of the chlorine content has been discussed previously (1,2), but as already mentioned, conclusions are diverse. In the present work three samples with different Cl-contents were analyzed by the combined STEM/EDX instrument, by H_2 chemisorption and by CP hydrogenolysis experiments.

The metal particles were observed as diffuse white spots on the annular dark-field STEM micrograph. Information about the composition of the particles was obtained by collecting EDX-spectra of 100 – 120 particles for each sample. Particle composition – size distribution diagrams, such as the ones shown in Figure 1 - 4, were made for all the samples.

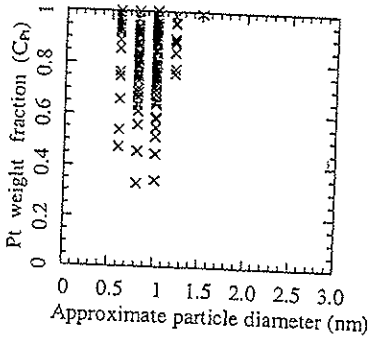

Fig.1. Approximate particle diameter and measured Pt fraction of individual metal particles in sample 5 (0.65 wt% Cl, dry reduction).

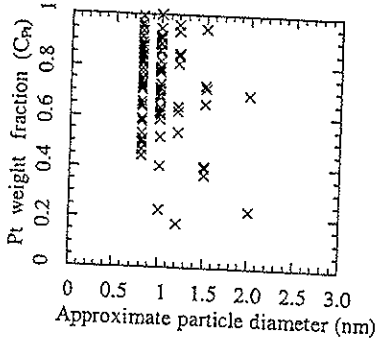

Fig.2. Approximate particle diameter and measured Pt fraction of individual metal particles in sample 7. (1.50 wt% Cl, dry reduction).

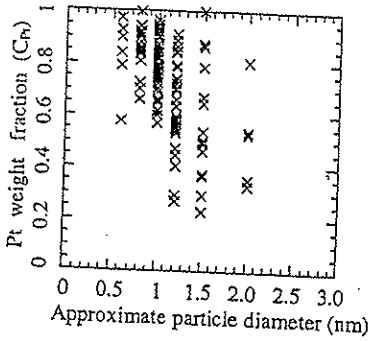

Fig.3. Approximate particle diameter and measured Pt fraction of individual metal particles in sample 8. (0.65 wt% Cl, moist reduction).

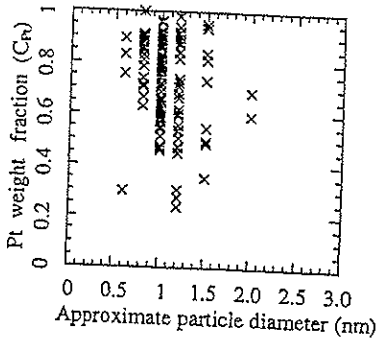

Fig.4. Approximate particle diameter and measured Pt fraction of individual metal particles in sample 10. (1.50 wt% Cl, moist reduction).

The average particle size and the average metal composition were calculated for each sample based on the data collected from the STEM/EDX analysis. These results give an indication of the state of the metal particles on the catalyst after reduction. From Figure 1 – 4, it is obvious that the averages are approximate, and care has to be taken when interpreting these results. However, it is possible to see trends toward differences in bimetallic formation by studying such diagrams.

Table 2
Effect of chlorine content, reduction in dry H_2

Sample	Chlorine level	STEM/ EDX C_{Pt}	STEM $D_{Particle}$ [nm]	CP conv. [%]	C_1 sel.	H/Pt
5	0.65	0.8	0.9	2.7	2.2	0.43
6	1.10	0.8	1.0	3.6	1.7	0.43
7	1.50	0.7	1.0	3.1	1.5	0.59

In Table 2, the calculated average particle platinum composition and the particle size are presented for catalysts with different chlorine levels reduced in dry H_2. The composition – size diagram of sample 5 and 7 is shown in Figure 1 and 2. The different chlorine levels do not show any differences with respect to the bimetallic formation. The EDX data (C_{Pt}) suggests a slight increase in the alloying degree with increasing chlorine content when reducing the catalyst under dry conditions (dried at 510 °C in air). However, the cyclopentane hydrogenolysis data and the hydrogen chemisorption results show an opposite trend suggesting that sample 7 with the highest chlorine content has the lowest degree of alloy formation.

After reducing the dry oxychlorinated samples in moist hydrogen (1500 ppm H_2O), STEM/EDX measurements indicate the formation of somewhat larger particles with higher Re contents as compared to the catalysts reduced in dry hydrogen (Table 3). This is also reflected in Figure 3 and 4. For these samples, the selectivity to methane increases significantly indicating more alloyed (bimetallic) particles. This shows the beneficial effect of moisture in the reduction process also when water is introduced during reduction after drying the catalyst at a rather high temperature (510 °C). High temperature combined with moisture may introduce some stripping of chlorine, and the removal of chlorine and subsequent sintering of the platinum crystallites. Due to instrumental limitations, volumetric chemisorption measurements were not performed for the samples 8 – 10.

Table 3
Effect of chlorine content, reduction in moist H_2

Sample	Chlorine level	STEM/ EDX C_{Pt}	STEM $D_{Particle}$ [nm]	CP conv. [%]	C_1 sel.	H/Pt
8	0.65	0.7	1.1	7.8	5.9	*
9	1.10	0.7	1.2	5.5	5.0	*
10	1.50	0.7	1.1	7.0	5.0	*

4. CONCLUSIONS

Drying the catalyst at higher temperatures in the absence of air inhibits the transport of mobile rhenium species on the surface and hence restricts intimate contact between the two metals. The EXAFS data analysis shows that moderate drying temperatures and air atmosphere provide the best conditions for transport of mobile rhenium species on the surface and alloy formation of Pt and Re. These trends are evident also from the basis of the STEM/EDX analysis performed.

The chlorine level of the catalyst samples was varied in the range 0.65 to 1.50 wt %, but only limited influence of the content was found when analysing with techniques such as STEM/EDX, model reactions and hydrogen chemisorption.

ACKNOWLEDGEMENTS

The financial support of the Norwegian Scientific Foundation VISTA and the Norwegian Research Council (NFR) is gratefully acknowledged. The assistance by Mr. D.W. Ackland with the STEM images is very much appreciated.

REFERENCES

1. Malet, P., Munuera, G. and Caballero, A., J. Catal. 115, (1989) 567.
2. Michel, C. G., Bambrick, W. E. and Ebel, R. H., Fuel Proc. Technol. 35, (1993) 159.
3. Augustine, S. M. and Sachtler, W. M. H., J. Phys. Chem. 91, (1987) 5953.
4. Isaacs, B. H. and Petersen, E. E., J. Catal. 85, (1984) 1.
5. Prestvik, R., Moljord, K., Grande, K. and Holmen, A., J. Catal. 174, (1998) 119.
6. Prestvik, R.Tøtdal, B., Lyman, C.E., and Holmen, A., J. Catal. 176, (1998) 246.
7. Rønning, M., Gjervan, T., Prestvik, R., Nicholson, D.G., and Holmen, A. *in prep.*

Paper II

Influence of pretreatment temperature on the bimetallic interactions in Pt-Re/Al_2O_3 reforming catalysts studied by X-ray absorption spectroscopy

Magnus Rønning,[a] Torbjørn Gjervan,[a] Rune Prestvik,[b] David G. Nicholson[c] and Anders Holmen[a]

[a]*Department of Chemical Engineering, Norwegian University of Science and Technology (NTNU), N-7491 Trondheim, Norway*

[b]*SINTEF Applied Chemistry, N-7465 Trondheim, Norway*

[c]*Department of Chemistry, Norwegian University of Science and Technology (NTNU), N-7491 Trondheim, Norway*

Running title:

Influence of pretreatment on reforming catalysts

Corresponding author:

Professor Anders Holmen

Department of Chemical Engineering, Norwegian University of Science and Technology (NTNU), N-7491 Trondheim, Norway

Fax: +47 73 59 50 47

E-mail: holmen@chembio.ntnu.no

Abstract

The influence of pretreatment temperature on the metal function of a commercial Pt-Re/Al_2O_3 reforming catalyst was studied by X-ray absorption spectroscopy. By simultaneously examining the rhenium L_{III} and platinum L_{III} EXAFS data, the bimetallic interaction and the metal – support interaction can be distinguished from the overall spectrum. The results show that if the catalyst is dried in air at temperatures ≤ 500°C before reduction at 480°C, bimetallic particles of platinum and rhenium are formed. Drying at higher temperatures and in absence of air inhibits the transport of mobile (rhenium) species on the surface causing no intimate contact between the two metals. Platinum L_{III} EXAFS data show that the average particle size of the bimetallic particles on the alumina surface is less than 10 Å. The results from the rhenium L_{III} EXAFS analysis confirm that rhenium is not completely reduced to metallic rhenium after reduction, with a significant fraction of the rhenium present in low, positive oxidation states and in intimate contact with the support. The EXAFS data are consistent with a structural model of flat rhenium metal particles with smaller platinum particles situated at the boundary of the rhenium particles, and that moderate heating in presence of air (i.e. moist) provide the best conditions for transport of mobile rhenium species on the surface, and hence alloy formation.

Keywords

Catalyst pretreatment, platinum catalysts, rhenium, catalytic reforming, EXAFS, bimetallic interaction

Introduction

The catalytic reforming of naphtha is usually performed using a bifunctional catalyst containing both a hydrogenating metal and an acid function. The metal function is platinum together with another component such as rhenium, tin, iridium or germanium. Chlorine promoted alumina with high surface area provides the acid function. It has been demonstrated that the addition of rhenium to Pt/Al_2O_3 leads to a catalyst with greater stability and improved selectivity [1]. However, the structure and exact role of rhenium in Pt-rhenium catalysts has been a matter of controversy. It has been proposed that metallic rhenium provides sites for hydrogenolysis of coke deposits [2] and that rhenium acts independently of platinum and is able to convert coke precursors into harmless products [3]. Others state that rhenium anchors platinum to the alumina support and thereby stabilise the platinum dispersion [4]. The structure insensitive conversion of methylcyclohexane (MCH) has been used as a measure of the platinum dispersion in the catalysts.

The most common explanation of the properties of the catalyst is based on Pt – Re alloy formation [5] and the interaction of such an alloy with sulphur [6-9]. It has been shown that the hydrogenolysis activity over bimetallic catalysts is significantly higher than over its monometallic counterparts [5,10,11] and also higher than for physical mixtures of Pt/Al_2O_3 and Re/Al_2O_3 [12]. Hydrogenolysis is a structure sensitive reaction and has therefore been used as a probe reaction to determine Pt – Re alloy formation. In addition, TPR-studies [13-15] have indicated possible reduction mechanisms leading to the formation of bimetallic Pt – Re metal particles. Previous studies indicate that the treatment of the catalyst prior to reduction strongly modifies the reducibility of rhenium and the

extent of Pt – Re alloy formation [16–19]. Varying degrees of alloy formation have been confirmed both by hydrogenolysis activity measurements and by hydrogen chemisorption experiments [17]. More direct evidence of alloy formation from physical characterisation techniques such as IR and XPS has been difficult to obtain due to the low metal loading and high metal dispersion in the Pt – Re reforming catalysts.

Studies using EDX and TEM [20,21] conclude that no rhenium can be detected in the platinum particles in the bimetallic system after reduction at 400°C, although the yields from reforming experiments indicate that a significant fraction of the rhenium must be present in the metallic state. However, in a recent study [18] a high resolution combined STEM and EDX instrument were able to detect bimetallic Pt – Re particles. It was established that bimetallic interaction in Pt-Re/Al_2O_3 catalysts is highly dependent on the pretreatment conditions. The highest degree of Pt – Re interaction was found when the catalyst was not dehydrated prior to reduction, while drying in N_2 at high temperatures before reduction cause sintering of platinum particles and low bimetallic interaction. Four different drying conditions were studied [18].

X-ray absorption spectroscopy (XAS) is a powerful technique for obtaining detailed information about the metal containing species in highly dispersed systems lacking long range order. Several XAS studies on Pt-Re/Al_2O_3 have been reported dealing with different aspects concerning the metal function of the catalyst system [22-30]. Recent studies have made use of TPR and binding energies from the XAS spectra to establish the correlation between calcination temperatures and bimetallic interaction [23]. It is reported that rhenium is completely reducible to metallic rhenium if the samples are calcined at

low temperatures and that the reduction step involves a rhenium intermediate with oxidation state close to +I [28] leading to complete alloying of platinum and rhenium. Michel *et al.* [24] found that the metal loadings and the Re/Pt ratio affect the reduction kinetics of rhenium but do not affect the final oxidation state of rhenium, and that even if the catalyst precursor is dried, all rhenium is coreduced with platinum at low temperatures when the catalyst contains ca. 1 wt% chlorine.

Successful second metal shell fitting has been achieved on catalysts with higher metal loading and on other types of oxide supports [26]. Fung *et al.* [31] used EXAFS spectroscopy to characterise Pt – Re clusters supported on γ-Al_2O_3 prepared from $[Re_2Pt(CO)_{12}]$, demonstrating that by using k^0 weighting (k being the wave vector) contributions from metal-support interactions and bimetallic interaction (Pt – Re) may be distinguished in the EXAFS data analysis. They conclude that the catalyst reduced at 400°C in H_2 contained a considerable fraction of bimetallic particles consisting of Re_4Pt_2 entities and displaying high dispersion (average particle size less than 10 Å) and strong interaction between rhenium atoms and the support. For further details, we refer to Xiao and Puddephatt [32], who have published a comprehensive review on the structure and reactivity of Pt – Re clusters.

There are several experimental obstacles associated with XAS data collection on this catalyst system, with the most important being low metal loading (0.3 wt%). Thus, a corresponding series of samples containing higher metal loading were made; A sample containing 0.9 wt% platinum and 0.9 wt% rhenium, a sample with 0.9 wt% platinum only and a sample with 1.75 wt% rhenium only (all on the same support material), were made

in order to make the data analysis more reliable. Samples with metal loadings as low as 0.3 wt% require the spectra to be recorded in the fluorescence mode rather than transmission. Furthermore, interference from overlapping EXAFS regions excludes part of the EXAFS region associated with the platinum L_{III} and L_{II} absorption edges [25]. Accordingly, one can either choose to use the limited EXAFS region associated with the platinum L_{III} and L_{II} edge or use the EXAFS associated with the platinum L_I edge which is not affected by intervening rhenium edges but exhibits a considerably weaker signal compared to the L_{III} edge signal. By comparing preliminary data for all three platinum L edges, data associated with the platinum L_{III} adsorption edge (11 565 eV) were found to be most suitable for this EXAFS study. Due to the similarity in backscattering properties for the two noble metals involved, simultaneous investigations of data taken from representative reference systems and the use of both k^0 and k^3 weighting schemes are important for the deconvolution of contributions from the different backscatterers [31]. We report here an examination of samples from 4 different pretreatment procedures by using EXAFS spectroscopy.

Experimental

Catalyst preparation

The standard EUROPT-4 commercial catalyst (CK433) containing 0.3wt% platinum and 0.3wt% rhenium supported on γ-Al_2O_3 was manufactured by Akzo, Holland. The chlorine loading was 0.95 wt%. The pre-calcined EUROPT-4 catalyst extrudates were finely grounded and sieved to give a particle size fraction of 0.25-0.075 mm. The samples containing 0.9 wt% platinum and 0.9wt% rhenium were prepared in the following

manner: The support material (γ-alumina, CK 300, with specific surface area of 188 m^2/g and pore volume of 0.50 cm^3/g) was dried at 120°C over night. A controlled amount of $H_2PtCl_6 \cdot H_2O$ was dissolved in HCl (0.2 M) and impregnated on the support (incipient wetness) in order to obtain 0.9 wt% platinum on the alumina. After calcination in air at 450°C for 4 hours, the catalyst was impregnated with an aqueous solution of $(NH_4)ReO_4$ to yield 0.9 wt% rhenium, before calcination in air at 450 °C for 4 hours.

Catalyst pretreatment procedure

In order to use the allocated beam time at the ESRF and Brookhaven laboratories as efficiently as possible the samples were dried and reduced *ex situ* in our home laboratory. After reduction, the samples were sealed in quartz capillary tubes as described below to prevent exposure to air. This procedure avoids time-consuming *in situ* pretreatment at the synchrotron facility. In order to verify that the sealing procedure was successful, some of the samples were reduced *in situ* using an environmental cell developed by Lytle *et al.* [33].

Pretreatment was carried out in a standard apparatus equipped with *Alltech* molsieves and O_2-traps for gas purification. Steady gas flows (30 ml/min) were maintained by using mass-flow controllers. The catalyst was placed on a quartz sinter inside a tubular flow-through quartz microreactor with quartz capillary tubes (from *Glas Technik & Konstruktion*, Germany) with outer diameter 2 – 3 mm and wall thickness of 0.02 mm attached to the reactor wall. The sample was heated to the desired temperatures using a furnace equipped with a temperature controller. Four different drying conditions prior to reduction at 480°C for 1 hour using a heating rate of 0.8°C/min were examined. After the

reduction was finished the reactor was flushed with helium for 30 minutes and cooled down to room temperature. The reactor was sealed off at both ends using stainless steel valves and turned upside down to allow the powdered sample to enter the capillary tubes. Using a relatively narrow sieve fraction of the catalyst powder (0.25 – 0.075 mm), easy filling and uniform distribution of the sample inside the capillary tube are ensured. The quartz tube containing the sample was sealed using a high temperature gas flame, and detached from the reactor. The inert atmosphere inside the reactor and the relatively high flame temperature (>1200°C due to the high melting point for quartz) prevented oxidation of the catalyst sample captured inside the capillary tube. In order to reduce heat transfer to the sample in the capillary, the length of sample material were such that 2 – 3 cm of empty capillary separated the sample from the flame. A summary of the samples involved and their characteristics is given in Table 1. The volumetric hydrogen chemisorption measurements were performed in a Micromeretics ASAP 2010 instrument at 25°C.

XAS measurements

XAS data were collected using the facilities of the Swiss-Norwegian Beamline (SNBL) at the European Synchrotron Radiation Facility (ESRF), France and at Beamline Station X11-A at the National Synchrotron Light Source (NSLS), Brookhaven National Laboratory, USA.

At SNBL, spectra were obtained on station EH1 at the platinum L_{III} edge (11 564 eV) and the rhenium L_{III} edge (10 535 eV). A channel-cut silicon(111) monochromator with an unfocussed beam was used to scan the X-ray spectra. The beam currents ranged from 130 - 200 mA at 6.0 GeV. Higher order harmonics were rejected by means of a chromium-

coated mirror angled at 3.5 mrad to give a cut-off energy of approximately 14 keV. The maximum resolution ($\Delta E/E$) of the Si(111) bandpass is 1.4×10^{-4} using a beam of size 0.6 $\times$ 7.2 mm as defined by the slits in the station. Ion chamber detectors with their gases at ambient temperature and pressure were used for measuring the intensities of the incident (I_0), transmitted (I_t) and fluorescent (I_f) X-rays. The detector gases were as follows: I_0, detector length 17 cm, 100% N_2; I_t, length 31 cm, 35% Ar, 65% N_2; I_f (Lytle detector, see below), 100% Ar.

XAS data were also collected at Beamline Station X11-A at Brookhaven National Synchrotron Light Source (NSLS), USA. The station is equipped with a double crystal silicon(111) monochromator and the storage ring is operated at 2.5 GeV with a ring current of 180-350 mA. The beam size was defined to be 0.5 x 10 mm and the resolution approximately 2.0×10^{-4} at the actual energies. Higher order harmonics were suppressed by tuning the monochromator crystals to 50% of maximum intensity.

The fluorescent radiation were collected using a detector of the type developed by Lytle *et al.* [33]. The signal-to-noise ratio was enhanced using a set of soller slits and Zn (3μ) and Ga (3μ) filters for rhenium and platinum edges, respectively. Due to the low metal loading, several scans were taken and summed for each sample. The energy calibration was checked by measuring the spectrum of a platinum foil (thickness 0.003 mm) and a rhenium foil (thickness 0.0125 mm) with the energy of the first inflection point being defined as the edge energy. The raw, unfiltered Re L_{III} and Pt L_{III} EXAFS spectra of samples A – D are shown in Figure 1.

EXAFS Data Analysis

The data were corrected for dark currents, converted to *k*-space, summed and background subtracted to yield the EXAFS function $\chi(k)$ using the *EXCALIB* and *EXBACK* programs [34]. Model fitting was carried out with *EXCURV90* using curved-wave theory and *ab initio* phase shifts [34,35]. During the least squares fitting it is important to minimise correlation effects between the parameters that strongly affect the EXAFS amplitude and those that influence the frequency of the EXAFS oscillations. Therefore, the EXAFS spectra were least squares fitted in *k* space using k^0 and k^3 weighted data. By carrying out this procedure on appropriate reference compounds as well as for the unknown spectra, more accurate coordination numbers can be obtained than what otherwise is the case. The errors in the refined parameters [36-38] are estimated to be 10% in coordination number (N), 1% in distance (R), 10% in Debye-Waller type factors ($2\sigma^2$) and 10% in the photoelectron energy at zero wave vector (E_0). As an indication on the quality of the fit, the residual index, R_χ (%) is defined as:

$$R_\chi = \frac{\sum_i [(\chi_i^{exp} - \chi_i^{calc})k^{WT}]^2}{\sum_i [(\chi_i^{exp})k^{WT}]^2} \times 100\%$$

The k^3 weighting scheme compensates for the diminishing photoelectron wave at higher *k* values. Low *k* weighting also enhances the contribution from lighter backscattering atoms such as oxygen, and thereby allowing metal-support interactions to be included in the analysis. However, due to overlapping EXAFS regions for the platinum L_{III} and rhenium L_{II} edges, platinum L_{III} spectra have to be truncated at approximately 9 $Å^{-1}$. Our approach to the data analysis was similar to that used by Fung *et al.* [31]. They demonstrated that by

analysing the XAFS data using k^0 weighting, it is possible to distinguish Pt – Re from the Pt – Pt and Re – Re interactions. The parameters obtained by Fung *et al.* have been used as first guesses for the bimetallic interactions due to the lack of suitable model compounds for the Pt – Re and Re – Pt scattering pairs. The preliminary data analysis involved testing models that include contributions from Pt, Re and O scatterers for both platinum and rhenium EXAFS data. Due to the narrow data range (3.5 $Å^{-1} < k < 9.0$ $Å^{-1}$) for the platinum L_{III} data, the distance (R) and disorder ($2\sigma^2$) for the Pt – Re coordination were kept fixed at the values obtained from the rhenium data analysis. This will keep the number of floating parameters (n) within the definition of the Nyquist criterion [39]:

$$n = \left(\frac{2\Delta k \Delta r}{\pi} \right) + 1$$

Tables 2 and 3 summarise the data ranges and Fourier filtering ranges used in the EXAFS data analysis. In addition to the platinum and rhenium metal foils, ReO_3, $(NH_4)ReO_4$ (both the solid salt and an aqueous solution containing ReO_4^-) and PtO_2 were used as model compounds to check the validity of the *ab initio* phase shifts and establish the general parameters *AFAC* (amplitude reduction factor) and *VPI* (accounts for inelastic scattering of the photoelectron) [34]. Structural parameters for the reference compounds [40-43] are listed in Table 4. The unreduced catalyst samples with higher metal loading (0.9wt%) were used to check the validity of the amplitudes obtained from reference compounds measured in transmission mode for use on the catalyst samples recorded in fluorescence mode.

XANES profile analysis

The XAS data analysis program *WinXAS* [44] was used for examining the XANES spectra of the reduced samples. The method of using a linear combination of the near-edge profiles from known reference compounds was used to obtain information about the composition of the samples of different pretreatment procedures. In order to establish the degree of reduction in the reduced samples, the edge profiles were analysed by linear combination of the reference profiles from the respective metal foil and the catalyst sample prior to reduction.

Results and discussion

EXAFS Analysis

The results from the rhenium L_{III} and platinum L_{III} EXAFS analysis are listed in Tables 5 and 6, respectively. The k^0 fitted rhenium EXAFS spectra of sample A through D together with their Fourier transforms are shown in Figure 2, and the platinum spectra of the same samples are presented in Figure 3. For the rhenium EXAFS, a structural model including four shells, Re – Pt, Re – Re and two different Re – O distances associated with Re(+VII) oxide species and support interaction, respectively, resulted in good fit and realistic structural parameters for all samples except sample D, which did not contain the contribution from the Re – Pt shell. The platinum spectra of samples A, B and C were best fitted using a model constructed from Pt – Re, Pt – Pt and one single Pt – O contribution, the latter originating from metal – support interaction. The EXAFS spectrum of sample D, consistently lacking the bimetallic interaction, was modelled by one Pt – Pt distance and two different Pt – O contributions.

The relatively large Re – Re and Re – Pt coordination numbers show that the rhenium containing metal particles of the samples in this study are significantly larger than the rhenium containing particles in the similar catalysts studied by Fung *et al.* [31]. This is also reflected in the EXAFS spectra in Figure 2, where the oscillations persist as far out as $k = 13$ Å^{-1}. The oscillations may also be affected by the extent of alloy formation in the metal particles since the Re – Re and the Re – Pt signals are out of phase within the region 10 – 13 Å^{-1} [31]. The total metal-to-metal coordination is 6 – 9 atoms for all of the samples except sample D, which is coordinated to only 1.5 metal atoms. A relatively high proportion of the rhenium atoms in sample D is not completely reduced, and therefore exhibits relatively high coordination to oxygen and thus correspondingly lower metallic coordination. Samples A and C display more composite rhenium EXAFS spectra than samples B and D. The spectrum from sample D is simplified due to the fact that there is only one metal - metal contribution. The complexity in the spectra from samples A and C may arise from contributions from oxides with rhenium in different oxidation states. For example, ReO_3 has a collinear arrangement of O – Re – O atoms and hence multiple scattering processes contributing to the spectrum. However, this contribution is not large enough to be extracted from the overall spectrum which may be reflected in the relatively poor quality of the fit for sample C (see Table 2). The slightly longer Re – O distance (1.76 Å) in sample C compared to ReO_4^- (1.74 Å) is consistent with this since the Re – O distance in ReO_3 is 1.87 Å. In Sample B, the Re – O distance is even longer (1.93 Å), being close to the Re – O distance found in Sample D at 1.96 Å. This Re – O distance is most likely associated with rhenium atoms in low oxidation states coordinated to oxygen in the support interface. The low coordination number (0.4) of the oxygen shell at 1.93 Å

in sample B coupled with the support interaction found at 2.13 Å, indicate that the reliability of this distance is limited. The coordination shell is, however, included in the fitting since the contribution is statistically significant at the 1% level [45].

From the rhenium EXAFS analysis, sample B and C have the highest degrees of alloy formation (highest Re – Pt coordination). Sample A which is not dehydrated prior to reduction, shows a significantly lower bimetallic coordination than sample B and C. This does not agree with previous reports [13,46] suggesting that rhenium is more easily reduced when water is present on the surface allowing mobile rhenium oxide species to transport rhenium to the platinum particles. The EXAFS data from sample B exhibits the most balanced coordination towards platinum and rhenium (4.8 and 5.2, respectively). Sample B also contains a larger fraction of completely reduced rhenium. Consequently, moderate heating in air (i.e. low drying temperature) prior to reduction, provides the most suitable conditions for transport of the mobile rhenium species on the surface, and hence alloy formation. For the sample dried in N_2 at high temperature (sample D), the EXAFS analysis for both elements is consistent with this model and also with our previous EDX results [18] confirming that very limited alloying take place under such conditions. The relatively low alloy formation in sample A is not reflected in the EXAFS analysis of the other element, platinum, which accords well with the aforementioned EDX results (see Table 6 and Table 7). The results from the platinum EXAFS analysis show only minor differences between samples A, B and C. All three samples are characterised by a Pt – Pt coordination of ca. 3 and Pt – Re coordination close to 1. The relatively weak metal – support interaction at ca. 2.7 Å found in sample B and C is not significant for sample C. It has been reported that this metal – oxygen distance is typical for support interfaces where

chemisorbed hydrogen is present and when reduced at temperatures less than 450°C [31,47,48]. It thus appear that raising the drying temperatures have similar impact on the platinum – support interface as raising the reduction temperatures when dried in air (i.e. in presence of moisture), since sample D has a similar Pt – O distance, although slightly contracted. Sample D displays a different spectrum from the other samples in the sense that, as stated above, it contains no bimetallic contribution and a somewhat stronger interaction with the support than the other samples. The strength of the interaction is reflected both in the higher Pt – O coordination and in the contracted metal – support bonding distance compared to the metal – support interaction in the other samples (see Table 6). Another difference is that sample D is not completely reduced (or alternatively passivated by oxygen after reduction). The Pt – Pt coordination is practically the same in this sample as for the three other samples. Thus, the larger particle sizes found in the STEM images of this sample [18] are not reflected in the EXAFS results. Since STEM is not able to distinguish between platinum metal and the oxide, this would indicate that the outermost atom layers of larger platinum particles are easily passivated [49,50] leading to smaller metal particles and hence reduced coordination numbers. This model consisting of passivated particles with a metal kernel is a more likely explanation of the Pt – O contribution than platinum not being completely reduced during the reduction step, which would form a metal particle with an oxide kernel.

The structural parameters obtained from the rhenium and platinum EXAFS analysis can be summarised as follows: rhenium metal shows relatively high coordination to both rhenium and platinum in addition to a strong metal – support interaction, suggesting that relatively large, flat rhenium particles are present on the surface. Platinum EXAFS

analysis shows high platinum dispersion (small particles consisting of only a few atoms) coordinated to both platinum and rhenium. These observations are consistent with a metal particle model in which rhenium particles are sited on the support interface. Smaller platinum particles are situated on or at the boundary of the rhenium particles, the latter being most likely because the rhenium surface species are believed to be the most mobile [18]. This is only true for samples A, B and C, which contain bimetallic particles. The EXAFS analysis of sample D confirms that the surface contains separate particles of rhenium and platinum metal.

Particle size and composition

The high surface relaxations observed in small metal particles may lead to a significant contraction of the metal-metal bond distances relative to the distances found for bulk metal and to anharmonic pair distribution functions [27,51-53]. For small metal particles, the average nearest-neighbour bond length decreases rapidly with decreasing particle diameter. Furthermore, the pair distribution functions become increasingly anharmonic for smaller particle sizes and may lead to significant errors in the estimation of coordination number and hence particle sizes. Consequently, particle size estimates from EXAFS are usually associated with relatively large uncertainty (ca. 20%). However, from the low Pt – metal coordination (ca. 4) in the investigated samples we conclude that the mean particle diameter in the platinum containing must be small. The contraction in Pt – Pt distances from 2.77 Å found for bulk platinum down to approximately 2.67 Å in the catalyst samples are also an indication of small particles [27]. Klimenkov *et al.* [53] showed in a TEM study that an Pt – Pt atomic distance of 2.65 Å corresponds to a mean particle size of ca. 15 Å while Diaz-Moreno *et al.* used EXAFS to determine that first shell Pt – Pt

coordination of 4 corresponded to a particle size of approximately 8 Å [52]. It has been suggested that Pt – Pt coordination of 4.8 atoms corresponded to particles of diameter ca. 9 Å and containing about 10 atoms [54,55]. It may therefore be concluded that all samples contain platinum metal particles of average diameter less than 10 Å and that the platinum dispersion is 100%.

The Re – Re distances are even more contracted compared to bulk rhenium (2.74 Å). Samples A, B and C have Re – Re bond lengths of ca. 2.6 Å even though the metal – metal coordination number is larger than for platinum. Such shortened Re – Re distances have been explained by presence of oxophilic rhenium in a low positive oxidation state [31]. The atomic fractions of platinum C_{Pt}, listed in Table 7 are calculated by dividing the Pt – Pt coordination number by the total Pt – metal coordination number. The results from the platinum EXAFS analysis show negligible difference in C_{Pt} for samples A, B and C, whereas sample D shows no alloy formation. These results are practically identical with the EDX results, although a weak trend towards higher Pt – Re interaction for the samples dried at the lowest temperature could be observed [18]. Note, however, that the EDX data display mass fractions while fractions determined from EXAFS is atomic fractions. The rhenium atomic fraction C_{Re}, is calculated in the same way by dividing the Re – Re coordination number by the total Re – metal coordination number. This is in contrast to the STEM/EDX studies, which assume that all the rhenium containing particles are bimetallic particles such that $C_{Re} = 1 - C_{Pt}$. The EXAFS results show that $C_{Re} > 1 - C_{Pt}$, indicating that the samples also contain monometallic particles. Sample B, which shows the highest hydrogenolysis activity of the four samples [18], has got the highest bimetallic interaction ($C_{Re} = 0.52$).

Linear combination of XANES spectra

The shape of the absorption edge features and the white line intensity contain information about the oxidation state and chemical environment of the element in question. The graphical presentation in Figure 4 of the rhenium L_{III} absorption edge profiles clearly show that rhenium is not completely reduced. From Table 8 it appears that linear combination of XANES profiles underestimates the degree of reduction of rhenium in the samples. However, in the amount of metallic rhenium deduced from the EXAFS data, the metal – support interaction is not included. By including the metal – support coordination number in the Re – O coordination number, the results from the EXAFS and XANES data converge to agreement. Sample B has a larger fraction of metallic rhenium than the other samples, suggesting that the higher reducibility of rhenium leads to a higher degree of alloying, thus supporting the previously proposed rhenium reduction mechanism [15,18].

The XANES analysis of platinum L_{III} edge data are consistent with the EXAFS data of the same element, showing that practically all platinum is present as metallic platinum in samples A, B and C, while sample D is slightly passivated (see Table 9). This is also reflected in the white line intensities of the platinum catalyst samples shown in Figure 5, which are all very similar to the profile of the platinum metal foil.

Passivation

Sample A was reduced *in situ* (in the X-ray beam) as a test in order to establish whether or not the sample was passivated in the quartz capillary tubes. The fitted EXAFS spectrum of the sample is shown in Figure 6. The EXAFS data in Table 10 show that the amount of

completely reduced rhenium is higher in the *in situ* reduced sample with the fraction of Re(0) being 78 % compared to 63 % in the sample sealed in a capillary tube. No significant passivation of platinum was found in the samples containing 0.3 wt% while ca. 20 – 30 % of the platinum in the samples with higher platinum loading (0.9 wt%), which also are included in Tables 8 and 9, were found to be in a positive oxidation state. Passivation by oxygen of supported platinum particles has been reported [49,55,56] as being mainly limited to the surface layer and hence proportional to the fraction of surface platinum atoms. The oxide layer has Pt - O distances close to that of PtO_2 (ca. 2.00 Å), which is the most stable platinum oxide. Surface chloride complexes may also be involved in the oxidation of the metal particles when chloride is present in the system [57,58]. No bimetallic interactions were found in the highly passivated samples with 0.9 wt% platinum and 0.9 wt% rhenium. We therefore conclude that rhenium stabilises the metal particles against passivation since no passivated platinum was found in the samples containing 0.3 wt% platinum and 0.3 wt% rhenium. The passivation of the samples with higher metal loadings may result from lower dispersion and larger particles on the surface, indicating that the platinum particles in sample D must be larger than in the other samples. The Re – Re coordination number is practically the same for the samples sealed in capillary tubes and the one reduced *in situ,* while the Re – Pt coordination is considerably lower and the Re – O coordination accordingly higher in the passivated sample (see Figure 7). These results may explain why Macleod *et al.* [21] in their TEM/EDX study were unable to detect any bimetallic interaction nor metallic rhenium in their catalyst samples. Most of the rhenium may have been oxidised to higher oxidation states since the bimetallic particles seem to be more prone to passivation than the particles containing only rhenium. The weakened bimetallic interaction in the quartz capillary sample

compared to the *in situ* sample also indicate that the true bimetallic contributions in the Pt – Re catalyst are larger than what are reported here.

Conclusions

The effect of the pretreatment conditions on the metal particles in Pt-Re/Al_2O_3 catalysts was studied for several pretreatment procedures, using X-ray absorption spectroscopy and by comparing these studies with previous results obtained by STEM/EDX [18] and catalytic measurements [17].

The results show that if the catalysts are dried in air at temperatures ≤ 500°C before reduction at 480°C, bimetallic particles of platinum and rhenium are formed. Drying at higher temperatures in absence of air inhibits the transport of mobile (rhenium) species on the surface causing no intimate contact between the two metals. Platinum L_{III} EXAFS data show that the average particle size of the bimetallic particles on the alumina surface is less than 10 Å. The results from the rhenium L_{III} EXAFS analysis confirm that rhenium is not completely reduced to metallic rhenium in the catalysts after reduction. The short Re – Re distance (ca. 2.6 Å) suggests that oxophilic rhenium in low, positive oxidation states are present. Rhenium interacts relatively strongly with the support, which is reflected in the Re – O interaction around 2.0 Å that displays an average coordination number close to 1.0.

EXAFS data from the rhenium edge exhibits higher coordination numbers towards platinum and rhenium than those provided by the platinum EXAFS data. The relatively

high Re – Re and Re – Pt coordination, together with the strong Re – support interaction, and platinum being coordinated to approximately 1 rhenium and 3 platinum atoms, agree with a structural model of flat rhenium metal particles with smaller platinum particles sitting at the boundary of the rhenium particles.

The catalyst sample (sample B) dried at 240°C in air prior to reduction at 480°C contains more completely reduced rhenium than the other samples. The EXAFS data from this sample exhibits the most balanced coordination towards platinum and rhenium. These results show that moderate heating in presence of air (i.e. moist) provide the best conditions for transport of mobile rhenium species on the surface, which is necessary for alloy formation.

Acknowledgements

The authors would like to thank the Research Council of Norway for the financial support of this work. We acknowledge the staff at the Swiss-Norwegian Beam Lines (SNBL) at ESRF for their assistance (Experiment Number 01-01-98), and we thank the Norwegian University of Science and Technology and the Research Council of Norway for grants towards construction and maintenance of SNBL. The Brookhaven National Synchrotron Light Source (Beamline X11A) is thanked for generously providing beamtime. The NSLS is supported by the U.S. Department of Energy under Contract numbers DE-AC02-76CH00016 and DE-FG05-89ER45384. Support from the Nansen Foundation and VISTA-Statoil (both to DGN). Scientific glassblower Tor Johannes Wærøe at SINTEF

Applied Chemistry is acknowledged for his assistance in the work involving the quartz capillary tubes.

References

[1] Kluksdahl, H. E., U.S. pat. 3,415,737 (1968)

[2] Parera, J.M., and Beltramini, J.N., J. Catal. **112**, 357 (1988)

[3] Bertolacini, R. J., and Pellet, R. J., in "Catalyst Deactivation" (Delmon, B., and Froment, G. F., Eds.), p. 73, Elsevier, Amsterdam, 1980

[4] Yermakov, Y.U., and Kuznetsov, B. N., J. Mol. Catal. **9**, 13 (1980)

[5] Betizeau, C., Leclercq, G., Maurel, R., Bolivar, C., Charcosset, H., Frety, R., and Tournayan, L., J Catal. **45**, 179 (1976)

[6] Biloen, P., Helle, J. N., Verbeek, H., Dautzenberg, F. M., and Sachtler, W. M. H., J. Catal. **63**, 112 (1980)

[7] Shum, V. K., Butt, J. B., and Sachtler, W. M. H., J. Catal. **96**, 371 (1985)

[8] Ribeiro, F. H., Bonivardi, A. L., Kim, C., and Somorjai, G. A., J. Catal. **150**, 186 (1994)

[9] Augustine, S. M., Alameddin, G. N., and Sachtler, W. M. H., J. Catal. **115**, 217 (1989)

[10] Haining, I. H. B., Kemball, C., and Whan, D. A., J. Chem. Research (S), 170 (1977)

[11] Haining, I. H. B., Kemball, C., and Whan, D. A., J. Chem. Research (S), 364 (1978)

[12] Shum, V. K., Butt, J. B., and Sachtler, W. M. H., J. Catal. **99**, 126 (1986)

[13] Wagstaff, N., and Prins, R., J. Catal. **59**, 434 (1979)

[14] Isaacs, B. H., and Petersen, E. E., J. Catal. **77**, 43 (1982)

[15] Augustine, S. M., and Sachtler, W. M. H., J Catal. **116**, 184 (1989)

[16] Prestvik, R., *Ph.D.-Thesis*, Norwegian Institute of Technology, Trondheim (1995)

[17] Prestvik, R., Grande, K., Moljord, K., and Holmen, A., J. Catal. **174**, 119 (1998)

[18] Prestvik, R., Tøtdal, B., Lyman, C.E., and Holmen, A., J. Catal. **176**, 246 (1998)

[19] Reitmaier, S.F., Subramaniam, A., and Sermon, P.A., Catal. Lett. **19**, 345 (1993)

[20] Huang, Z., Fryer, J.R., Park, C., Stirling, D., and Webb, G., J. Catal. **148**, 478 (1994)

[21] Macleod, N., Fryer, J.R., Stirling, D., and Webb, G., Catal. Today **46**, 37 (1998)

[22] Short, D.R., Khalid, S.M., Katzer, J.R. and Kelley, M.J., J. Catal. **72**, 288 (1981)

[23] Hillbrig, F., Michel, C., and Haller, G.L., J. Phys. Chem., **96**, 9893 (1992)

[24] Michel, C., Bambrick, W.E., Ebel, R.H., Larsen G., and Haller, G.L., J. Catal. **154**, 222 (1995)

[25] Meizner, G., Via, G.H., Lytle, F.W., and Sinfelt, J.H., J. Chem. Phys. **87**(11), 6354 (1987)

[26] Purnell, S.K., Chang, J.R., and Gates, B.C., J. Phys. Chem. **97**, 4196 (1993)

[27] Caballero, A, Villain, F., Dexpert, H., LePeltier, F., and Lynch, J., J. Chem. Soc., Faraday Trans. **89**, 159 (1993)

[28] Fernandez-Garcia, M., Chong, F.K., Anderson, J.A., Rochester, C.H., and Haller, G.L., J. Catal. **182**, 199 (1999)

[29] Bensaddik, A., Caballero, A., Bazin, D., Dexpert, H., Didillon, B., and Lynch, J., Applied Catalysis A **162**, 171 (1997)

[30] Caballero, A, Villain, F., Dexpert, H., LePeltier, F., Didillon, B., and Lynch, J., Catal. Lett. **20**, 1 (1993)

[31] Fung, A.S., Kelley, M.J., Koningsberger, D.C., and Gates, B.C., J. Am. Chem. Soc. **119**, 5877 (1997)

[32] Xiao, J., and Puddephatt, R.J., Coord. Chem. Rev. **143**, 457 (1995)

[33] Lytle, F.W., Greegor, R.B., Marques, E.C., Sandstrom, D.R., Via, G.H., and Sinfelt, J.H., J. Catal. **95**, 546 (1985) and Lytle, F.W., Greegor, E.C., Sandstrom, R.B., Marques, D.R., Wong, J., Spiro, C.L., Huffman, G.P., and Huggins, F.D., Nucl. Instr. and Meth. **226**, 542 (1984)

[34] *EXCALIB, EXBACK* and *EXCURV90* programs, Binsted, N., Campbell, J.W., Gurman, S.J., and Stephenson, P.C., *SERC Daresbury Laboratory, 1990*

[35] Gurman, S.J., Binsted, N., and Ross. I., *J. Phys. C: Solid State Phys.* 17, 143 (1984)

[36] Koningsberger, D.C., and Prins, R., (Editors) *X-ray Absorption: Principles, Applications, Techniques of EXAFS, SEXAFS and XANES*, Wiley, New York (1988)

[37] *Report of the International Workshop on Standards and Criteria in X-ray Absorption Spectroscopy*, Eds: Lytle, F.W., Sayers, D.E., and Stern, E.A., Physica B **158**, 701 (1989) and *Report of the International Workshop on Standards and Criteria in X-ray Absorption Spectroscopy*, Ed: Hasnain, S.S., X-ray Absorption Fine Structure, Hellis Horwood, Chicester (1991)

[38] Vaarkamp, M., Catal. Today **39**, 271 (1998)

[39] Stern, E.A., Phys. Rev. B 48, 9825 (1993)

[40] MacGillavry, C.H., Riek, G.D., Lonsdale, K., (Editors) *International Tables of X-ray Crystallography*, Kynock Press, Birmingham, Vol III, 281 (1962)

[41] Meisel, K., Z. Anorg. Allg. Chem. **207**, 121 (1932)

[42] Brown, R.J.C., Segel, S.L., and Dolling, G., Acta Crystallogr. **B36**, 2195 (1980)

[43] Range, K.-J., Rau, F., Klement, U., and Heyns, A.M., Mat. Res. Bull. **22**, 1541 (1987)

[44] Ressler, T., J. Physique IV; **7**, C2 (1997)

[45] Joyner, R.W., Martin, K.J., and Meehan, P., J. Phys. C: Solid State Phys. **20**, 4005 (1987)

[46] Bolivar, C., Charcosset, H., Frety, R., Primet, M., Tournayan, L., Betizeau, C., Leclercq, G., and Maurel, R., J. Catal. **39**, 249 (1975)

[47] van Zon, F.B.M., Maloney, S.D., Gates, B.C., and Koningsberger, D.C., J. Am. Chem. Soc. **115**, 10317 (1993)

[48] Vaarkamp, M., Modica, F.S., Miller, J.T.,, and Koningsberger, D.C., J. Catal. **144**, 611 (1993)

[49] McCabe, R.W., Wong, C., and Woo, H.S., J. Catal. **114**, 354 (1988)

[50] Shido, T., Lok, M., and Prins, R., Topics in Catalysis **8**, 223 (1999)

[51] Clausen, B.S., Topsøe, H., Hansen, L.B., Stolze, P., and Nørskov, J.K., J. Catal. **114**, 463 (1994)

[52] Diaz-Moreno, S., Koningsberger, D.C., and Munoz-Paez, A., Nucl. Instr. Met. Phys. Res. B **133**, 15 (1997)

[53] Klimenkov, M., Nepijko S., Kuhlenbeck, H., Bäumer, M., Schlögl, R., and Freund, H.-J., Surf. Sci. **391**, 27 (1997)

[54] Kip, B.J., Duivenvoorden, F.B.M., Koningsberger, D.C., and Prins, R., J. Catal. **105**, 26 (1987)

[55] Borgna, A., Le Normand, F., Garetto, T., Apesteguia, C.R., and Moraweck, B., Catal. Lett. **13**, 175 (1992)

[56] Markusse, A.P., Kuster, B.F.M., Koningsberger, D.C., and Marin, G.B., Catal. Lett. **55**, 141 (1998)

[57] Le Normand, F., Borgna, A., Garetto, T., Apesteguia, C.R., and Moraweck, B., J. Phys. Chem. **100**, 9068 (1996)

[58] Borgna, A., Garetto, T., Apesteguia, C.R., Le Normand, F., and Moraweck, B., J. Catal. **186**, 433 (1999)

Table 1.

Previously obtained data for the catalyst samples involved [16,17]. All samples were reduced at 480°C in H_2 for 1 hour after the indicated drying sequence.

Sample *Pt-Re/γ-Al_2O_3 (CK433)*	*Metal loading*	*Drying conditions*	*H/Pt ratio*[a]	*MCH Conversion*[b]
Sample A	0.3 wt%	No drying	0.23	–
Sample B	0.3 wt%	240°C/ air	0.31	41 %
Sample C	0.3 wt%	500°C/ air	0.44	42 %
Sample D	0.3 wt%	680°C/ N_2	0.16	27 %
Pt-Re/γ-Al_2O_3	0.9 wt%	No drying	*Model systems*[c]	
Pt-Re/γ-Al_2O_3	0.9 wt%	500°C/ air		
Pt/γ-Al_2O_3	0.9 wt%	No drying		
Pt/γ-Al_2O_3	0.9 wt%	500°C/ air		
Re/γ-Al_2O_3	1.75 wt%	No drying		

a) Volumetric hydrogen chemisorption at 25°C

b) Methylcyclohexane (MCH) conversion at 300°C, 1.1 bar, WHSV=25h^{-1} and H_2/MCH=40

c) Used as structural references only. Activity and chemisorption data are therefore not included

Table 2.

Details concerning the Re L_{III} EXAFS analysis:

Sample	*Metal loading*	*Drying conditions*	*Data analysis range, Δk ($Å^{-1}$)*	*Fourier filtering range, ΔR (Å)*	*Quality of fit[a] (%)*
Sample A	0.3/0.3 wt%	No drying	3.5 – 13	1.0 – 3.5	22.89
Sample B	0.3/0.3 wt%	240°C/air	3.5 – 13	1.0 – 3.5	20.66
Sample C	0.3/0.3 wt%	500°C/ air	3.5 – 13	1.0 – 3.5	31.81
Sample D	0.3/0.3 wt%	680°C/ N_2	3.5 – 13	1.0 – 3.5	12.10

a) Defined in the text

Table 3.

Details concerning the Pt L_{III} EXAFS analysis:

Sample	*Metal loading*	*Drying conditions*	*Data analysis range, Δk ($Å^{-1}$)*	*Fourier filtering range, ΔR (Å)*	*Quality of fit[a] (%)*
Sample A	0.3/0.3 wt%	No drying	3.5 – 9	1.3 – 3.4	17.64
Sample B	0.3/0.3 wt%	240°C/air	3.5 – 9	1.3 – 3.4	10.30
Sample C	0.3/0.3 wt%	500°C/ air	3.5 – 9	1.3 – 3.4	18.91
Sample D	0.3/0.3 wt%	680°C/ N_2	3.5 – 9	1.0 – 3.4	9.63

a) Defined in the text

Table 4.

Crystallographic data for the EXAFS model compounds used to check the validity of the *ab initio* phaseshifts and backscattering amplitudes.

Compound	*Model pair*	*R (Å)*[a]	*N*[b]	*Reference*
Re foil	Re – Re	2.74	12	[40]
$(NH_4)ReO_4$	Re – O	1.74	4	[42]
ReO_3	Re – O	1.87	6	[41]
Pt foil	Pt – Pt	2.77	12	[40]
PtO_2	Pt – O	2.00[c]	2+4	[43]

a) Interatomic distance, b) Coordination number (multiplicity), c) Mean coordination distance, 2×1.989 Å $+ 4 \times 2.003$ Å $\cong 2.00$ Å

Table 5.

Results from the EXAFS analysis of data from the Re L_{III} edge after pretreatment and reduction at 480°C.

Sample	*Drying conditions*	*Coordination shell*	$E_0(eV)^a$	N^b	$2\sigma^2(Å^2)^c$	$R(Å)^d$
Sample A	No drying	Re – Pt	20.4(2)	2.0(2)	0.033(3)	2.75(2)
		Re – Re		4.1(2)	0.025(1)	2.56(1)
		Re – O		1.5(1)	0.003(0)	1.72(1)
		Re – $O_{support}$		1.3(1)	0.004(0)	2.02(1)
Sample B	240°C/air	Re – Pt	18.2(2)	4.8(2)	0.033(2)	2.75(1)
		Re – Re		5.2(2)	0.023(1)	2.59(1)
		Re – O		0.4(1)	0.003(1)	1.93(1)
		Re – $O_{support}$		1.1(1)	0.006(1)	2.13(1)
Sample C	500°C/ air	Re – Pt	12.2(5)	5.2(4)	0.030(2)	2.75(1)
		Re – Re		3.3(3)	0.014(1)	2.55(1)
		Re – O		1.5(1)	0.004(0)	1.76(1)
		Re – $O_{support}$		2.4(1)	0.006(0)	2.05(1)
Sample D	680°C/ N_2	Re – Pt	9.5(1)	0	–	–
		Re – Re		1.5(1)	0.024(2)	2.74(1)
		Re – O		2.0(1)	0.004(0)	1.74(0)
		Re – $O_{support}$		0.9(1)	0.004(1)	1.96(0)

a) Energy threshold, b) Number of neighbours (multiplicity), c) Debye-Waller type factor (disorder), d) Interatomic distance

Table 6.

Results from the EXAFS analysis of data from the Pt L_{III} edge after pretreatment and reduction at 480°C.

Sample	*Drying conditions*	*Coordination shell*	E_0 *(eV)*[a]	N[b]	$2\sigma^2$ *(Å²)*[c]	R *(Å)*[d]
Sample A	No drying	Pt – Re	14.8(3)	1.1(2)	0.033([e])	2.75([e])
		Pt – Pt		2.9(1)	0.005(1)	2.66(4)
		Pt – $O_{support}$		0.2(1)	0.012(4)	2.69(7)
Sample B	240°C/air	Pt – Re	10.5(3)	1.1(2)	0.033([e])	2.75([e])
		Pt – Pt		2.5(1)	0.004(1)	2.67(2)
		Pt – $O_{support}$		0.5(0)	0.005(4)	2.70(8)
Sample C	500°C/ air	Pt – Re	24.7(5)	1.3(3)	0.030([e])	2.75([e])
		Pt – Pt		2.9(1)	0.006(1)	2.67(4)
		Pt – $O_{support}$		0	–	–
Sample D	680°C/ N_2	Pt – Re	14.1(1)	0	–	–
		Pt – Pt		3.6(1)	0.007(1)	2.67(3)
		Pt – $O_{support}$		0.8(1)	0.005(3)	2.63(6)
		Pt – O[f]		1.4(1)	0.006(1)	1.97(1)

a) Energy threshold, b) Number of neighbours (multiplicity), c) Debye-Waller type factor (disorder), d) Interatomic distance, e) Disorder ($2\sigma^2$) and distance (R) are kept fixed at values obtained from the Re L_{III} EXAFS analysis (see Table 5), f) Pt – O coordination associated with passivated/unreduced Pt

Table 7.

Comparison of average platinum and rhenium mass fractions and particle size estimates for the catalyst samples from STEM/EDX analysis [18] and atomic fractions from EXAFS analysis.

Sample	*Pt fraction, C_{Pt}*		*Re fraction, C_{Re}*		*Average particle diameter (nm)*	
	EDX	EXAFS	EDX	EXAFS	*STEM*	*EXAFS*[a]
Sample A	0.68	0.72	0.32	0.67	0.9	< 1.0
Sample B	0.71	0.69	0.29	0.52	1.0	< 1.0
Sample C	0.85	0.69	0.15	0.39	1.8	< 1.0
Sample D	0.96	1.00	0.04	1.00	2.3	< 1.0

a) Derived from Pt L_{III} EXAFS data. Mean particle diameter estimated from Pt EXAFS data as described by Borgna *et al.* [53]

Table 8.

Fraction of metallic Re (%) determined from linear combination of XANES profiles by using Re foil and the unreduced sample as reference compounds compared to results obtained from EXAFS by dividing the Re – O coordination number by the Re – O coordination number for the unreduced sample (N = 4).

Sample pretreatment	*Sample A*[a]		*Sample B*		*Sample C*		*Sample D*	
and metal loading	*XANES*	*EXAFS*	*XANES*	*EXAFS*	*XANES*	*EXAFS*	*XANES*	*EXAFS*
0.3wt%Re/0.3wt%Pt	44%	63%	45%	90%	11%	63%	4%	50%
0.9wt%Re/0.9wt%Pt	21%	48%			0%	37%		
1.75wt%Re	24%	65%						

a) For sample A reduced *in situ*: XANES; 54%, EXAFS; 78%

Table 9.

Fraction of metallic Pt (%) determined from linear combination of XANES profiles by using Pt foil and the unreduced sample as reference compounds compared to results obtained from EXAFS by dividing the Pt – O coordination number by the Pt – O coordination number for the unreduced sample (N = 6).

Sample pretreatment	*Sample A*		*Sample B*		*Sample C*		*Sample D*	
and metal loading	*XANES*	*EXAFS*	*XANES*	*EXAFS*	*XANES*	*EXAFS*	*XANES*	*EXAFS*
0.3wt%Re/0.3wt%Pt	97%	100%	98%	100%	100%	100%	100%	77%
0.9wt%Re/0.9wt%Pt	83%	70%			81%	75%		
0.9wt%Pt	70%	69%						

Table 10.

Comparison of the Re L_{III} EXAFS data from sample A reduced *in situ* and the same sample reduced *ex situ* (at our home laboratory) and subsequently sealed in a quartz capillary tube

	Reduced in situ		*Reduced ex situ*	
Backscattering pair	N^a	R (Å)^b	N^a	R (Å)^b
Re – Pt	5.2	2.75	2.0	2.75
Re – Re	3.8	2.63	4.1	2.56
Re – O	0.9	1.77	1.5	1.72
Re – $O_{support}$	1.5	2.04	1.3	2.02

a) Coordination number (multiplicity), b) Interatomic distance

Figure captions

Figure 1. The raw, unfiltered EXAFS spectra of samples A – D from both the Re L_{III} edge (left) and the Pt L_{III} edge (right).

Figure 2. Re L_{III} EXAFS spectra (left) and corresponding Fourier transforms (right) of samples A – D, using Δk = 3.5 – 13 Å^{-1} and ΔR = 1.0 – 3.5 Å. Experiment is shown in solid lines, and k^0 fit in dotted lines.

Figure 3. Pt L_{III} EXAFS spectra (left) and corresponding Fourier transforms (right) of samples A – D, using Δk = 3.5 – 9.0 Å^{-1} and ΔR = 1.3 – 3.4 Å. Experiment is shown in solid lines, and k^0 fit in dotted lines.

Figure 4. Normalised Re L_{III} edge profiles and white line intensities for the catalyst samples shown together with the profiles of a rhenium foil and the unreduced sample (CK433) as references.

Figure 5. Normalised Pt L_{III} edge profiles and white line intensities for the catalyst samples shown together with the profiles of a platinum foil and the unreduced sample (CK433) as references.

Figure 6. Re L_{III} EXAFS spectrum (left) and corresponding Fourier transform (right) of sample A reduced *in situ*, using Δk = 3.5 - 13 Å^{-1} and ΔR = 1.0 - 3.5 Å. Experiment is shown in solid lines, and k^0 fit in dotted lines.

Figure 7. Fourier transforms of the Re L_{III} EXAFS spectra of sample A reduced *in situ* (solid line) and of the same sample reduced *ex situ* and sealed in a quartz capillary tube (dotted line).

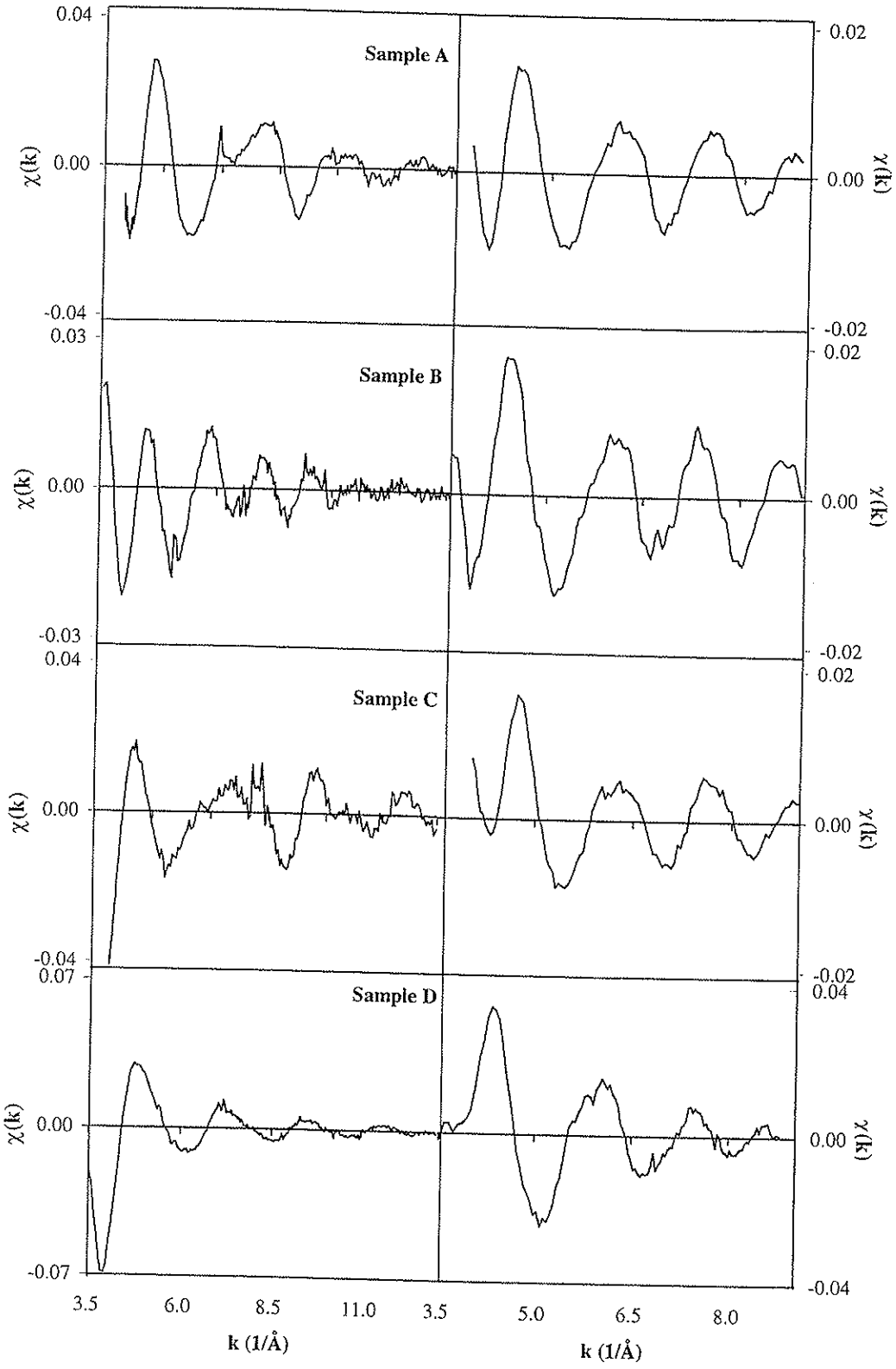
Sample A
Sample B
Sample C
Sample D
χ(k)
χ(k)
0.04
0.00
-0.04
0.02
0.00
-0.02
0.03
0.00
-0.03
0.02
0.00
-0.02
0.04
0.00
-0.04
0.02
0.00
-0.02
0.07
0.00
-0.07
0.04
0.00
-0.04
3.5
6.0
8.5
11.0
3.5
5.0
6.5
8.0
k (1/Å)
k (1/Å)

Figure 1

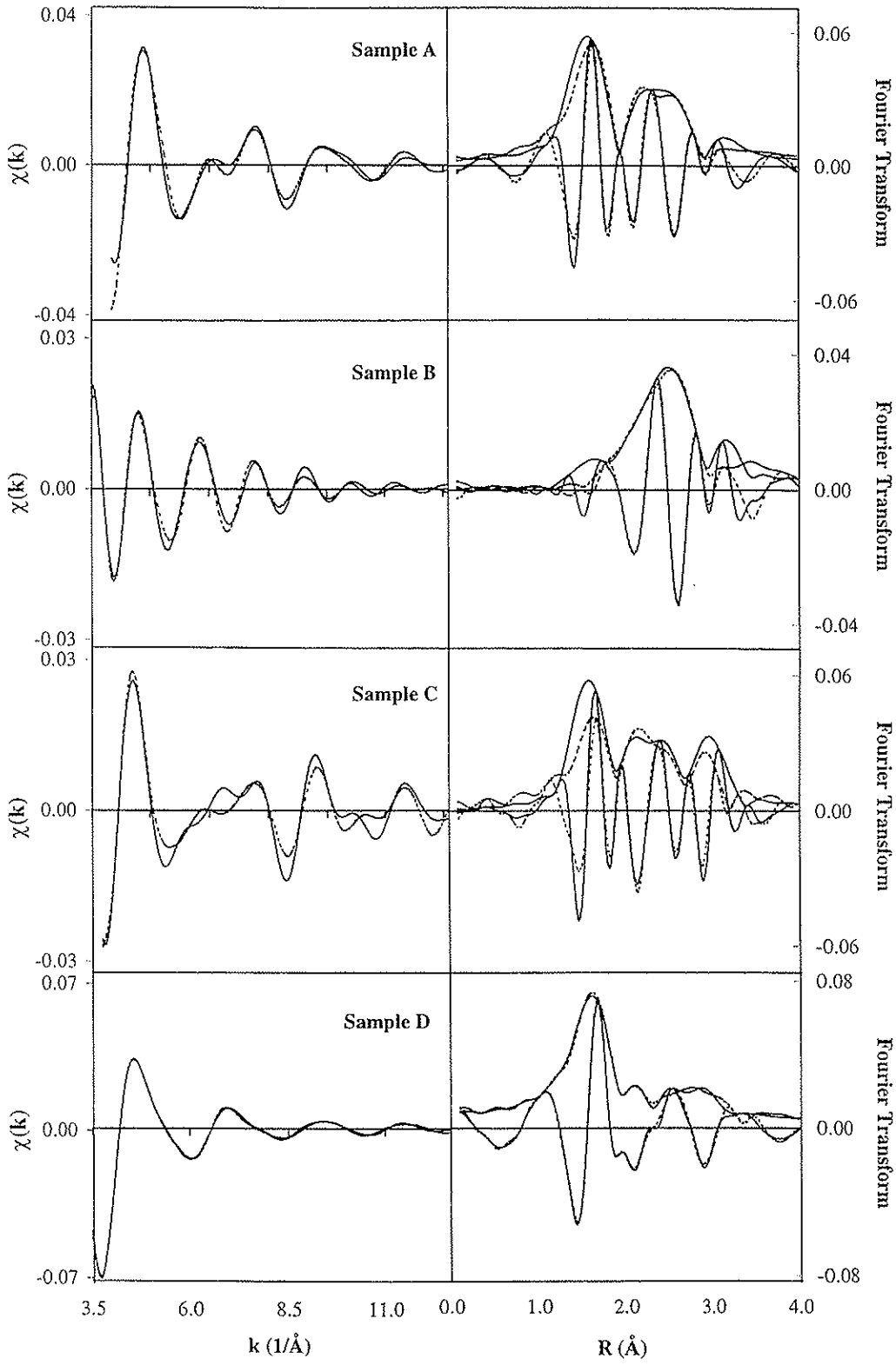
Sample A
Sample B
Sample C
Sample D
χ(k)
Fourier Transform
0.04
0.00
-0.04
0.06
-0.06
0.03
-0.03
0.07
-0.07
0.08
-0.08
3.5
6.0
8.5
11.0
k (1/Å)
0.0
1.0
2.0
3.0
4.0
R (Å)

Figure 2

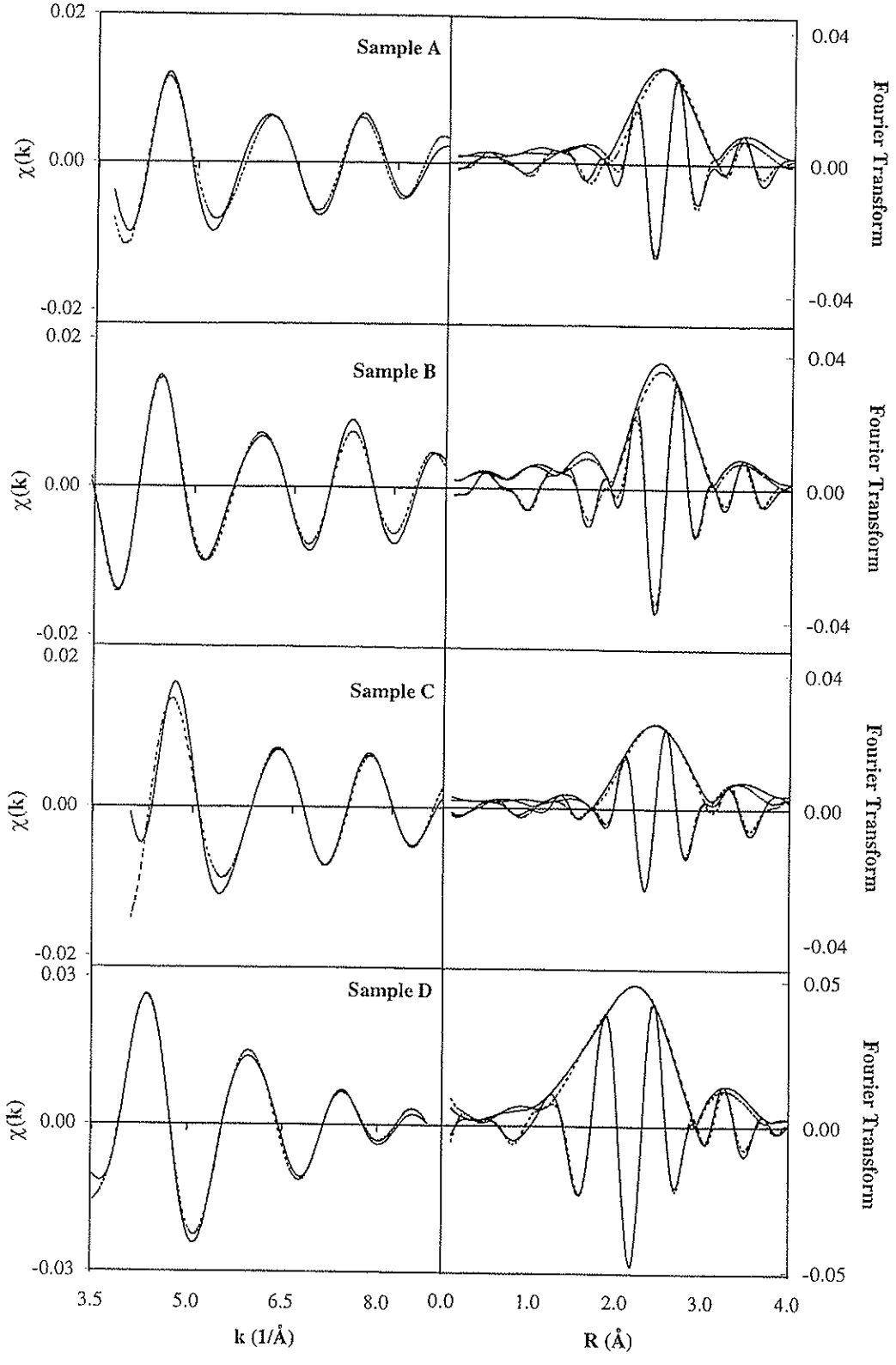
Sample A
Sample B
Sample C
Sample D
χ(k)
Fourier Transform
k (1/Å)
R (Å)
0.02
0.00
-0.02
0.04
-0.04
0.03
-0.03
0.05
-0.05
3.5
5.0
6.5
8.0
0.0
1.0
2.0
3.0
4.0

Figure 3

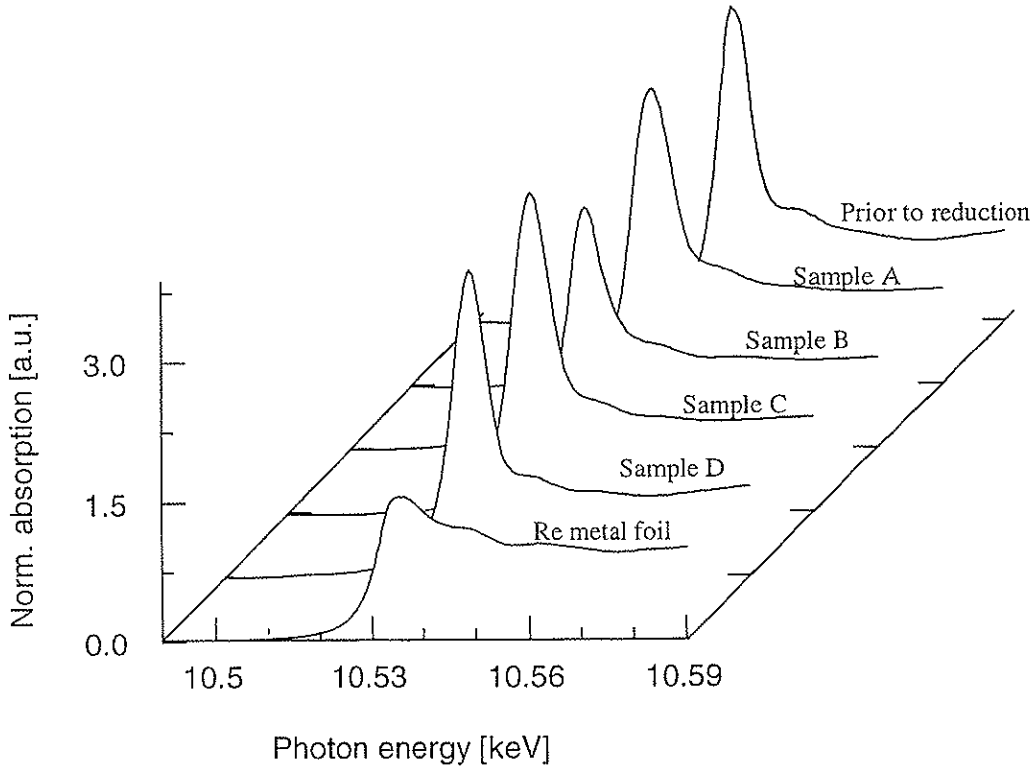
Prior to reduction
Sample A
Sample B
Sample C
Sample D
Re metal foil
Norm. absorption [a.u.]
3.0
1.5
0.0
10.5
10.53
10.56
10.59
Photon energy [keV]

Figure 4

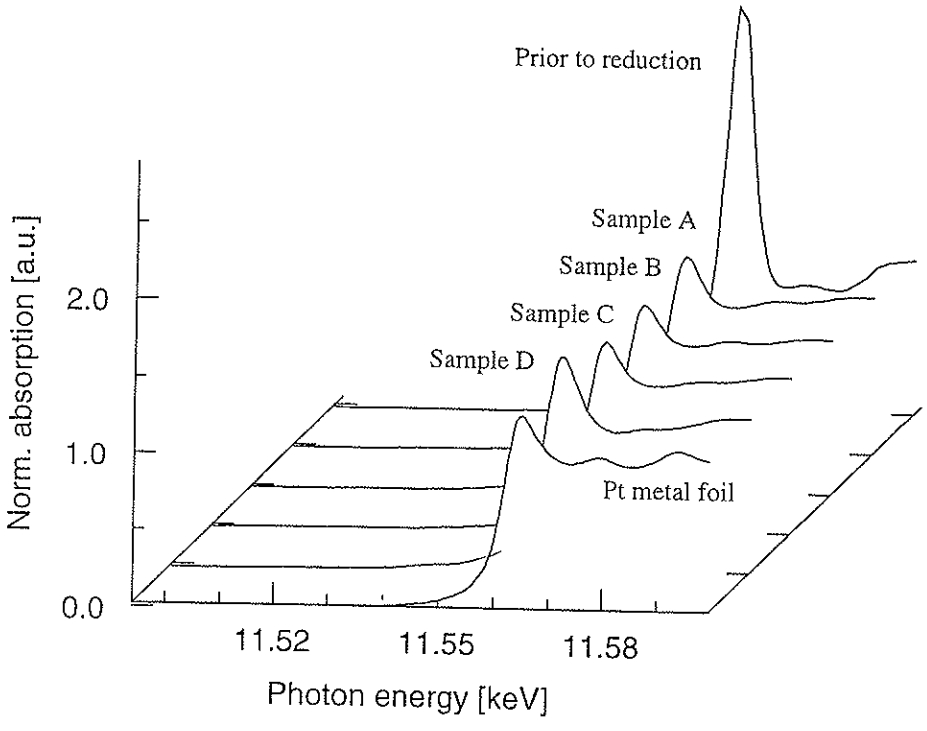
Prior to reduction
Sample A
Sample B
Sample C
Sample D
Pt metal foil
Norm. absorption [a.u.]
2.0
1.0
0.0
11.52
11.55
11.58
Photon energy [keV]

Figure 5

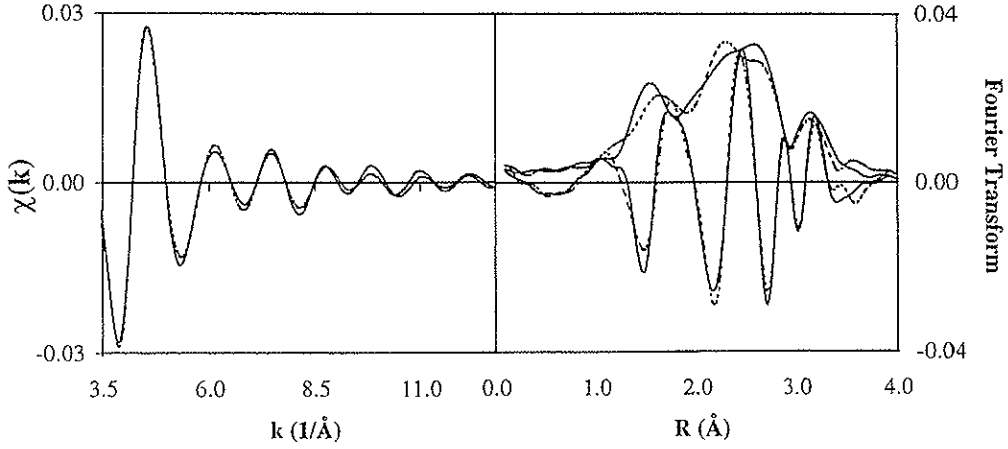
0.03
0.00
-0.03
χ(k)
3.5
6.0
8.5
11.0
k (1/Å)
0.04
0.00
-0.04
Fourier Transform
0.0
1.0
2.0
3.0
4.0
R (Å)

Figure 6

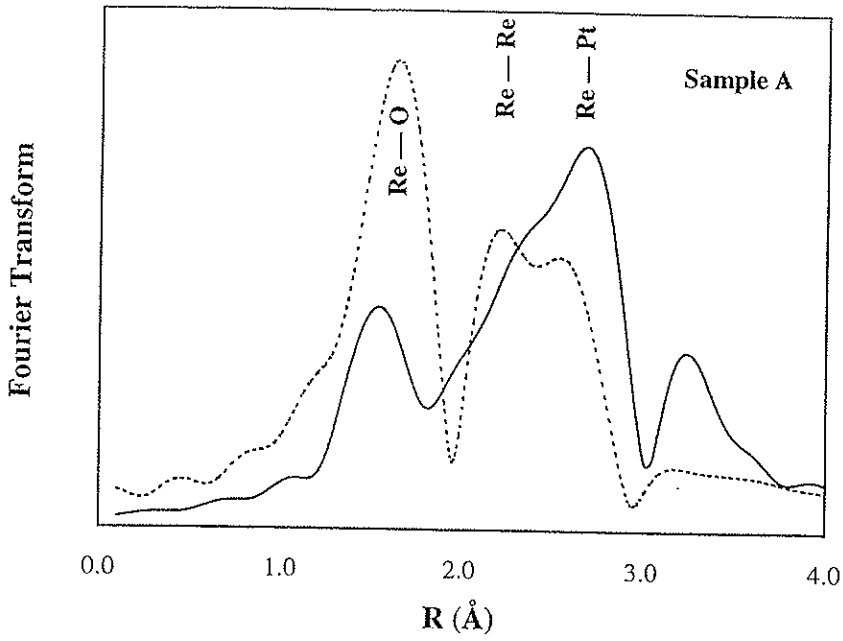

Figure 7

Paper III

The influence of the chlorine content on the bimetallic particle formation in Pt-Re/Al_2O_3 studied by STEM/EDX, TPR, H_2 chemisorption and model reaction studies

[a]T. Gjervan, [b]R. Prestvik, [c]B. Tøtdal, [d]C.E. Lyman, and [a]A. Holmen

a Dept. of Chemical Engineering, Norwegian University of Science and Technology (NTNU), 7491 Trondheim, Norway

b SINTEF Applied Chemistry, 7465 Trondheim, Norway

c Dept. of Physics, NTNU, 7491 Trondheim, Norway

d Dept. of Materials Science and Engineering, Lehigh University, Bethlehem, PA 18015, USA

Abstract

A Pt-Re/Al_2O_3 reforming catalyst with different levels of chlorine content prior to reduction has been studied by various techniques such as combined STEM/EDX, TPR, H_2 chemisorption and model reactions in order to investigate the effect of the chlorine content on the bimetallic particle formation. TPR, H_2 chemisorption and model reactions show that chlorine inhibits the formation of bimetallic particles in the PtRe/Al_2O_3 catalyst. The effect of chlorine is, however, limited. Direct measurements by STEM/EDX analysis could not reveal any significant difference in alloy formation by varying the chlorine content from 0.6 to 1.5 wt%. In comparison, the effect of adding water during reduction has a greater impact on the final state of the metal particles.

Keywords: PtRe/Al_2O_3 catalyst; Chlorine content; STEM/EDX; TPR; Cyclopentane; n-butane

1. Introduction

Since the introduction of the PtRe(S)/γ-Al_2O_3-Cl catalyst in catalytic reforming [1], it has been extensively studied with regard to the role of rhenium. This is a bifunctional catalyst where platinum catalyses hydrogenation/dehydrogenation reactions, and the acidic support catalyses isomerisation and cracking reactions. The acidity is adjusted by adding chlorine. Over time the bimetallic catalyst loses its activity especially due to coking. The addition of rhenium to the monometallic Pt/Al_2O_3-Cl catalyst increases its stability, but the way that rhenium modifies this system is not clear. It seems to be a general agreement [2-6] that rhenium has to be present "alloyed" with platinum in small bimetallic particles in order to have a beneficial effect. In industrial units sulphur is added to the catalyst in order to suppress undesired reactions. After a certain time on stream, the catalyst has to be regenerated by burning off the coke. Under these conditions platinum will sinter, and in order to re-establish the platinum dispersion and to restore the acidity of the support, the catalyst undergoes oxychlorination treatment followed by reduction. It has been reported that the chlorine level prior to reduction is critical to the alloy formation, but the conclusions are diverse. Michel et al [7] suggest that there is a mobile rhenium oxychloride involved in the reduction mechanism, whereas others [8-9] claim that chlorine inhibits Pt-Re interaction. Previously our group has studied formation of alloy particles on the PtRe/Al_2O_3 catalyst employing STEM/EDX, TPR, H_2 chemisorption and model reactions with respect to the pretreatment condtions [10,11]. Evidence for alloy formation was found and the drying temperature prior to reduction determined the degree of alloy formation. The present study is aimed to investigate the effect of the chlorine content on the bimetallic particle formation in the same catalyst system.

2. Experimental

2.1 Catalysts

The catalyst used was EUROPT-4 (Akzo) 0.3-0.3wt% PtRe/γ-Al_2O_3. As received it contained approximately 1.0 wt% Cl. To adjust the chlorine level, the catalyst was subjected to oxychlorination treatment at 500°C by using a flow of air saturated with different ratios HCl /H_2O. Finally, the catalyst was dried in air at 510 °C. The chlorine content of these samples was measured to be 0.6, 1.1, and 1.5 wt%, respectively by Escha dissolution and silver nitrate titration using chromate as indicator (Mohr method). Before performing the catalyst test reaction, the catalyst was reduced from 200°C to 480 °C at 0.8 °C/min and held at 480 °C for 1h in dry or moist (5000 ppm H_2O) hydrogen. The sample of the lowest chlorine content was called sample 1, whereas the samples containing 1.1 and 1.5 wt% chlorine were named sample 2 and 3, respectively. When reduced in moist hydrogen, the same samples are referred to as sample 4,5, and 6, with 0.6, 1.1, and 1.5 wt% Cl prior to reduction respectively.

2.2 Model reactions

Hydrogenolysis has been used as a probe reaction to distinguish between different degrees of alloy formation [12]. As reactants, n-butane and cyclopentane were used separately. The hydrocarbon/hydrogen mixture (molar ratio of 1/17 for n-butane and of 1/12 for cyclopentane, respectively) was pulsed (1.2 ml) over the catalyst bed (0.15 g) with regular intervals in a helium flow (250 ml/min) with a reactor temperature of 250 °C and 270°C, respectively. The product was analysed on-line using a HP 5890 series II gas chromatograph equipped with an flame ionisation detector (FID). The hydrocarbons were separated on a 50 m GC alumina column (J&W Scientific).

2.3 Temperature Programmed Reduction

Temperature programmed reduction (TPR) was used to further examine the degree of alloy formation of the PtRe catalyst. The TPR instrumentation has been described elsewhere [13]. 0.5 g of catalyst sample was heated slowly at 0.8°C/min, and dried at 510°C for 4 h. The TPR runs were performed with a heating rate of 10°C/min to 900 °C, using a mixture of 7% H_2 in Ar (30 ml/min). The hydrogen consumption was monitored by a thermal conductivity detector (TCD).

2.4 Hydrogen chemisorption

Volumetric hydrogen chemisorption was measured at 25°C using a Micromeretics ASAP 2010 Chemi instrument. The samples were dried, reduced, and analysed in the chemisorption apparatus after oxychlorination treatment *ex situ*. The dispersion, or hydrogen to platinum ratio (H/Pt), is calculated based on the volume of hydrogen chemisorbed on the sample. The volume adsorbed was obtained by making two subsequent isotherms with evacuation to 10^{-5} torr for 30 minutes in between. The values reported in Table 1 were obtained by subtracting the second isotherm from the first isotherm. It is assumed that the adsorption stoichiometry for H_2 on Pt is H/Pt =1, and that Re does not chemisorb H_2 at 25°C [14,15].

2.5 STEM/EDX particle analysis

Combined STEM/EDX particle analysis was performed at Lehigh University with a VG microscope HB-603. The particle sizes were found from the STEM images, whereas the EDX data yielded information on the composition. Detailed description of the analysis procedure is given elsewhere [11].

3. Results and discussion

3.1 Model reactions and hydrogen chemisorption

The results from the hydrogenolysis of n-butane performed on sample 1,2, and 3 are presented in Table 1, and the data given is from the first pulse. The selectivity to methane is taken as a measure of the degree of Pt-Re interaction, and it can be observed that the sample of the highest chlorine content show the lowest activity for n-butane conversion and selectivity to methane. Sample 2 show a slightly higher selectivity to methane than sample 1, but the difference is hardly significant. As sample 3 displays the lowest selectivity, it appears that the chlorine content of the catalyst prior to reduction has a significant effect on the final state of the metal phase. The presence of platinum and rhenium in intimate contact yields more active sites for hydrogenolysis than clusters of the respective atoms alone due to electronic interaction between the metal atoms. Hydrocarbons adsorb strongly on Re, but weaker on Pt. In such bimetallic clusters an intermediate heat of adsorption will result, giving the highest rate of reaction and methane formation. Reactions on the acid support, such as cracking, will also occur but the hydrogenolysis reaction and the formation of methane is catalysed by the metal sites. When comparing the methane selectivity of catalysts of various chlorine content care has to be taken in order to account for the additional cracking activity of the acid sites. However, the conversion of n-butane is similar for sample 1 and 2 and even lower for sample 3. The difference in catalytic performance is therefore attributed to differences in the metal particle characteristics.

The results from the hydrogen chemisorption studies are also presented in Table 1 and they show that sample 3 adsorbs significantly more hydrogen than sample 1 and 2. Assuming that the dispersion is the same for all samples a possible interpretation for this behaviour is that a higher degree of alloy formation results in a lower H/Pt ratio. In an alloy fewer contiguous platinum atoms are present allowing less dissociative hydrogen chemisorption to take place.

Table 1
Conversion of n-butane on the $PtRe/Al_2O_3$ catalyst containing different levels of chlorine (Average values expressed in molar units). Temperature = 250°C, C_4/H_2 = 1/17. Reduction in dry H_2.

Sample	Chlorine level	n-butane conv. [%]	C_1 sel.	H/Pt
1	0.65	16	36	0.43
2	1.10	17	39	0.43
3	1.50	11	26	0.59

In order to obtain bimetallic particles it is important that the rhenium oxide species present on the surface may be able to migrate to the platinum atoms which have already been reduced. Rhenium oxide in intimate contact with platinum will then be catalytically reduced resulting in alloy formation. The interpretation of the results presented in Table 1 is therefore that a too high surface concentration of chlorine will possibly inhibit the mobility of the rhenium species resulting in lower degrees of alloy formation.

Table 2 shows the results from cyclopentane hydrogenolysis, and again the results indicate that the catalyst with the lowest level of chlorine has the highest degree of Pt-Re interaction. In this case sample 1 shows a higher selectivity to methane even though the conversion of cyclopentane is lower than for sample 2 and 3. This could be due to acid catalysed cracking reactions of sample 1 and 2 due to the promoting effect of chlorine.

Table 2
Conversion of cyclopentane (CP) on the $PtRe/Al_2O_3$ catalyst containing different levels of chlorine prior to reduction (Average values expressed in molar units). Temperature = 270°C, CP/H_2 = 1/12. Reduced in dry H_2.

Sample	Chlorine level	CP conv. [%]	C_1 sel.
1	0.65	2.7	2.2
2	1.10	3.6	1.7
3	1.50	3.1	1.5

The catalysts were also reduced in moist H_2 in order to study the effect of water in the reduction process. As all catalyst samples were dried at 510 °C in air prior to reduction they are relative dehydrated [10]. From Table 3, it can be observed that the conversion of cyclopentane and the selectivity to methane increase for all catalyst samples when 5000 ppm of water is being introduced together with hydrogen during the reduction process. This increased activity can be explained by a higher degree of alloy formation due to an increased level of hydration during reduction as the presence of water in form of hydroxyl groups increases the mobility of surface rhenium oxide species.

Sample 4, which contains the lowest amount of chlorine prior to reduction in moist hydrogen, shows the highest conversion of cyclopentane and the highest selectivity to methane. The effect of chlorine content on alloy formation can be debated as high temperature treatment in moist atmosphere introduce some stripping of chlorine. Hydroxyl groups will replace the surface chlorine atoms and thus both enhance the mobility of rhenium oxide by ensuring a higher level of surface hydration and reducing the inhibiting effect of chlorine. The sample with the lowest chlorine level will in this case also contain most bimetallic particles after reduction. The catalytic performance of all samples will be affected by the removal of chlorine as the acidity of the support will be altered. In spite of this the conversion of cyclopentane is higher after reduction in moist hydrogen and the increased conversion must be attributed to a higher degree of alloy formation. Water in the reduction gas could also lead to sintering of platinum, but as the structure sensitive hydrogenolysis reaction is favoured on small metal particles this effect is not significant.

Table 3
Conversion of cyclopentane (CP) on the $PtRe/Al_2O_3$ catalyst containing different levels of chlorine prior to reduction (Average values expressed in molar units). Temperature = 270°C, CP/H_2 = 1/12. Reduced in moist H_2.

Sample	Chlorine level	CP conv. [%]	C_1 sel.
4	0.65	7.8	5.9
5	1.10	5.5	5.0
6	1.50	7.0	5.0

Both n-butane and cyclopentane hydrogenolysis studies indicate that the chlorine level has an effect on the alloy formation. The selectivity to methane is highest for all samples containing the lowest amount of chlorine, also when water is added to the reduction gas.

3.3 STEM/EDX

The metal particles can be observed as diffuse white spots on the annular dark-field STEM micrograph. Information about the composition of the particles was obtained by collecting EDX-spectra of 100 - 120 particles for each sample. Particle composition - size diagrams, such as the ones shown in Figures 1 - 4 were made for all samples.

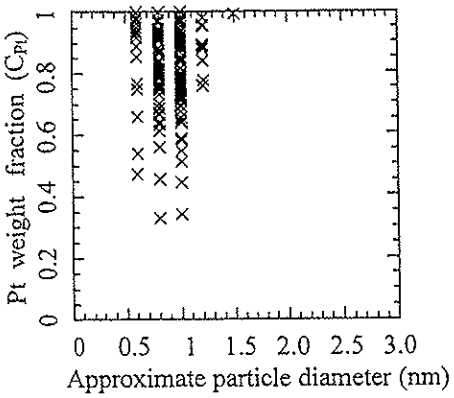

Fig.1. Approximate particle diameter and measured Pt fraction of individual metal particles in sample 1 (0.65 wt% Cl, dry reduction).

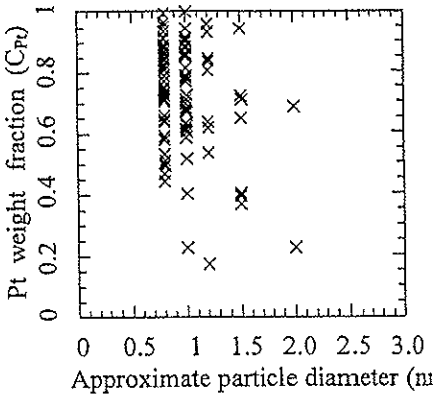

Fig.2. Approximate particle diameter and measured fraction of individual metal particles in sample 3. (1 wt% Cl, dry reduction).

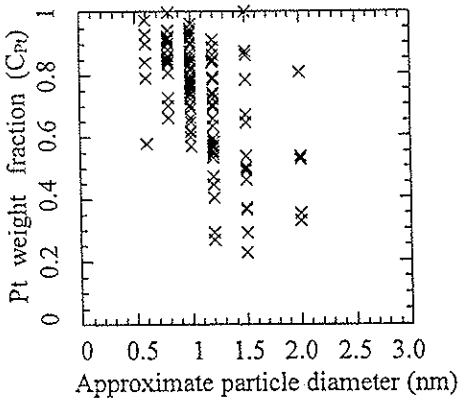

Fig.3. Approximate particle diameter and measured Pt fraction of individual metal particles in sample 4. (0.65 wt% Cl, moist reduction).

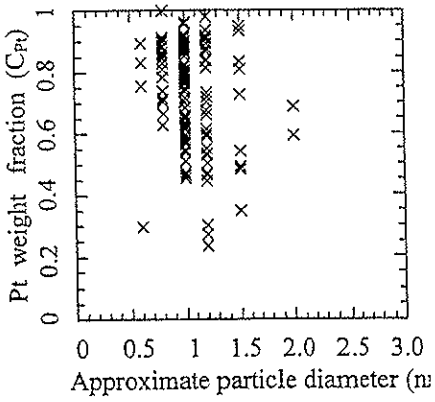

Fig.4. Approximate particle diameter and mea fraction of individual metal particles in sample wt% Cl, moist reduction).

The metal particles of the $PtRe/Al_2O_3$ catalyst are very small (≤ 2nm). This makes direct studies of the metal sites very difficult due to the resolution limitation of conventional instruments. Previous studies [11] using combined STEM and EDX to describe the PtRe alloy formation for the same catalyst system, have indicated that no rhenium was alloyed with platinum. However, it seems that the particles studied in this case were too large (2-3nm) to represent the system. The instrument used here (VG Microscope HB 603) has been specially designed for high spatial resolution [16], and studies of particles smaller than 1 nm are possible.

Figs. 1 through 4 show the the composition - size diagrams obtained from the STEM/EDX analysis of sample 1,2,3, and 4. The average particle size and the average metal composition were calculated for each sample based on the data collected from the STEM/EDX analysis, and are given in Table 5 and 6. These results give an indication of the state of the metal particles on the catalyst after reduction. It is obvious that the average particle size and composition is very approximate as the distribution of both parameters are so broad and it is therefore hard to see useful trends from these data. It can be concluded that the effect of the effect chlorine level on the bimetallic particle formation is too limited to be observed using this technique. The lack of significant results can be attributed various factors such as a limitation in the number of particles analysed. However, by comparing the shape of the composition - size diagrams in Fig. 1 and 3 one can observe that the particles are somewhat larger and more alloyed when water is added to the reducing gas. It can be speculated that the effect of moisture introduced in the reduction gas is to induce the formation of larger particles. As previously discussed, water ensures rhenium mobility and platinum sintering, creating larger particles as observed.

Table 5
Average platinum compositions (C_{Pt}) and particle sizes (D_{Pt}) obtained from combined EDX/STEM analysis of the $PtRe/Al_2O_3$ catalyst containing different levels of chlorine. Reduction in dry H_2.

Sample	Chlorine level	EDX C_{Pt}	STEM $D_{Particle}$ [nm]
1	0.65	0.8	0.9
2	1.10	0.8	1.0
3	1.50	0.7	1.0

The results presented in Table 5 show that there is no significant individual difference between samples 1 to 3. This is as expected from observations of the composition - size diagrams shown in Figs. 1 - 2.

Table 6
Average platinum compositions (C_{Pt}) and particle sizes (D_{Pt}) obtained from combined EDX/STEM analysis of the $PtRe/Al_2O_3$ catalyst containing different levels of chlorine. Reduction in moist H_2.

Sample	Chlorine level	EDX C_{Pt}	STEM $D_{Particle}$ [nm]
4	0.65	0.7	1.1
5	1.10	0.7	1.2
6	1.50	0.7	1.1

After reduction of the dry (510°C in air) oxychlorinated samples in moist (5000 ppm H_2O) hydrogen, the STEM/EDX data presented in Table 6 indicate that the average particle diameter is larger than when reducing in dry hydrogen and a higher degree of alloy formation is present. The composition – size diagrams of sample 4 and 6 are presented in Figure 3 and 4. The effect of water can be interpreted as being beneficial for the mobility of rhenium oxide species as previously discussed. However, it is not possible to find significant differences in alloy formation with varying chlorine content. As discussed previously, the introduction of water may introduce some stripping of chlorine, and this will also effect the formation of bimetallic clusters during reduction. The influence of water can thus be

both ascribed to the removal of chlorine and introduction of more hydroxyl groups on the catalyst surface. Both effect the mobility of rhenium, and thus the alloy formation.

3.2 TPR

From the TPR profiles in Figure 5, it is observed a first peak at about 250°C which can be assigned to the reduction of Pt. At 350°C an other peak, or "shoulder" appears which is characteristic of further reduction of Pt and the catalytic reduction

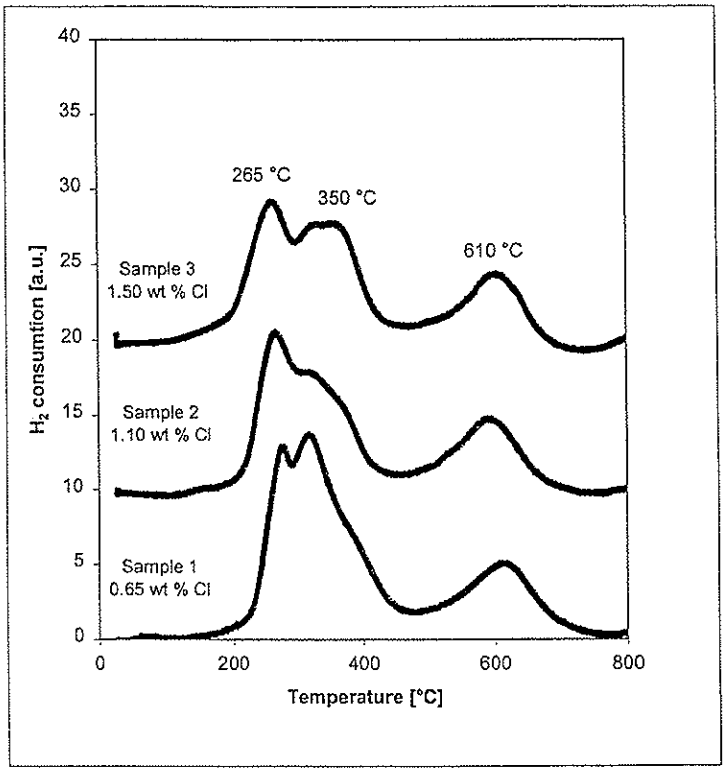

Fig.5.TPR profiles of PtRe catalyst with different chlorine content. Sample 1: 0.65 wt% Cl, Sample 2 1.10 wt% Cl and Sample 3: 1.50 wt% Cl.

of Re by Pt. The further reduction of rhenium can be seen as a peak at 610°C. Sample 1 to 3 differ in their TPR profile. Sample 1, with the lowest chlorine level, has the narrowest and largest peak in the low temperature region. Sample 2 and sample 3 have a lower H_2 consumption in this area reflected by the smaller peaks. This is as an indication of more formation of alloyed particles on sample 1 with the lowest chlorine level. Measurements of H_2 consumption and calculation of the degree of reduction of the metals are complicated by the fact that there might be some reduction and removal of chlorine. However, according to Barbier [17] the chlorine level is approximately constant at low concentrations. Using the monometallic Pt catalyst (CK 300) as a standard, and assuming 100% reduction, the degree of reduction of Re can be calculated (both the co-reduction with Pt and the reduction at 610 °C) by subtracting the hydrogen consumed by Pt. Re in sample 1 is reduced to ca. 80 %, whereas the reduction degree of sample 2 and 3 is as low as 30 %. The difference is reflected in the different size of the first peaks in the low temperature region. A higher degree of reduction of rhenium in the low temperature region in sample 1 can be interpreted such that this catalyst contains more alloyed particles than sample 1 and 2.

4. Conclusions

Using both physical and indirect experimental techniques, the effect of the chlorine content prior to reduction on the bimetallic formation in the Pt-Re/Al_2O_3 catalyst has been studied. Indirect methods such as model reactions, hydrogen chemisorption, and TPR studies indicate that too much chlorine on the catalyst surface during reduction is undesirable with respect to bimetallic particle formation. Chlorine has apparently an inhibiting effect on the mobility of Re in the reduction process. The effect of chlorine on the bimetallic formation is, however, limited as compared to the effect of water during reduction. Addition of water enhances the formation of alloyed particles and this might be due to increased rhenium oxide mobility and stripping of chlorine of the support. Direct physical measurements employing combined EDX/STEM does not reveal any significant differences in alloy formation with increasing chlorine content due to the broad distribution of both size and composition of the particles. However, by comparing the shape of the composition - size diagrams in Fig. 1 and 3 one can observe that the particles are somewhat larger and more alloyed when water is added to the reducing gas.

Acknowledgements

The financial support of the Norwegian Scientific Foundation VISTA is gratefully acknowledged.

References

1. Kluksdahl, H.E., U.S. Patent 3,415,737 (1968)
2. Betizeau, C., Leclerq, G., Maurel, R., Bolivar, C., Charcosset, H., Frety, R., and Tournayan, L., *J. Catal.*, **45**, 179 (1976).
3. Biloen, P., Helle, J.N., Verbreek, H., Dautzenberg, F.M., and Sachtler, W-M.H., *J. Catal.* **63**, 112 (1980)
4. Shum, V.K., Butt, J.B., and Sachtler, W.M., *J. Catal.* **96**, 371 (1985)
5. Riberio, F.H., Bonivardi, A.L., Kim, C., and Somorjai, G.A., *J. Catal.* **150**, 186 (1994)
6. Augustine, S.M., Alameddin, G.N., and Sachtler, W.M.H., *J. Catal.* **115**, 217 (1989)
7. Michel, C.G., Bambrick, W.E., and Ebel, R.H., *Fuel Proc. Technol.* **35**, 159 (1993)
8. Malet, P., Munuera, G., and Caballero, A., *J. Catal.* **115**, 567 (1989)
9. Pieck, C.L., Marecot, P., Parera, J.M., and Barbier, J., *Appl. Catal.* **126**, 153 (1995)
10. Prestvik, R., Moljord, K., Grande, K., and Holmen, A., *J. Catal.* **174**, 119 (1998)
11. Prestvik, R., Tøtdal, B., Lyman, C.E., and Holmen, A., *J. Catal.* **176**, 246 (1998)
12. Augustine S.M., and Sachtler, W.M.H., *J. Catal.* **106**, 417 (1987)
13. Blekkan, E. A., Holmen, A., and Vada, S., *Acta Chemica Scandinavia* **47**, 275 (1993)
14. Freel, J., *Prepr. Amer. Chem. Soc. Div. Petrl. Chem.* **18**, 10 (1973)
15. Isaacs, B.H., Petersen, E.E., *J. Catal.* **85**, 1 (1984)
16. Lyman, C.E., Goldstein, J.I., Williams, D.B., Ackland, D.W., von Harrach, S., Nocholls, A.W., and Statham, P.J., *Journal of Microscopy* **176**, 85 (1994)
17. Barbier, J., Bahloul, D., and Marecot, P., *J. Catal.* **137**, 377 (1992)

Paper IV

Catalytic reforming

Torbjørn Gjervan[1], Rune Prestvik[2], and Anders Holmen[1]

[1] Department of Chemical Engineering, Norwegian University of Science and Technology (NTNU), 7491 Trondheim, Norway
E-mail: Holmen@chembio.ntnu.no
[2] SINTEF Applied Chemistry, 7465 Trondheim, Norway

Abstract: Catalytic reforming is an important refinery process for the production of high-octane gasoline, hydrogen, and aromatics from naphtha. The most important reactions occurring are dehydrogenation of naphthenes, dehydrocyclisation of paraffins, isomerisation, and dehydroisomerisation. In addition, the process suffers from catalyst deactivation by coking. The catalyst employed in reforming is bifunctional in nature consisting of a noble metal supported on alumina. Hydrogenation/Dehydrogenation reactions are catalysed by the noble metal, e.g. platinum. Isomerisation reactions are catalysed by the support, which is acidic in nature. The alumina supported platinum catalyst has been used for decades but has been improved by the addition of a second element such as rhenium, tin or iridium. The chemical state of the second element and the exact role of the element in bringing about higher stability in catalytic reforming have been intensively studied for many years. Due to environmental concerns the aromatic content of gasoline will have to be reduced. In addition, the possible introduction of hydrogen as an alternative motor vehicle fuel may seriously threaten the role of catalytic reforming in the future.

1.1 Introduction

Catalytic reforming is an important process in today's refineries and is one of the largest users of catalysts in the chemical industry. According to the International Petroleum Encyclopedia (1999) [1] there are 755 catalytic reforming plants world-wide with a total capacity of more than 11 million barrels per calendar day. The reforming process involves the reconstruction of low-octane hydrocarbons boiling in the gasoline range into more valuable high-octane gasoline components, such as aromatics and highly branched paraffins, without significantly changing their carbon numbers. Catalytic reforming is a major refining process due to the large and still increasing demand for motor fuel, and for high-value aromatic hydrocarbons such as benzene, toluene and xylenes (BTX) being important building blocks of the petrochemical industry.

Fig. 1.1 illustrates how the catalytic reforming unit is integrated in a typical motor fuels refinery. Feedstocks are hydrodesulphurised straight-run heavy naphthas and cracker naphthas. The liquid C_{5+} product (reformate) from the reformer typically account for 30-50% by volume of the total gasoline pool [2].

The reformate is blended with other available refinery streams such as isomerate (branched paraffins), naphtha from catalytic cracking, coking, and visbreaking (rich in olefins and aromatics), alkylate (highly branched paraffins), and straight run naphtha in order to obtain the desired gasoline properties. Tetraethyl lead are still being added as an octane booster to the gasoline in some countries, but are most likely to be phased out globally due to strong environmental concerns and the introduction of car exhaust catalysts that are poisoned by lead. It is expected that 84% of all gasoline sold in the world will be unleaded in 2005 [3]. MTBE has been used in gasoline to replace lead and aromatics as octane-boosting components and to increase the content of oxygen in reformulated gasoline, but due to concerns about MTBE contamination in groundwater the use of this additive has become very controversial. Small amounts (ca 1%) of other additives are put in to protect against engine corrosion, condensation (water) and deposition of coke.

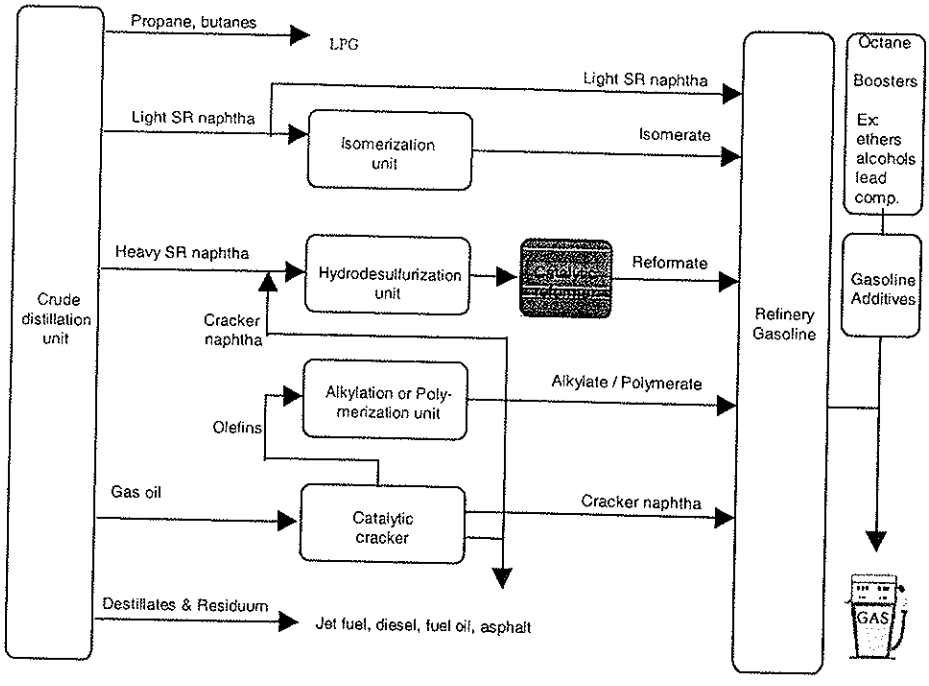

Fig. 1.1. Example of a processing scheme for refinery gasoline production with catalytic reforming. SR = Straight-Run

Hydrogen is an important product from the reforming process and it is usually the main hydrogen source for hydroprocessing, such as hydrodesulphurization and

hydrodenitrification, demetallation and aromatic saturation. The hydrogen yield is typically in the range of 1-5 wt%. The unwanted light paraffins that are also formed in the reaction (5-20 wt% yield) are normally used as fuel gas (C_1-C_2) and liquefied petroleum gas (C_3-C_4). The butanes may also be mixed into the gasoline pool to increase volatility.

1.2 Fundamentals

1.2.1 Feedstocks / octane ratings

The feedstocks for reforming are characterized by their distillation range, their hydrocarbon composition and a number of overall properties (density, molecular weight, octane number), as well as the concentrations of sulphur and nitrogen. The reformer feed properties vary depending on the type of crude, the initial and end point distillation cuts and the amount of the feedstock originating from heavier parts of the crude. A normal feedstock contains 40-70% paraffins, 20-50% naphthenes, 5-20% aromatics and 0-2% olefins and the density is in the range of 0.68-0.76 g/ml. The amount of sulphur and nitrogen has been reduced to ppm levels by hydrotreating in order not to poison the reforming catalyst (and the car exhaust catalyst). Olefins, most of that are present in the cracker naphtha, will be hydrogenated as well. The distillation range is usually cut between C_6 and C_7 in the light end because the C_6 fraction partly will crack to gases and partly form unwanted benzene (in a fuels refinery). In addition the C_6 naphthenes have a higher octane number than their dehydrogenated products as shown in Table 1.1. The light fraction of the naphtha is instead usually upgraded by isomerisation. As the reforming catalyst is more subjected to coke formation using heavier hydrocarbons, the end boiling point is also limited normally up to 150-180°C. For a refinery in BTX operation the preferred naphtha feedstock is narrowed to a pure C_6-C_8 cut.

The purpose of catalytic reforming is to increase the octane number of the feedstock up to a level that makes it suitable as an automotive fuel. Taking the gasoline specifications and the available blending stocks into account an octane number for reformate of 95-102 is usually needed. The octane number represents the ability of a gasoline to resist detonation or knocking during combustion of the compressed air/gasoline mixture in the engine cylinder. The higher the octane number, the less is the tendency for knocking - which strongly limits the efficiency of the automobile engine. In practice two ratings are usually measured and are designated Research Octane Number (RON) and Motor Octane Number (MON) and differ only in the type of engine and test procedure used. RON represents the engine performance at low speed while MON is representative for high speed driving. The octane number displayed on the pumps at service stations is usually either the RON value or an average octane value ½ (RON + MON). In the literature usually RON is used if nothing else is stated. By definition the octane number of n-heptane is zero and the octane number of iso-octane (2,2,4-

trimethylpentane) is 100. The octane number for a gasoline is defined as the volume percent of iso-octane in blending with n-heptane that equals the knocking performance of the gasoline being tested. Some gasoline components have octane numbers exceeding 100 and have to be characterized by use of mixtures. A usual mixture contains 20% of the actual compound and 80% of an n-heptane/iso-octane (40:60) mixture. A hypothetical "blending octane number" is then obtained by extrapolating from 20 to 100 % concentration. The blending octane number is specific for the mixture and usually different from the octane number of the pure component as seen for a range of different hydrocarbons with octane numbers < 100 in Table 1.1.

Table 1.1. Research octane numbers for a range of pure hydrocarbons and in blending [4].

Hydrocarbon	Research Octane Number Pure	Research Octane Number Blending
Paraffins		
n-Butane	94	113
Isobutane	>100	122
n-Pentane	62	62
2-Methylbutane	92	100
n-Hexane	25	19
2-Methylpentane	73	82
n-Heptane	0	0
3-Methylhexane	52	56
n-Octane	<0	-18
n-Nonane	<0	-18
Naphtenes		
Methylcyclopentane	91	107
Ethylcyclopentane	67	74
Cyclohexane	83	110
Aromatics		
Benzene	-	98
Toluene	>100	124
1,2-Dimethylbenzene	-	120
1,3-Dimethylbenzene	>100	145
1,4-Dimethylbenzene	>100	146

Table 1.1 shows that aromatics generally have much higher octane numbers than naphthenes, olefins, and paraffins and are therefore the most desired products. The octane number of the aromatics (except for benzene) is always above 100. Straight chain paraffins have very low octane numbers (RON < 0 for n-octane and n-nonane), but the octane number increases markedly with the degree of branching (RON > 100 for 2,2,3-trimethylbutane). The octane number of the paraffins declines as the number of carbon atoms increases and is very low for paraffins with more than seven carbon atoms. Unsaturation (paraffins to olefins) also result in an octane enhancement. Branching does not positively influence naphthenic hydrocarbons and their octane values are in average not very high. The above comparison show that the desired products for obtaining high octane numbers are aromatics and highly branched paraffins or olefins, although the latter group is not formed in the reformer due to thermodynamic limitations. An increase in the octane number can therefore best be obtained by transformation of naphthenes into aromatics and of linear paraffins into branched paraffins - or even better into aromatics.

1.2.2 Reactions

The major reactions contributing to the improvement of the octane number are (a) dehydrogenation of cyclohexanes to aromatics, (b) dehydroisomerization of alkylcyclopentanes to aromatics, (c) isomerization of straight-chain paraffins to branched paraffins and (d) dehydrocyclization of paraffins into aromatics. Other important reactions are (e) hydrocracking and hydrogenolysis (carbon-carbon bond scissions), which result in low molecular weight paraffins, and (f) coke formation. Like most other hydrocarbon reactions at elevated temperatures, reforming reactions are accompanied by formation of carbonaceous residue (coke) which may poison the active sites of the catalyst. The relative importance of the reforming reactions depends on the nature of the catalyst, the composition of the feedstock and the conditions of operation.

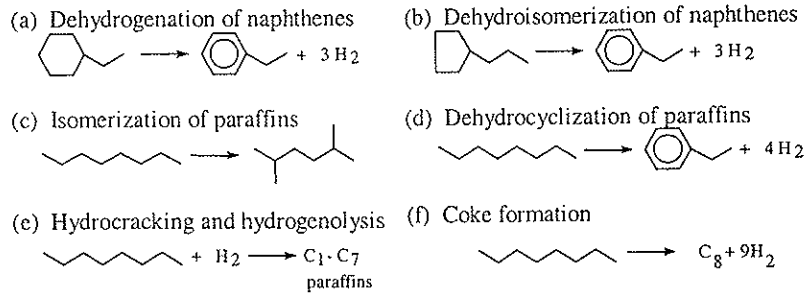

Fig. 1.2. Major catalytic reforming reactions exemplified with some C_8 hydrocarbons

Fig. 1.2 gives examples of these major reactions in the reforming of C_8 hydrocarbons. The reforming catalyst is a bifunctional catalyst with a metal function for hydrogenation and dehydrogenation reactions and an acid function for hydrocarbon rearrangements. Both the metal and acid sites on the Pt/Al_2O_3 catalyst are dispersed on the surface of the carrier material. The two catalyst functions interact through the olefins, which are key intermediates in the reaction network. The bifunctional reaction network shown in Fig. 1.3. was originally proposed by Mills and co-workers [5] but has later been modified [6]. The vertical paths in the figure take place on the metal and the horizontal paths proceed on the acid sites. The conversion of n-hexane into iso-hexanes first involves dehydrogenation on the metal to yield n-hexene. The hexene migrates to a neighboring acid site where it is isomerized (carbonium ion mechanism). Finally the iso-paraffin is formed by hydrogenation of the iso-olefin at a metal site. It has been shown that mechanical mixtures of particles containing each of the two functions are active for isomerization at rates comparable to the rates for the dual function catalyst [7]. Therefore, the two types of sites in the dual function catalyst can operate individually and the olefin intermediates can migrate between the sites by gas phase diffusion.

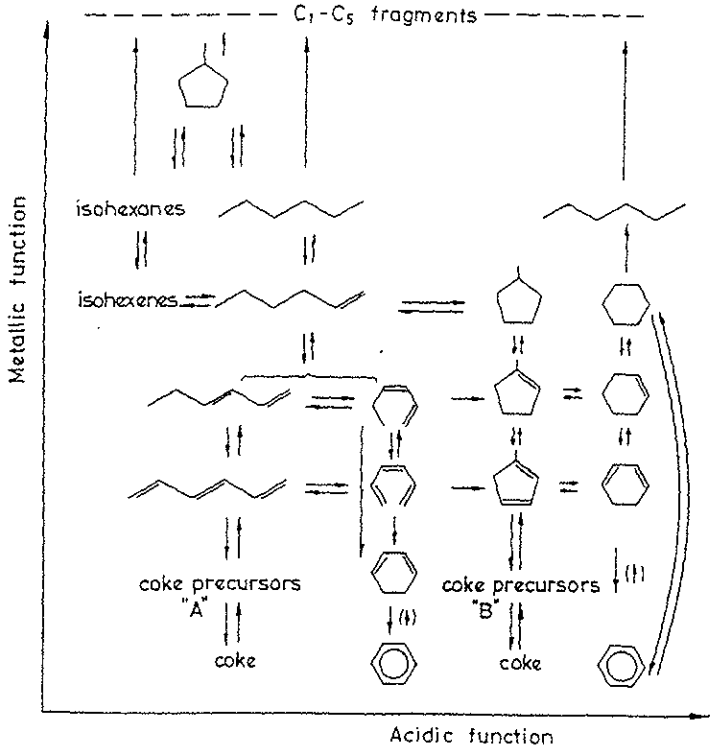

Fig. 1.3. Reaction network for the reforming of C_6 hydrocarbons [6].

1.2.3 Thermodynamics

Table 1.2 shows equilibrium constants and heats of reaction for some reactions of C_6 and C_7 hydrocarbons occurring at 500°C, reflecting the overall thermodynamics of catalytic reforming. Generally, the heats of reaction depend only slightly on the number of carbon atoms in the molecule. The formation of aromatics from cyclohexanes produces a significant RON increase, and from Table 1.2 it can be observed that the dehydrogenation of cyclohexanes to yield aromatics is strongly endothermic and the conversion is favoured by high temperature and low pressure. The equilibrium constants show that the reactions are almost completely displaced to the aromatics at 500°C. An increase in hydrogen partial pressure or total pressure will, however, shift the equilibrium toward the naphthenes. The effects of temperature and pressure on the concentration of toluene in equilibrium with C_7 naphthenes are shown in Fig. 1.4.

Table 1.2. Thermodynamic data, at 500°C, of some typical reforming reactions with C_6 and C_7 hydrocarbons.

Reaction type	Reaction	K_p (p in atm)	ΔH_R (kJ/mol)
Dehydrogenation	Cyclohexane ⇔ Benzene + 3 H_2	6×10^5	221
	Methylcyclohexane ⇔ Toluene + 3 H_2	2×10^6	216
	n-Hexane ⇔ 1-Hexene + H_2	0.04	130
Dehydroisomerization	Methylcyclopentane ⇔ Benzene + 3 H_2	5.2×10^4	75
Isomerisation	n-Hexane ⇔ 2-Methylpentane	1.14	-5
	n-Heptane ⇔ 2-Methylhexane	41.69	-6
	Methylcyclopentane ⇔ Cyclohexane	0.09	-16
Dehydrocyclisation	n-Hexane ⇔ Benzene + 4 H_2	7.8×10^4	266
	n-Heptane ⇔ Toluene + 4 H_2	2.1×10^6	252
Hydrocracking	n-Heptane + H_2 ⇔ Propane + n-butane	3.1×10^3	-52
Hydrogenolysis	n-Heptane + H_2 ⇔ Methane + n-Hexane	1.2×10^4	-62

Source: Calculated from API Research Project [8].

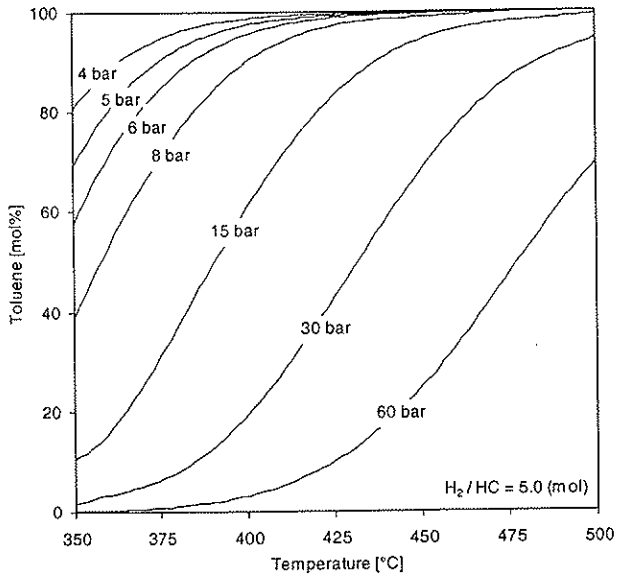

Fig. 1.4. The effect of temperature and pressure on the concentration of toluene in thermodynamic equilibrium with H_2 and C_7 naphthenes.

The thermodynamics of the dehydroisomerisation of cyclopentanes is similar to that of the dehydrogenation reactions, but the reaction is slightly less endothermic and the equilibrium constant is lower. Since the reaction involves an isomerisation step, the rate is lower than for pure dehydrogenation reactions, but high enough for the equilibrium to be approached under normal reforming conditions.

Paraffin dehydrocyclisation is a key reaction in catalytic reforming. It results in the highest RON improvement of all the reactions occurring in the process. Conversion of n-heptane into toluene equals a difference of over 100 RON units. The thermodynamics is similar to that of dehydrogenation of naphthenes. However, the rate of the reaction is slow, thermodynamic equilibrium is not reached and the reaction is kinetically controlled.

The isomerisation of paraffins is rapid and the conversion to isoparaffins is limited by the thermodynamic equilibrium. The heat of reaction is low (mildly exothermic) and temperature has only a moderate effect on the conversion within the temperature window typically applied in catalytic reforming (450-520°C). A low reaction temperature is the most favourable thermodynamically. Since the number of reactant and product molecules in the reaction are equal, neither the total nor the hydrogen pressure influences the equilibrium notably. Most fortunately, the equilibrium favours the more desirable (higher-octane) branched isomers. Isomerisation therefore makes a significant contribution to the octane improvement.

Paraffin dehydrogenation is strongly endothermic. At equilibrium, only very small concentrations of olefins can exist at the hydrogen partial pressures normally employed in reforming as reflected by the small K_p in Table 1.2. Thus the contribution of olefins to the octane number of reformate remains very low. Nevertheless, the olefins are important reaction intermediates in some of the reforming reactions. The thermodynamics sets an upper limit on the attainable concentration of olefins in the system and may therefore limit the overall rate for these reactions. In addition, the olefins may be further dehydrogenated and polymerised, particularly at low hydrogen pressure, and form carbonaceous residue (coke) covering the active surface.

The naphthenes isomerisation reactions are mildly exothermic. The equilibrium between methylcyclopentane and cyclohexane clearly favours the former at typical reforming conditions. The reaction is, however, relatively rapid and equilibrium is established under reforming conditions.

Hydrocracking is promoted under hydrogen pressure. It involves rupture of carbon-carbon bonds producing light paraffins as products. The reaction results in a loss of reformate yield, valuable hydrogen is consumed and is therefore in general unwanted. However, a limited degree of hydrocracking - transforming the heaviest paraffins into lighter ones having higher octane ratings as well as concentrating the aromatics - will increase the octane number of the reformate and is often needed to reach a specified RON level. The cracking reaction involves a classical carboniumion mechanism that favours the formation of propane and butanes.

Hydrogenolysis is a carbon-carbon bond scission reaction that is, as for hydrocracking, very feasible thermodynamically. Both hydrocracking and hydrogenolysis are very exothermic and highly favoured by low temperature from a thermodynamic point of view. However, the reaction rates are relatively slow and the reaction is solely kinetically controlled. Unlike hydrocracking, hydrogenolysis produces large amounts of methane and ethane.

1.2.4 Kinetics

Dehydrogenation reactions occur readily on commercial reforming catalysts at the temperatures employed during catalytic reforming, and equilibrium is reached relative fast. Isomerisation of paraffins is also a fairly rapid reaction, and equilibrium is usually approached. However, the equilibrium concentration of some of the products is not fully attained. Dehydrocyclisation, hydrocracking, and coking are reactions that are kinetically controlled, and the product composition will depend on the relative rates of the various reactions, controlled by factors such as temperature, pressure and catalyst composition.

The temperature has an obvious impact on the kinetics of the reforming reactions. Fig. 1.5 a) clearly demonstrates that the research octane number (RON) of the liquid product increases as the temperature is increased during reforming of straight-run naphtha from North Sea crude [9]. Even though it is favourable from a thermodynamic point of view with high temperature conditions, the selectivity to unwanted cracking products will increase more than the desired products. This is due to a higher activation energy of the cracking reaction compared to reactions such as dehydrocyclisation. It is evident from Fig. 1.5 b) that the reformate yield decreases with increasing temperature due to increased selectivity to unwanted reactions such as hydrocracking.

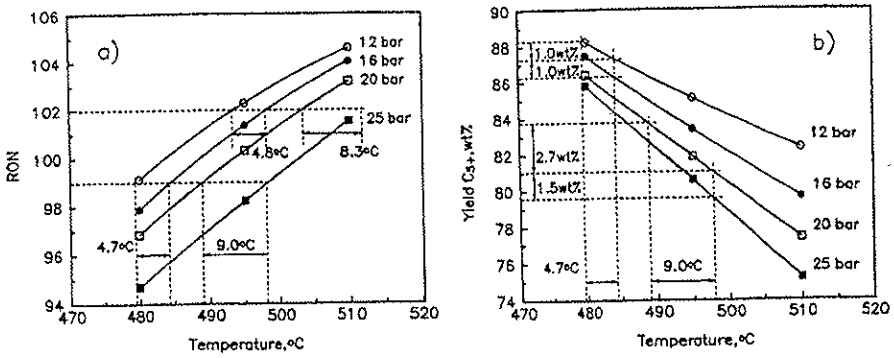

Fig. 1.5. RON (a) and reformate yield (b) as a function of the reaction temperature at different reaction pressures [9].

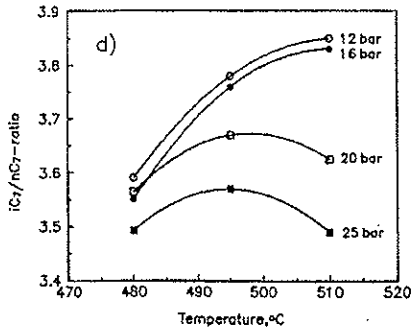

Fig. 1.6. iC_7/nC_7 ratio as a function of the reaction pressure at 12,16,20, and 25 bar [9].

Higher selectivity to cracking as a function of temperature can also be observed from Fig. 1.6, which shows the *i/n*-ratio of C_7 paraffin isomers at different reaction temperatures and reaction pressures. Multi-branched isomers are secondary products formed via single-branched isomers [10], and equilibrium is largely attained between normal paraffins and their single-branched isomers [11]. However, *i*-C_7 cracks more easily than *n*-C_7 and the *i/n*-ratio is therefore not thermodynamically controlled. At low reaction pressures this trend is not evident and the selectivity to *i*-C_7 increases with increasing temperature until thermodynamic equilibrium is attained at 510°C at 12 and 16 bar. At higher reaction pressure there is a net consumption of *i*-heptanes due to hydrocracking and there is a large drop in the *i/n*-ratio.

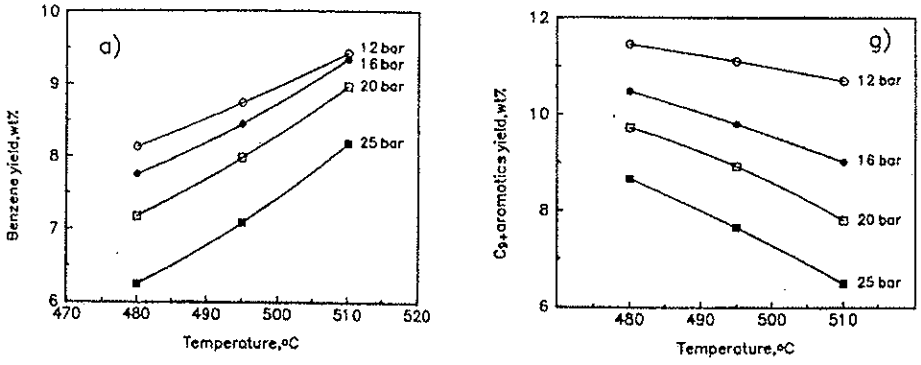

Fig. 1.7. Yield of benzene and C_{9+} aromatics as a function of reaction temperature and pressure [9].

As dehydrogenation and dehydrocyclisation are favoured at high temperature the yield of benzene increases with increasing temperature as shown in Fig. 1.7. Furthermore, benzene production is favoured at low reaction pressures. On the contrary the yield of C_{9+} aromatics (for example) decreases with increasing temperature and increasing pressure as a consequence of side chain hydrodealkylation.

Figs. 1.5, 1.6, and 1.7 all demonstrate the beneficial effect of low reaction pressure operation in order to obtain high yields of reformate and high-octane products. From Fig. 1.5 a) it can be observed that for a given severity in the range 99-102 RON, the temperature can be lowered by 8-9°C when going from 25 bar to 20 bar. At the same time the formation of carbonaceous deposits is favoured and it is therefore important to keep a certain pressure in order to suppress catalyst deactivation caused by coke formation. In order to be able to run at low-pressure conditions emphasis must be put on catalyst optimisation to make the catalyst more stable and active at less severe process conditions.

Measurements of individual reaction rates during reforming are made difficult by the complexity of the overall reaction and due to catalyst deactivation during operation. There exist several kinetic simulation models that describe the reaction kinetics during catalytic reforming. In such models certain simplifications are made in order to reduce the number of reaction species and reaction pathways involved.

1.2.5 Catalyst

The catalyst used in commercial reforming processes is a bifunctional catalyst involving an acidic function and a dehydrogenation-hydrogenation function. The latter is provided by a noble metal such as platinum. Most modern reforming catalysts consist of platinum promoted with elements such as Re, Sn, and Ir in order to enhance the stability and selectivity of the catalyst. The metals are usually deposited on a chlorinated porous high surface area alumina which act as the acidic function of the catalyst.

The catalyst support

The acidic function of the catalyst promotes skeletal rearrangement and the support usually consists of one of the two alumina crystallite forms η-Al_2O_3 or γ-Al_2O_3 [12]. In order to selectively crack low octane n-paraffins acidic zeolites having shape-selective cracking properties have also been employed together with conventional reforming catalyst [13-15].

The aluminas are made from aluminium hydrates, η-Al_2O_3 from gibbsite or bayerite and γ-Al_2O_3 from bohemite, by calcination in air or vacuum. Both forms are highly stable aluminas with a spinel structure (cubic close packing) characterised by high surface area. Both Brønstedt and Lewis acidity may exist on the alumina surface and the fraction of each depend on the degree of hydration [16]. Based on techniques such as ammonia adsorption and IR measurements Peri [16-18] proposed an idealised model for the surface alumina and suggested that

the catalytic activity of these supports were closely related to certain acid sites (aluminium ions that act as Lewis acids) created by the desorption of hydroxyl groups on the surface. On the other hand, Knözinger and Ratnasamy [19] have shown that the catalytic activity is primarily not due to such Lewis acid sites. These authors attributed the catalytic activity to OH groups with neighbouring defects sites created in the partially dehydroxylated surface.

The acidity of the support is enhanced by treating the alumina with halogens, preferable chloride in the form of HCl or carbon chlorides. Gates et al [20] proposed a model illustrated in Fig. 1.8 where the acidity of the OH groups are strengthened by the inductive effect exerted by an adjacent Cl^- ion.

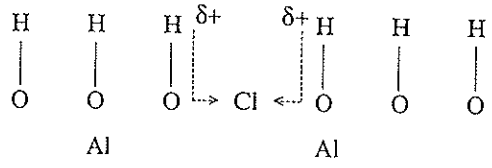

Fig. 1.8. Enhancement of the Brønstedt acidity by adjacent Cl^- ions [20]

Increasing the acidity of the support with a high chlorine content will lead to excessive unwanted hydrocracking while a low content results in low activity for isomerization and dehydrocyclization. Chlorine is removed from the support by water present in the feedstock and during operation the chlorine content must be maintained by continuously adding chlorine to the feedstock at a fixed Cl/H_2O ratio.

The Pt/Al_2O_3 catalyst

Platinum is the preferred metal in reforming catalyst both due to its high activity and to its good selectivity characteristics. Table 1.3 shows the results obtained by Ciapetta et al. [21] when comparing the activities for dehydrogenation of benzene on various metal-oxide catalysts and other supported metals. It is clearly illustrated that platinum is by far the most active metal for dehydrogenation even when compared to palladium, iridium and rhodium.

Table 1.3. Cyclohexane dehydrogenation activities of supported metal and metal oxide catalysts [21].

Catalyst, wt%	Dehydrogenation acivity (μmoles benzene/g catalyst/s)
34% Cr_2O_3 cogelled with Al_2O_3	0.5
10% MoO_3 coprecipitated with Al_2O_3	3
5% Ni on Al_2O_3 or SiO_2-Al_2O_3	13
5% Co on Al_2O_3	13
0.5% Ir on Al_2O_3	190
1% Pd on Al_2O_3	200
5% Ni on SiO_2	320
1% Rh on Al_2O_3	890
0.5% Pt on Al_2O_3 or SiO_2-Al_2O_3	1400-4000

Differential flow reactor at 427°C, 6.8 atm, H_2/HC = 6 (mole ratio), activity determined after 30 min on stream, pre-treated with H_2 at reaction conditions, LHSV varied to give differential operation

Except for naphthene dehydrogenation, which is structure insensitive and is depending on the number of exposed platinum atoms only, the other reforming reactions are favoured kinetically by small crystallite sizes [22]. The smaller the platinum ensembles are, the more stable and resistant to coke formation is the catalyst [23]. Considering also the high cost of the platinum metal, it is desirable to deposit it onto the porous alumina support in a highly dispersed form possibly atomically dispersed. Sufficient activity and high dispersion require only small amounts of platinum and the current commercial catalysts typically contain in the order of 0.2-0.4 wt% of platinum. Depending on the preparation technique the metal particle size can vary in the range 0.8 to 1000 nm [20]. Fig. 1.9. shows an annular dark field image of a Pt-Re/Al_2O_3 catalyst (single piece of alumina) and a corresponding X-ray spectrum of one metal particle obtained using combined scanning transmission electron microscopy and electron-dispersive X-ray analysis [24]. The metal particles detected, observed as small white dots, varies from 1 nm to 0.5 nm in size. Particles below this size were not measurable due to resolution limitations of the microscope applied [25].

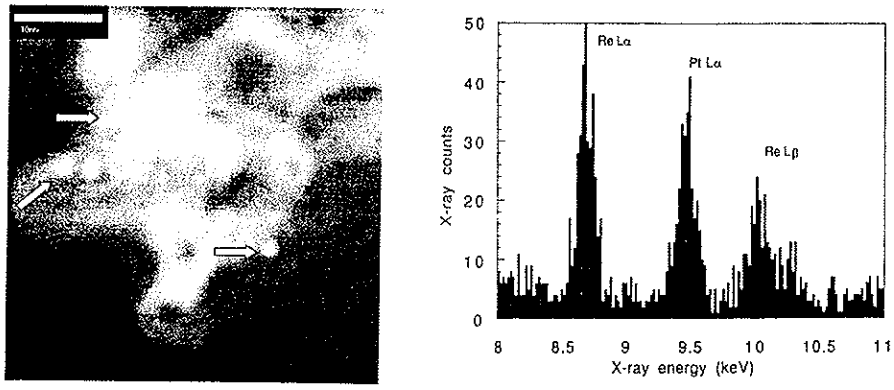

Fig. 1.9. Annular dark field image of a single piece of a $PtRe/Al_2O_3$ catalyst and a X-ray spectrum of a single particle [24].

The dispersion of the platinum on the support can be measured be a number of techniques such as electron microscopy, X-ray line broadening, small-angle x-ray scattering, and gas chemisorption [26]. Metal dispersion measurement by selective H_2 chemisorption and H_2-O_2 titration is a frequently applied for characterisation of reforming catalysts. In order to calculate the dispersion from H_2 chemisorption the H/Pt stoichiometry has to be defined, and in most studies a H/Pt stoichiometry of unity has been applied [27]. Volumetric chemisorption of hydrogen of the standard 0.3 wt% Pt/Al_2O_3 Akzo CK 303 catalyst, typically yields a dispersion of 90-95% [28].

The $PtRe/Al_2O_3$ catalyst

One of the first bimetallic catalysts was introduced by Chevron in 1969 [29] and was based on platinum and rhenium. Today, catalysts based on these elements are among the most important in industrial catalytic reforming. Other common additives ranged in commercial availability are tin [30], iridium [31] and germanium [32]. In the patent literature a number of other additives have also been reported. The most frequently studied and utilised catalyst will be described in the following chapters.

The presence of rhenium markedly decreases the rate of deactivation by coke formation allowing long runs at relatively low pressures. Due to the high hydrogenolysis activity of rhenium sulphur is added to deactivate the rhenium sites. The rhenium content in an industrial catalyst is similar to the amount of platinum. However, the tendency points toward higher rhenium to platinum ratios (for example 0.2 wt% Pt-0.4 wt% Re) which presumably will increase the dilution of platinum with rhenium.

The higher stability of the Pt-Re(S) catalyst compared to the monometallic Pt/Al_2O_3 catalyst has been claimed to be due to a different location of the coke [33] and to a different nature of the coke [34] rather than due to a lower amount of coke deposited. Pt-Re catalysts may operate satisfactorily with coke levels approaching 25 wt% [35]. In Table 1.4. the change in the nature and amount of the coke with the addition of Re and S is shown. After having added sulphur to the catalyst, the carbon deposition is reduced from 200 to 116 μmol/g cat, and the carbon species are much richer in hydrogen [36].

Table 1.4. Carbon and hydrogen retained on the catalyst [36]

Catalyst	Carbon retained (μmol/g cat)	Hydrogen retained (μmol/g cat)	H/C
Pt/Al_2O_3-Cl	342	126	0.37
$PtRe/Al_2O_3$-Cl	200	101	0.51
$PtRe(S)/Al_2O_3$-Cl	116	185	1.58

Different theories have been proposed to explain the beneficial role of Re in modifying the catalytic performance of the Pt-Re system. It has been claimed that Re prevents sintering of Pt [29,37] or that Re acts independently as an active ingredient in the modification of the carbonaceous deposits [38]. The most common explanation of the effect of Re on the catalytic properties of the Pt-Re catalyst is that Re is associated with Pt in bimetallic particles and the interaction of such bimetallic particles with sulphur [39-43]. Sulphur adsorbs primarily on rhenium atoms and suppresses the unwanted high hydrogenolysis activity known for Pt-Re alloys. Biloen et al [43] proposed a model, shown schematically in Fig. 1.10 where the rhenium atoms which adsorb sulphur divide the metal crystallite surface effectively into smaller platinum entities and become obstacles against the transformation of soft coke into deleterious graphitic coke, a reaction demanding larger surfaces.

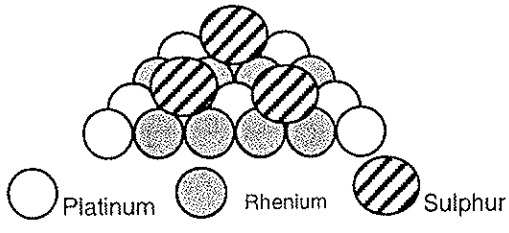

Fig. 1.10. A model for the active surface sites of $Pt\text{-}Re/Al_2O_3$ [43]

Since sulphur mainly adsorbs on rhenium, the number of surface platinum atoms is not significantly reduced upon sulphurisation. It has been demonstrated that sulphur is preferentially bound to the Re atom. Michel et al [44] have observed that after sulphiding and hydrogen stripping only 10% of the Pt and all

of the Re was covered with irreversibly adsorbed S. This has been attributed to the much lower electron affinity of Re [45], and the increases in the electron affinity of Pt by the Re-S bond.

Direct evidence for bimetallic particle formation has been difficult to obtain because of the extremely small size of the metal crystallites (<10 Å) and the subject has been a matter of controversy for over two centuries. However, modern characterisation techniques have clearly proven the existence of bimetallic Pt-Re particles as demonstrated in Fig. 1.11. The individual particle size was found from studying STEM images, whereas the composition is obtained from EDX analysis of each metal particle (A STEM image of a Pt-Re/Al_2O_3 catalyst is shown in Fig. 1.9) [24].

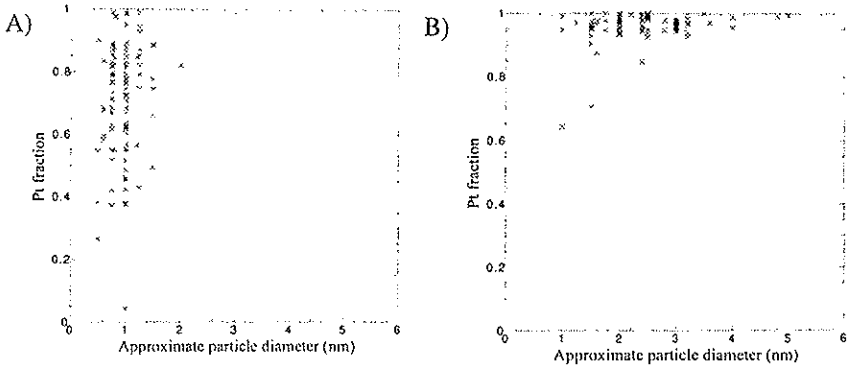

Fig. 1.11. Pt content vs crystallite size measured by ultra high-resolution combined STEM/EDX analysis of individual (x) Pt-Re crystallites on the EUROPT-4 catalyst (0.3-0.3 wt% Pt-Re/Al_2O_3) [24]. (A) High (B) Low 'alloying' degree.

The PtSn/Al_2O_3 catalyst

The catalyst stability of Pt-Sn/Al_2O_3 catalysts is close to that of Pt-Re/Al_2O_3, but the selectivity is better at low pressures and the resistance to platinum sintering is high. Tin does not possess any hydrogenolysis activity and therefore the catalyst does not have to be treated with sulphur prior to use. These features make this catalyst preferable in low-pressure reforming units with frequent regeneration.

To explain the advantageous effect of Sn in the Pt-Sn system two different mechanisms have been proposed. Either is Pt modified by an "ensemble effect" where Sn decreases the number of contiguous Pt atoms, or Sn changes the electronic environment of the Pt atoms. The exact role of Sn in the Pt-Sn system is closely related to the chemical state of Sn in the system. Diverging results from the literature may be due to different catalyst preparation, pre-treatment and experimental techniques applied.

Dautzenberg et al [46] have argumented for the formation of an alloy and that the beneficial effect of Sn is due to the "ensemble" effect. Bacaud et al [47] suggest that alloying accounts for the decrease in catalytic activity related to Pt. In addition it was also suggested that if part of the Pt was unalloyed, its activity is also inhibited due to an electronic effect of Sn ions. Coq and Figueras [48] studied the conversion of methyl cyclopentane on the Pt-Sn system. It was observed that the addition of Sn had a stabilisation effect on the catalytic activity and resulted in a decrease of the hydrogenolysis. Thus, it was concluded that the main role of Sn is to dilute the Pt surface. Li et al [49] concluded that the presence of Sn oxides improves the stability of the catalyst by blocking Pt particle sintering, and that the presence of Pt-Sn bimetallic particles significantly depresses hydrogenolysis. Paál et al [50] rationalised the changes in activity and selectivity brought about by Sn in terms of geometric effects, with Sn as a solid solution in Pt or as an alloy diluting multiatomic Pt sites.

Burch [47] suggested that the special properties of Pt-Sn catalysts cannot be due to a geometrical effect in which Sn divides the surface up in small clusters of Pt atoms as not sufficient metallic Sn was found. The beneficial effect of Sn was attributed to the change in the electronic properties of small Pt crystallites and to the modification of the acidic properties of the support [51]. As a result self-poisoning is reduced and the selectivity to nondestructive reactions is increased. Sexton et al [52] supported the conclusions made by Burch suggesting that Sn(II) is a surface modifier of γ-Al_2O_3 and that the reactivity changes are most likely due to the changes in the electronic interaction between Pt and Sn(II)-γ-Al_2O_3. Parera et al [53] stated that the alloying of Pt with Sn could result in an electron transfer from Pt to Sn, creating electron deficient Pt atoms, which influence markedly the adsorption-desorption steps of the catalytic reaction. It was also suggested that both electronic and geometric effects act together to yield the great decrease in hydrogenolysis.

Catalyst preparation and pretreatment

The procedures for catalyst preparation and pretreatment are very important for the properties of the final catalyst. Platinum metal and the second metal is usually incorporated onto the alumina support by one or two successive impregnations of solutions containing HCl and metal precursors such as H_2PtCl_6, $HReO_4$ and $SnCl_4$. The catalysts are then dried, oxidised (400-600°C), and finally reduced (500-550°C) in hydrogen to convert the platinum oxide species into active zero valent metal. While platinum is usually fully reduced at these temperatures, the reduction degree of rhenium and tin has been a matter of discussion [39,46,47,54-58]. The Pt-Sn catalyst is fully activated after reduction, but the Pt-Re catalyst needs first to be sulphurised. Sulphur is added in the form of H_2S or some carbon sulphide diluted in hydrogen until Re saturation as recognised by sulphur breakthrough at the rector exit. Weakly adsorbed sulphur on platinum is flushed off by H_2 prior to naphtha introduction.

The pretreatment conditions and drying temperature has a significant influence on the final state of the metal particles of the Pt-Re/Al_2O_3 and Pt-Sn/Al_2O_3. In order to obtain bimetallic particles, intimate contact between Pt and the second metal has to be ensured. In the case of the Pt-Re catalyst contact can be obtained

during reduction as the Re oxide species can migrate on the surface. The mobility is controlled by the degree of surface hydration and the drying temperature prior to reduction is very important. Fig 1.12 shows the characteristic TPR profiles of two catalyst samples dried at 240°C and 520°C, respectively [57].

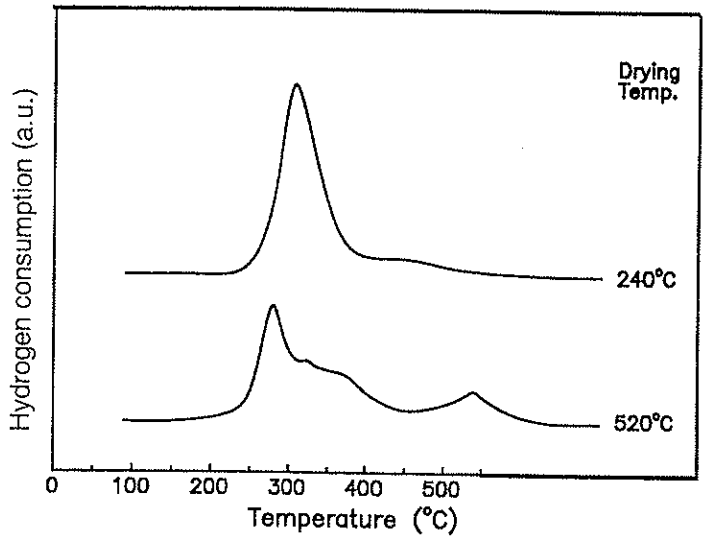

Fig. 1.12. TPR profiles of the $PtRe/Al_2O_3$ catalyst dried at 240°C and 520°C [57].

The TPR profile of the catalyst dried at 240°C show only one peak at 300°C and the hydrogen consumption corresponds to almost complete reduction [57]. This profile is characteristic of simultaneous reduction of Pt and Re and hence the formation of bimetallic particles. Mobile Re oxide species are catalytically reduced by Pt metal atoms on the surface when they get in contact. The catalyst dried at 520°C display a more complex TPR curve which can be attributed to the fact that some of the Re is reduced at higher temperatures forming monometallic particles. The reduction mechanism of the Re oxide species is schematically presented in Fig. 1.13. Hydroxyl groups on the support enables Re oxide species to migrate when the catalyst is dried at 240°C (Fig. 1.13 a). When the catalyst is dried at 520°C the surface is more dehydrated resulting in less Re oxide mobility (Fig 1.13.b).

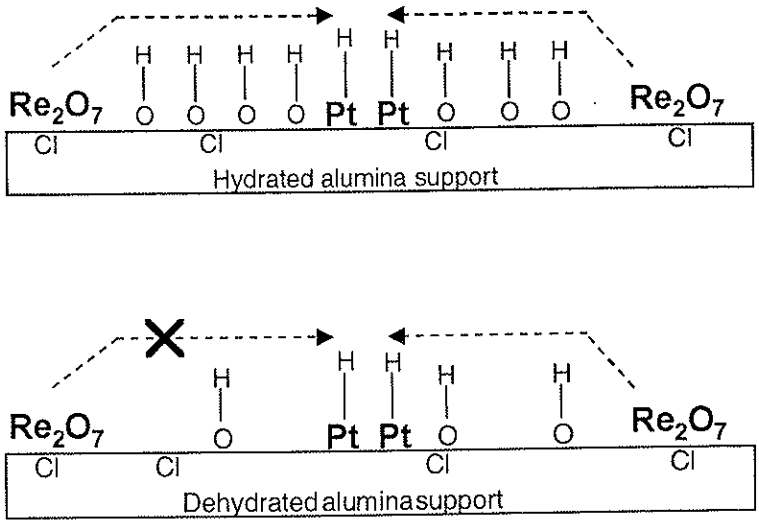

a)
b)

Fig. 1.13. Proposed reduction mechanism for the platinum catalysed reduction of rhenium for catalyst dried at 240°C a) and 520 °C b) [28].

Even if the valence state of Sn is debated in the Pt-Sn system it seems to be a general agreement that Pt may catalyse the reduction of Sn oxides [29,59]. Sn oxides are less able to migrate than Re oxides due to the very strong interaction with the alumina support. Lieske and Völter [59] reported that high temperature calcination (500°C) results in more alloyed particles as Pt (IV) and/or Sn (IV) oxide species are mobile at these conditions. According to the same authors an increasing Sn content gives an increasing amount of alloyed particles. In order to obtain bimetallic PtSn particles, contact between Pt and Sn can be obtained during the preparation step by employing a PtSn complex precursor such as $[Pt(NH_3)_4][SnCl_6]$ [50,60-62] and $[PtCl(SnCl_3)(PPh_3)_2]$ [63]. Investigation of both the Pt-Sn/Al_2O_3 [52,64] and the Pt-Sn/SiO_2 system [65] has shown that the impregnation procedure is very important and that co-impregnation leads to more bimetallic formation than a sequential impregnation procedure.

1.2.6 Catalyst deactivation and regeneration

Catalyst deactivation by coke formation

During reforming operation the catalyst may be subjected to deactivation by poisoning, sintering, and by the formation of coke. Coke formation is the main cause for deactivation determining the cycle length of the catalyst. Coke formation is favoured at high temperatures and low hydrogen pressures, which are also

conditions favourable for the formation of aromatic compounds. Reactions leading to coke formation on the support are acid catalysed polymerisation and cyclisation of olefins to give higher molecular weight compound that undergoes further dehydrogenation, cyclisation, and further polymerisation. Poisoning begins on the metal sites with the formation of olefins and aromatics. These species can slowly be transformed to coke on the metals or migrate to the acid support by gas phase transport or surface diffusion. Coke formed on the acid sites is more resistant, and this poisoning is probably the origin of long term deactivation in reforming. In order to keep constant conversion when the coke builds up on the catalyst, the temperature is increased. This usually results in a liquid yield reduction unless the deactivation of acid sites balances the activity increase caused by the higher temperature.

During reforming carbonaceous deposits are removed by hydrogen cleaning on the catalyst surface. Strong dehydrogenation reactions involved in coking are suppressed by the presence of hydrogen. A small amount of coke is deposited on the metal sites on bifunctional catalysts, whereas the majority of the coke is accumulated on the support. The mechanism of coke removal involves hydrogen spillover from the metal to the alumina support. Iridium and rhenium is known to promote the methanation of coke. The degree of platinum dispersion affects the ease of coke removal, as coke formed on large platinum ensembles is more dehydrogenated than the coke formed on well-dispersed catalysts and will be less reactive with hydrogen.

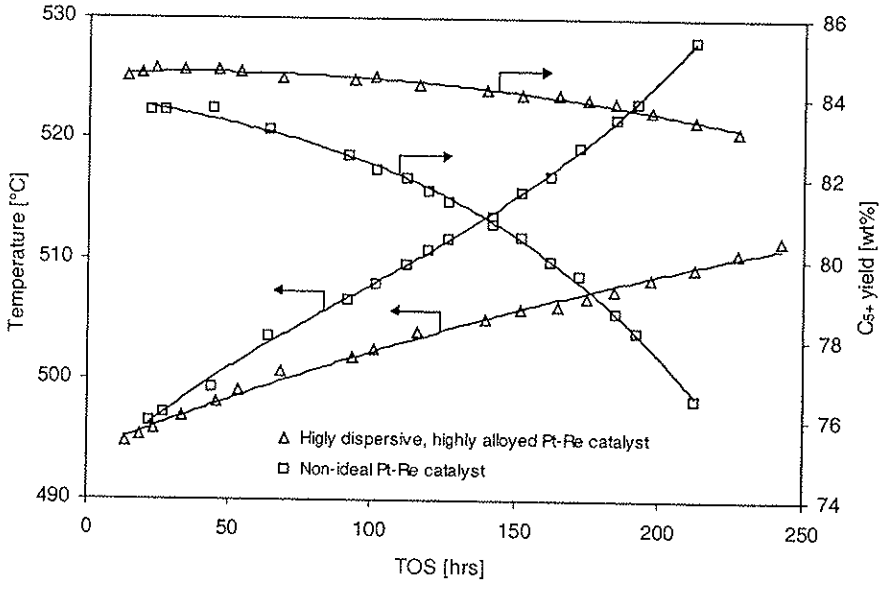

Fig. 1.14. Reaction temperature and reformate yield as a function of time on stream during accelerated deactivation of commercial Pt-Re catalyst (Unpublished results).

Fig. 1.14 shows the activity decline and the change in reformate yield due to coke formation of a commercial reforming catalyst as a function of time on stream. The beneficial effect of having the metal particles present in a highly alloyed form is also demonstrated. By adjusting the pre-treatment conditions as discussed previously it is possible to control the degree of alloy formation and thus obtaining better performance of the catalyst. The addition of rhenium and sulphur to the Pt/Al_2O_3 catalyst greatly enhances the stability of this catalyst system. This has been claimed to be due to changes in the location [33] and nature [34] of the coke rather than only due to the amount produced. The quantity of the coke can be characterised by techniques such as temperature programmed oxidation (TPO) whereas the composition of the coke can be analysed by investigating the coke combustion products or by IR studies of the hydrocarbon deposits [66]. Fig. 1.15 shows examples of TPO profiles of the Pt/Al_2O_3, Re/Al_2O_3, and $Pt\text{-}Re/Al_2O_3$ catalyst (coke formed during nC_6 reaction) obtained when monitoring the CO_2 evolution during temperature programmed oxidation [36]. The peaks identified can be assigned to carbon formed on either Pt (low temperature peaks) or the support. The two first peaks of the $Pt\text{-}Re/Al_2O_3$ catalyst have been attributed to oxidation of carbon formed on Pt and the peak in the middle to the oxidation of carbon located on Re. It is assumed that coke formed on the Pt sites is either catalytically oxidised or that the nature of coke surrounding the metal sites is different resulting in an oxidation at lower temperatures. The two last peaks are therefore attributed to the oxidation of carbon located on the support.

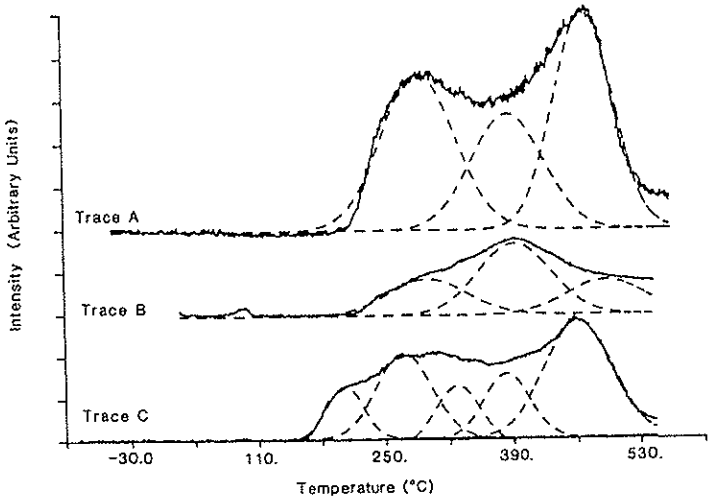

Fig. 1.15. TPO profiles obtained when measuring the CO_2 evolution during temperature programmed oxidation [36]

Coke formation is favoured at high temperatures and low hydrogen pressures, which are also conditions favourable for the formation of aromatic compounds. It

is therefore a question of process costs and frequency of regeneration when optimising the operation conditions. In addition to temperature and pressure, the rate of coke formation is obviously also dependent of the feedstock composition. The deactivation rate is faster if the feed contains aromatics, naphthenes, and paraffins in the C_8-C_{10} hydrocarbon range than if it contains lower molecular weight hydrocarbons. Fig.1.16 clearly demonstrates the effect of the final boiling point (FBP) of naphtha on catalyst deactivation [67].

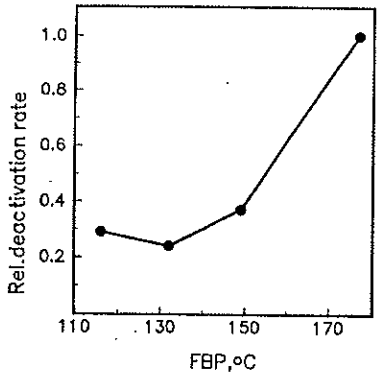

Fig. 1.16. The deactivation rate relative to the one for the base naphtha, as a function of naphtha FBP. The deactivation rate was measured as the temperature rise needed to maintain 102.4 RON [67].

Catalyst deactivation by poisoning

Poisoning refers to the strong adsorption of impurities in the feedstock, resulting in temporary or permanent inhibition of active sites. Typical impurities associated with the naphtha feed are sulphur in form of organic sulphides, nitrogen compounds, metals, and halides. In addition products formed during reaction may cause poisoning.

Table 1.5 shows the initial toxicity of the various impurities on the Pt/Al_2O_3 catalyst as measured by Barbier et al [68]. The initial toxicity is defined as number of platinum atoms poisoned by one molecule/atom of poison. It can be seen that Hg^{2+} is extremely toxic to the catalyst inhibiting as many as 15 Pt atoms by adsorption. Generally, metal impurities show strong affinity for platinum and form stable chemical compounds. Metal poisons are rarely eliminated by catalyst regeneration and will cause permanent damage.

Table 1.5. Initial toxicity of some compounds on Pt/Al_2O_3 [68].

Poison	Initial toxicity	Relative metal activity at poison saturation
SO_2	1.0	0
Thiophene	5.0	0
Dibenzothiophene	4.5	0
NH_3	0.1	0.67
Pyridine	0.12	0.042
CO	1.18	0
H_2O	0.00018	0.5
$As(C_6H_5)_3$	1.9	0
Na^{2+}	0	0
Fe^{2+}	1.1	0
Cu^{2+}	2.0	0
Hg^{2+}	15	0
Pb^{2+}	5.2	0

Sulphur is considered as the major poison of reforming catalysts and is present in the feed as organic sulphur compounds at concentrations up to 1500 ppm [69]. Although the adsorption of small amounts of sulphur is beneficial to the Pt and Pt-Re catalyst, excessive sulphurisation will affect the metal activity strongly. The toxicity of sulphur is a result of both the blocking of active sites and the modification of the electronic properties of these sites. It is important to use proper pretreatment conditions of the naphtha feed in order to avoid severe poisoning of the catalyst. In case of the $Pt\text{-}Re/Al_2O_3$ catalyst a maximum sulphur level of 0.5 ppm is recommended [29].

Nitrogen compounds in form of organic compounds decomposing into ammonia will inhibit the acid function of the catalyst. In the presence of water ammonia results in the leaching of chlorine by the formation of ammonium chloride [70]. Water and oxygenates will also cause leaching of chloride resulting in decreased acidity of the alumina, whereas halides present in the feed will have the opposite effect.

Catalyst deactivation by sintering

Sintering is the loss of active surface area of the catalyst due to high temperatures and most of the sintering in reforming catalysts occurs during regeneration by coke burning.

Metal sintering is the agglomeration and growth of metal crystallites. The extent and rate of this process is very much influenced by factors such as the temperature, atmosphere, and chloride content. Changes in Pt dispersion during treatment in oxygen atmosphere has been reviewed by Wanke et al [71]. The authors proposed a model where the sintering of Pt particles is governed by the formation of Pt^{4+} species. The stability and mobility of these surface species determines the degree of sintering of the catalyst, and at high temperatures sintering occurs rapididly.

In order to decrease the extent of sintering the catalyst must contain a sufficient amount of chlorine, as it is known to slow down sintering. The addition of a

second metal to the Pt catalyst has also been claimed to induce an beneficial effect on the sintering characteristics of Pt. Kluksdahl [29] attributed the higher stability of the Pt-Re catalyst to the increased resistance to sintering due to the formation of Pt-Re alloys.

In addition to sintering of the metal particles sintering of the alumina support occur. This is the change in pore structure causing loss of surface area and acidity. In opposition to metal particle sintering this is an irreversible process and determines therefore the total lifetime of the catalyst.

Catalyst regeneration

When the activity and selectivity of the reforming catalyst is too low for economical use after a certain time on stream, it has to be regenerated by oxidative removal of the coke. Coke combustion with oxygen starts at the coke deposited on the metal particles due to the catalytic action of platinum and the higher hydrogen content of deposits. This has been demonstrated by TPO experiments as shown in Fig. 1.15. By the action of oxygen spillover the coke burning will spread to the support. Because of the exothermic nature of oxidation, the procedure usually starts at a fairly low temperature (200-300°C) and with a low oxygen concentration (1-2%) in order to avoid temperature runaway and hot spots in the catalyst bed. The temperature and oxygen concentration is gradually increased up to 500°C and 21% (air). After coke combustion the chlorine content is low and the metal is partly sintered.

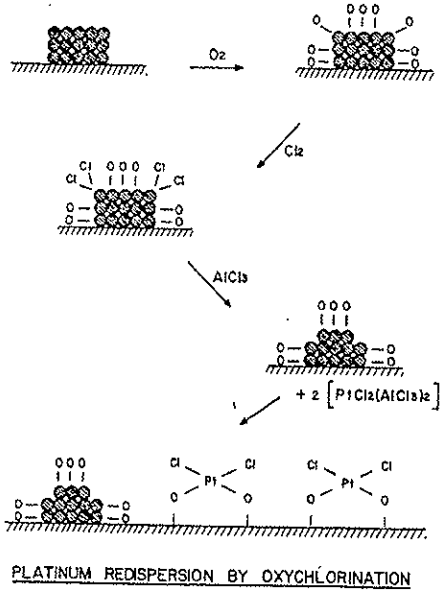

Fig. 1.17. Schematically presentation of the mechanism of redispersion by oxychlorination of Pt/Al_2O_3 catalysts [70].

After combustion of the coke the catalyst has to be rejuvenated in order to get it back to its initial state and the restoration of acidity and metal dispersion is obtained by oxychlorination. Fig. 1.17 shows the schematic presentation of the mechanism of redispersion by oxychlorinaton [70]. Here, the catalyst is exposed to chlorine (HCl, Cl_2 or carbon chlorides) together with oxygen at approximately 500°C, leading to a displacement of OH groups with Cl and a complete metal redispersion probably involving oxychlorinated platinum intermediates [72]. In the case of bimetallic catalysts the amount of chlorine prior to reduction may influence on the degree of alloyed metal particles [73]. After reduction the catalyst is sulphided in order to deactivate the superactive sites responsible of unwanted hydrogenolysis and hydrocracking reactions.

1.3 Industrial application

1.3.1 History

The first catalytic reformer started its operation in 1940. This was the fixed-bed Hydroforming process, using a molybdenum alumina catalyst. The catalyst lost activity as a result of coke deposition, but most of the original activity was regained on regeneration in air. However, the major breakthrough came with the introduction of alumina-supported platinum catalysts and the commercialisation by UOP of the Platforming process in 1949. The catalyst was more active by an order of magnitude or more than the first generation of molybdenum-based catalysts. The operating conditions (450-510°C, 35-50 bars) were selected to minimise coke laydown and the catalyst was not regenerated. In the 1950's more than 10 new commercial processes based on the platinum catalysts were developed. Most of these included facilities for catalyst regeneration, allowing operation at higher temperatures and lower pressures.

During the 1960's, higher-octane gasolines were necessitated by improvements in automobile engines, and in the 1970's and 1980's, environmental concerns, especially the phasing out of lead were the main driving forces. A significant catalyst improvement occurred in the late 1960's with the introduction of the Pt-Re alumina catalyst by Chevron in 1968 [29] and the new Rheniforming process two years later. The catalyst was more stable and could be operated at lower pressures and higher temperatures favouring the thermodynamics of aromatic formation. Subsequently, other bimetallic or multimetallic catalysts incorporating metals such as Ir, Sn and Ge came into the market. The higher stability and selectivity produced by the new catalysts does, however, require extensive feed purification because they are more vulnerable to sulfur poisoning. The new generation of bimetallic catalysts lead to the introduction of new processes, especially designed for low-pressure operation. The most significant innovation was the introduction of continuous catalyst regeneration (CCR) by UOP. This allows steady-state reforming operation with fresh catalyst performance at optimum process conditions. Most new units are of this type.

The platinum based bimetallic catalysts Pt-Re and Pt-Sn are dominating the present market. Because of the high stability, Pt-Re is usually the catalyst choice for units with periodical regeneration while Pt-Sn catalysts are used in CCR units because of better reformate selectivity at low pressures. The patent literature describes a number of new catalyst materials for reforming (such as metals on zeolites) and the combined use of different catalysts in the reactors. However, their catalytic performance has to be improved in order to replace the current Pt/alumina based systems. In fact, the catalysts in present use are still being improved as is seen by a continuous increase in commercial cycle lengths (run time in between regeneration). Modern semi-regenerable units may in fact operate for two to three years between regenerations at relatively severe operating conditions.

1.3.2 Reactor design and operation conditions

The overall reforming process is endothermic and the most endothermic reactions occur very rapidly. It follows that a large amount of heat must be added to the reactants in order to maintain a desired temperature level throughout the catalyst bed. Addition of heat to packed beds is associated with technical difficulties. Considering the heat duties, a fluidized bed reactor would be preferable, but the high cost of the reforming catalyst makes it uneconomical. The solution is to divide the catalyst charge among several reactors (usually 3 to 4) which are run adiabatically and with interstage heating in between.

When the feedstock enters the first reactor, the temperature falls rapidly as the cyclohexanes are dehydrogenated and almost quench the reactions. As a result, the residence time is short and the size of the first reactor is small compared to the other reactors. The effluent is reheated and enters the second reactor where it undergoes further dehydrogenation, dehydroisomerization and isomerization. The temperature drop of the second reactor is lower than in the first one. In the last reactor, which often contains about half of the total catalyst charge, the slower reactions, namely dehydrocyclization, hydrocracking and hydrogenolysis dominate. The exothermic cracking reactions in the last reactor causes a lower delta T (higher exit temperature) in the last reactor and shifts the naphthene-aromatic equilibria in favour of further dehydrogenation as well.

The reforming processes are classified according to the frequency and mode of regeneration. Semiregenerative processes are characterised by operation over long periods until complete plant shutdown during regeneration. This is suited for operating conditions where the catalyst deactivation is slow. The majority of reformers are of this type.

Cyclic processes have an additional 'swing' reactor that replaces one of the others when its catalyst charge needs to be regenerated. This type of process is not the most common because it requires that the reactors are of equal size and because of the technical complexity. Most new reforming units are based on continuous catalyst regeneration (CCR). In this design the reactors are usually stacked on top of one another. The catalyst is continuously withdrawn from the bottom of the reactor section, transported to a regeneration unit, regenerated and returned to the top of the reactor train.

High-pressure processes (20-50 bar) are operated at temperatures in the range of 470-520°C, high hydrogen to hydrocarbon mol ratios (4-10) and liquid hourly space velocities ranging from 1 to 6. Medium pressure (10-20 bar) and low-pressure (3-10) processes operate at slightly higher temperatures to optimise conversion into aromatics. The choice of conditions will depend on the feedstock quality, the product octane required, the catalyst stability and the regeneration capacity available. High-pressure operation causes higher rate of hydrocracking and therefore a lower reformate yield. On the other hand the rate of deactivation is reduced. The recent development of much more stable catalysts has increased the interest in low-pressure reforming. Since reformers are operated adiabatically and because the catalyst charge is unevenly divided among the reactors space velocity and temperatures are not constant. The space velocity in the first reactor may be more than twice of that for the last reactor. To evaluate catalyst activity, a weighted average bed temperature (WABT) is often calculated. WABT is the sum of the average of the inlet and outlet temperatures of each reactor multiplied with the weight fraction of catalyst in each reactor. The operating conditions of a modern medium-pressure unit are given in Table 1.6.

Table 1.6. Operating conditions for a semi-regenerative medium pressure unit.

H_2/HC inlet	Reactor			
	1	2	3	Total
Inlet temperature [°C]	485	485	485	
Exit temperatur [°C]e	395	440	460	
Average pressure [barg]	12	11	9	
WHSV per reactor [h^{-1}]	8	5	1.1	0.8
Percent of total catalyst charge	10	16	74	100

Reformers are operated to give a constant product octane number. As the catalyst is deactivated, the reactor temperature is gradually increased. The temperature increase during a cycle may be in the range of 20-40 degrees and the coke content of the catalyst may reach levels of 10-40 wt%. The decline in reformate yield in the cycle, if any, depends heavily on the catalyst stability (coke amount and coke tolerance).

1.4 Outlook

1.4.1 Reforming and the environment

In the recent decades it has become clear that the rapid utilisation of hydrocarbons as fuels are associated with strong environmental concerns. The inevitable formation of CO_2 upon combustion is recognised as a global problem and is a driving force for the development of more efficient engines and alternatives to hydrocarbons as fuels. The combustion of gasoline results in a

number of additional emissions such as CO, NO_x, SO_x and unburned hydrocarbons. Unsaturated gasoline components (aromatics and olefins) increase the formation of exhaust particles (smog). The air pollution related to traffic cause severe health problems in highly populated areas. The exposure to gasoline vapours during handling and the possibilities of leakage during storage and transportation are other problems of consideration. The hazards of benzene exposure (carcinogenic) are known.

To meet these problems, governments have progressively implemented stronger regulations on the specifications of gasoline and other fuels. Exhaust catalysts have been introduced to reduce emissions of CO and NO_x. Tetraethyl lead is being phased out as an octane booster as it is both an unwanted contaminant and because it poisons the exhaust catalysts. Both volatility and end boiling points in gasoline are being reduced and maximum levels of benzene, sulfur, total olefins and total aromatics are set. In the US, the Clean Air Act Amendments forced refiners to add minimum levels of oxygen (as oxygenates) to the fuel in order to reduce emissions of unburned hydrocarbons. The most common oxygenate was methyl tert butyl ether (MTBE) which has a high octane number (RON 120). Ethanol (RON 99) is used to a lesser extent. Table 1.7 outlines the gasoline specifications in the US, the European Union and in Japan for year 2000 and 2005.

Table 1.7. Gasoline specifications for the US, the European Union and Japan [74-76].

Specifications	USA	EU		Japan
Max. values	2000	2000	2005	2000
RVP [kPa]		60		78
S [wppm]	50	150	50	100
O [wppm]	2.2	2.7		
Benz. [vol%]	1.0	1		1
Arom. [vol%]	35	45	35	
Olef. [vol%]	15	18		
Lead (max.) [g/l]	-	0.005	-	

The new regulations will have great impact on reformers operating conditions and refineries configuration. Reid vapour pressure constraints will result in eliminating butanes from gasoline. Reduction of the benzene content can be achieved by processing the C_6 fraction by isomerization, by choosing reaction conditions disfavouring aromatics dealkylation (cracking) or by fractionation of the reformate. With aromatics being the main product from catalytic reforming and contributing most to the octane enhancement, aromatics reduction requires high amounts of other high-octane gasoline blending stocks. The alkylation and oligomerisation processes will likely become more important in the future, as the product is purely paraffinic, sulphur free and with high octane ratings. Olefins reduction sets an upper level of the amount of cracker naphtha as blending stock. Cracker naphtha is also practically the only source of sulphur in gasoline and the new specifications will require increased CCR hydroprocessing capacity. The use of MTBE, especially in the US, as an oxygen source and octane booster has been necessary in order to fulfil the specifications for unleaded gasoline. However, the high stability and high solubility of MTBE in water was not anticipated by the

industry and USA is faced with groundwater contamination due to unavoidable leakage. Odour and taste problems and questions regarding the toxicity of MTBE are about to ruin a number of large drinking water reserves. The use of MTBE is likely discontinued within two or three years. As a new main source of oxygen, other compounds such as methyl carbonate and ethanol (used in parts of the world already), will have to be considered.

1.4.2 Reforming outlook

The demand for aromatics for the petrochemical industry (BTX) and for high-octane gasoline will increase, especially in the developing countries of the world. Because of gasoline regulations, the importance of the reforming process as a gasoline supplier will be reduced. However, refineries are dependent on the valuable hydrogen produced by reforming for hydroprocessing purposes. In the future, gasoline-range components in the crude oil (naphtha) will likely be fractionated and the different components converted by various processes according to their potentials. For instance, the isomerization reaction equilibria favoured by low reaction temperatures have suffered in the reforming process. Although the reforming process and the reforming catalysts are considered mature, the research for more stable and more selective catalysts will continue. Advanced research instrumentation gives a better understanding of the chemistry involved. New speciality materials with strong shape selective properties (such as zeolites) may have potentials as future catalysts.

The main purpose of catalytic reforming is to produce high-octane gasoline components. Due to environmental concern of the ever-increasing number of cars, focus is recently been put on fuel cell cars using H_2 as the fuel. H_2 is a clean and very efficient energy carrier and is by many believed to be the fuel of the future. H_2 can be produced from a number of sources including water, but it is most likely that oil and gas will be the main source of H_2. H_2 can be produced in large units, filled and stored onboard the vehicle or it can be produced onboard by reforming of liquid fuels such as methanol or straight run gasoline. In any case such a development will have a great impact on the refinery configuration and in particular on catalytic reforming.

Acknowledgements

Odd Arne Rokstad is acknowledged for his contribution in calculating the thermodynamic data in Fig. 1.4.

References

1. International Petroleum Encyclopedia, vol 32. (Penn Well Publishing Co, Tulsa, OK 1999)
2. J.H. Gary and G.E. Handwerk : *Petroleum Refining Technology and Economics*, 3 edn. (Marcel Dekker, Inc., New York 1994)
3. M. Walsh : *The Global Phaseout of Leaded Gasoline: A Successful Initiative* (1999) http://earthsummitwatch.org/gasoline.html. (Earth Summit Watch Program)
4. American Petroleum Institute Research Project 45 (1954) Sixteenth Annual Report.
5. G.A. Mills, H. Heinemann, T.H. Milliken and A.G. Oblad, Ind.Eng.Chem **45**, 134 (1953)
6. Z. Paal, J. Catal. **105**, 540 (1987)
7. P.B. Weisz and E.W. Swegler, Science **126**, 31 (1957)
8. F.D. Rossini, K.S. Pitzer, R.L. Arnett, R.M. Braum and G.C. Pimentel : *API Research Project 44: Selected Values of Physical and Thermodynamic Properties of Hydrocarbons and Related Compounds.* (Carnegie Press, Pittsburgh 1953)
9. K. Moljord, H.G. Hellenes, A. Hoff, I. Tanem, K. Grande and A. Holmen, Ind. Eng. Chem.Res., **35**, 99-105 (1996)
10. P.A.Van Trimpont, G.B. Marin, G.F. Froment, Ind. Eng. Chem.Res, **27**, 51 (1988)
11. W.S. Kmak, A.N. Stuckey: Powerforming Process Studies with a Kinetic Simulation Model (Paper N0. 56a), AIChE National Meeting, New Orleans, March 1973.
12. J.P. Boitiaux, J.M. Devés, B. Didillon and C.R. Marcilly : Catalyst Preparation, in *Catalytic Reforming of Naphtha*, G.J. Antos, A.M. Aitani, and J.M. Parera (Eds.) (Marcel Dekker, Inc., New York 1995)
13. N.Y. Chen and W.E. Garwood, J. Catal. **52**, 453 (1978)
14. C.J. Plank, E.J. Rossininski and E.N. Givens (1973): US Patent US 4,141,859.
15. N.Y. Chen (1973): US Patent 3,729,409.
16. J.B. Peri, The Journal of Physical Chemistry **69**, 211 (1965)
17. J.B. Peri, The Journal of Physical Chemistry **69**, 220 (1965)
18. J.B. Peri, The Journal of Physical Chemistry **69**, 231 (1965)
19. H. Knözinger and P. Ratnasamy, Catal.Rev.-Sci.Eng. **17**, 31 (1978)
20. B.C. Gates, J.R. Katzer and G.C.A. Schuit : *Chemistry of Catalytic Processes.* (McGraw-Hill inc., New York 1979)
21. P.H. Emmet : *Catalysis. Alkylation, Isomerization, Polymerization, Cracking and Hydroreforming*, vol VI. (Reinhold Publishing Corporation, New York 1958)
22. G.A. Somorjai and J. Carrazza, Ind. Eng. Chem. Fundam. **25**, 23 (1986)
23. J. Barbier, G. Corro, Y. Zhang, J.P. Bournonville and J.P. Franck, Appl. Catal. **13**, 245 (1985)
24. R. Prestvik, B. Tøtdal, C.E. Lyman and A. Holmen, J. Catal. **176**, 246 (1998)

25. C.E. Lyman, J.I. Goldstein, D.B. Williams, D.W. Ackland, S. von Harrach, A.W. Nicholls and P.J. Statham, Journal of microscopy **176**, 85 (1994)
26. C.R. Adams, H.A. Benesi, R.M. Curtis and R.G. Meisenheimer, J. Catal. **1**, 336, (1962)
27. J.E. Benson and M. Boudart, J. Catal. **4**, 704, (1965)
28. R. Prestvik : Characterization of the metal function of a Pt-Re/Al2O3 reforming catalyst, Doctor of engineering Dissertation, The Norwegian Institute of Technology (1995)
29. H.E. Kluksdahl: U.S. Patent 3415737 (1968).
30. R.E. Rausch: U.S Patent 694872 (1977)
31. J.H. Sinfelt: U.S. Patent 3953368 (1976)
32. G.J. Antos: U.S. 803693 (1978)
33. J. Beltramini and D.L. Trimm, Appl. Catal. **32**, 71 (1987)
34. W.M.H. Sachtler, J.Mol.Catal. **25**, 1 (1984)
35. A.S. AlKabbani, Hydrocarbon Processing, July 1999, 61 (1999)
36. S.M. Augustine, G.N. Alameddin and W.H.M. Sachtler, J. Catal. **115**, 217, (1989)
37. Y.I. Yermakov and B.N. Kuznetsov, J.Mol.Catal. **9**, 13 (1980)
38. R.J. Bertolacini and R.J. Pellet : The function of Rhenium in Bimetallic Reforming Catalysts, in *Catalyst Deactivation* (Elsevier Scientific Publishing Company, Amsterdam 1980) pp. 73-77
39. D.R. Short, S.M. Khalid and J.R. Katzer, J. Catal. **72**, 288 (1981)
40. F.H. Ribeiro, A.L. Bonivardi and G.A. Somorjai, Catal. Lett. **27**, 1 (1994)
41. V.K. Shum, J.B. Butt and W.H. Sachtler, J. Catal. **96**, 371 (1985)
42. A. Bensaddik, A. Caballero, D. Bazin, H. Dexpert, B. Didillon and J. Lynch, Appl. Catal. **162**, 171 (1997)
43. P. Biloen, J.N. Helle, H. Verbeek, F.M. Dautzenberg and W.M.H. Sachtler, J. Catal. **63**, 112 (1980)
44. C.G. Michel, W.E. Bambrick and R.H. Ebel, Fuel Processing Technology **35**, 159 (1993)
45. J. Biswas, G.M. Bickle, P.G. Gray, D.D. Do and J. Barbier, Catal.Rev.-Sci.Eng. **30**, 161 (1988)
46. F.M. Dautzenberg, J.N. Helle, P. Biloen and W.M.H. Sachtler, J. Catal. **63**, 119 (1979)
47. R. Burch, J. Catal. **71**, 348 (1981)
48. B. Coq and F. Figureras, J. Catal. **85**, 197 (1984)
49. Y.-X. Li and K.J. Klaubunde, J. Catal. **126**, 173 (1990)
50. Z. Paál, A. Györy, I. Uszkurat, S. Olivier, M. Gurin and C. Kappenstein, J. Catal. **168**, 164, (1997)
51. R. Burch and L.C. Garla, J. Catal. **71**, 360 (1981)
52. B.A. Sexton, A.E. Hughes and K. Foger, J. Catal. **88**, 466 (1984)
53. J.M. Parera, J.N. Beltramini, C.A. Querini, E.E. Martinelli, E.J. Churin, P.E. Aloe and N.S. Figoli, J. Catal. **99**, 39 (1986)
54. B.H. Isaacs and E.E. Petersen, J. Catal. **77**, 43 (1982)
55. F. Hilbrig, C. Michel and G.L. Haller, The Journal of Physical Chemistry **96**, 9893 (1992)

56. C. Bolivar, H. Charcosset, R. Frety, M. Primet, L. Tournayan, C. Betizeau, G. Leclercq and R. Maurel, J. Catal. **39**, 249 (1975)
57. R. Prestvik, K. Moljord, K. Grande and A. Holmen, J. Catal. **174**, 119 (1998)
58. C. Meitzner, G.H. Via, F.W. Lytle, S.C. Fung and J.H. Sinfelt, The Journal of Physical Chemistry **92**, 2925 (1988)
59. H. Lieske and J. Volter, J. Catal. **90**, 96 (1984)
60. A. El Abed, S.E. El Qebbaj, M. Guérin, C. Kappenstein, H. Dexpert and F. Villain, J. Chim. Phys. **94**, 54 (1997)
61. C. Kappenstein, M. Guerin, K. Lazar, K. Matusek and Z. Paak, J.Chem.Soc.Faraday.Trans. **94**, 2463 (1998)
62. C. Kappenstein, M. Saouabe, M. Guérin and P. Marecot, Catal. Lett. **31**, 9 (1995)
63. J. Llorca, P. Ramírez de la Piscina, J.L.G. Fierro, J. Sales and N. Homs, J.Mol.Catal. **118**, 101 (1997)
64. G.T. Baronetti, S.R. Miguel, O.A. Scelza and A.A. Castro, Appl. Catal. **24**, 109 (1986)
65. S.M. Stagg, C.A. Querini, W.E. Alvarez and D.E. Resasco, J. Catal. **168**, 75 (1997)
66. P. Marecot and J. Barbier : Deactivation by coking, in *Catalytic Naphtha Reforming*, G.J.Antos, A.M. Aitani, and J.M. Parera (Eds.) (Marcel Dekker, Inc., New York 1995)
67. K. Moljord, K. Grande, I. Tanem, and A. Holmen, in *Deactivation and testing of hydrocarbon-processing catalysts*, P. O'Connor, T. Takatsuka, G.L. Woolery (Eds.), ACS Symposium Series No. 634 (ACS 1995) pp. 268-282
68. J. Barbier: *Deactivation and Poisoning in Catalysis.* (Marcel Dekker, New York 1985), p.121
69. J.N. Beltramini: Deactivation by Poisoning and Sintering , in *Catalytic Naphtha Reforming*, G.J. Antos, A.M. Aitani, and J.M. Parera (Eds.) (Marcel Dekker, Inc., New York 1995)
70. P. Franck and G. Martino: *Progress in Catalyst Deactivation.* (Martinus Nijhoff, The Hague 1982)
71. S.E. Wanke, J.A. Szymura and T.T. Yu : *Catalyst Deactivation* (Marcel Dekker, New York 1986)
72. H. Lieske, G. Lietz, H. Spindler and J. Völter, J. Catal. **81**, 8 (1983)
73. T. Gjervan, M. Rønning, R. Prestvik, B. Tøtdal, C.E. Lyman, and A. Holmen, in *Studies in Surface Science and Catalysis*, A. Corma, F.V. Melo, S. Mendioroz, J.L.G. Fierro (Eds.), Proceedings of the 12th ICC, Granada, Spain, July 9-14 2000, Vol 130A (Elsevier, Amsterdam 2000), pp. 3189-3194
74. G. Martino: Catalysis for oil refining and pertochemistry, recent developments and future trends, in *Studies in Surface Science and Catalysis*, A. Corma, F.V. Melo, S. Mendioroz, J.L.G. Fierro (Eds.), Proceedings of the 12th ICC, Granada, Spain, July 9-14 2000, Vol 130A (Elsevier, Amsterdam 2000), pp. 83-103
75. E.L. Hartman, D.W. Hanson, B. Weber, Hydrocarbon Processing, 77 (1998)
76. Petroleum Association of Japan: *Annual Review 1999* (http://www.paj.gr.jp/html/english/index.html)